DISTORTION DATA ANALYSIS

Michael T. Moore

General Electric Company

Prepared for:

Air Force Aero Propulsion Laboratory

February 1973

AFAPL-TR-72-111

DISTORTION DATA ANALYSIS

M.T, Moore
Aircraft Engine Group
General Electric Company

TECHNICAL REPORT AFAPL-TR-72-111

February 1973

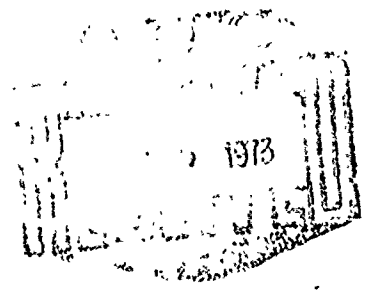

AIR FORCE AERO PROPULSION LABORATORY
AIR FORCE SYSTEMS COMMAND
WRIGHT-PATTERSON AIR FORCE BASE, OHIO 45433

194

NOTICE

When Government drawings, specifications, or other data are used for any purpose other than in connection with a definitely related Government procurement operation, the United States Government thereby incurs no responsibility nor any obligation whatsoever; and the fact that the government may have formulated, furnished, or in any way supplied the said drawings, specifications, or other data, is not to be regarded by implication or otherwise as in any manner licensing the holder or any other person or corporation, or conveying any rights or permission to manufacture, use, or sell any patented invention that may in any way be related thereto.

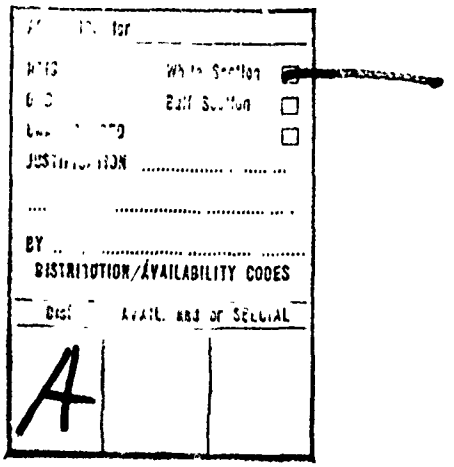

Copies of this report should not be returned unless return is required by security considerations, contractual obligations, or notice on a specific document.

UNCLASSIFIED

Security Classification

DOCUMENT CONTROL DATA - R & D

(Security classification of title, body of abstract and indexing annotation must be entered when the overall report is classified)

1. ORIGINATING ACTIVITY (Corporate author)	2a. REPORT SECURITY CLASSIFICATION
General Electric Company Cincinnati OH	UNCLASSIFIED
	2b. GROUP

3 REPORT TITLE

Distortion Data Analysis

4 DESCRIPTIVE NOTES (Type of report and inclusive dates)

Final Report February-November 1972

5. AUTHOR(S) (First name, middle initial, last name)

Michael T. Moore

6. REPORT DATE	7a. TOTAL NO. OF PAGES	7b. NO. OF REFS
December 1972	128	4

8a. CONTRACT OR GRANT NO	9a. ORIGINATOR'S REPORT NUMBER(S)
33615-72-C-1763	
b. PROJECT NO. 3066	
c. Task No. 11	9b. OTHER REPORT NO(S) (Any other numbers that may be assigned this report)
d. Work Unit 11	AFAPL-TR-72-111

10. DISTRIBUTION STATEMENT

Approved for public release; distribution unlimited

11. SUPPLEMENTARY NOTES	12. SPONSORING MILITARY ACTIVITY
	AF Aero Propulsion Laboratory Wright-Patterson AFB, Ohio 45433

13. ABSTRACT

A detailed study of the characteristics of inlet distortion has been conducted. Data was selected from inlet and engine/inlet test with various duct diameters and various levels of steady-state distortion. A similarity parameter was developed which showed consistent trends in dynamic distortion relative to steady-state distortion over different scale sizes. These trends were consistent when the GE "Method D" Phase 0 Distortion Parameter, "ID", was used and not when gross overall distortion parameters were used.

(Distribution of this abstract is unlimited)

DD FORM 1473

DISTORTION DATA ANALYSIS

M.T. Moore

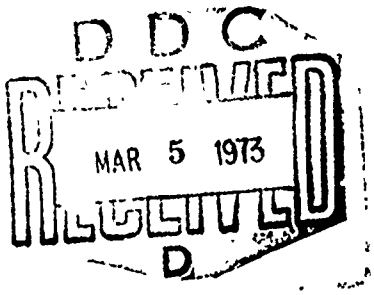

ic

FOREWORD

This report was prepared by the Aircraft Engine Group of the General Electric Company for the Aero Propulsion Laboratory, United States Air Force, Air Force Systems Command, under Contract No. F33615-72-C-1763, Project No. 3066, Task No. 11, Work Unit 11.

The work reported herein was conducted under the technical cognizance of Mr. John E. Lueke, Turbine Engine Division, Aero Propulsion Laboratory.

This program was initiated on February 25, 1972 and was concluded on January 25, 1973. The principal investigator for General Electric was Mr. Michael T. Moore. This report was submitted on December 5, 1972.

This technical report has been reviewed and is approved.

The author expresses his gratitude for the support of this study by S.M. Tripp and P.H. Gibson. Mr. Tripp, as operator of the SMAL, programmed the ADA and processed the analog distortion data; Mrs. Gibson processed the steady-state and dynamic distortion data through the GE635 computer. Their efforts were major factors in the success of this study.

Ernest C. Simpson

ERNEST C. SIMPSON, Director
Turbine Engine Division
AF Aero Propulsion Laboratory

ABSTRACT

A detailed study of the characteristics of inlet distortion has been conducted. Data were selected from inlet and engine/inlet tests with various duct diameters and various levels of steady-state distortion. A similarity parameter was developed which showed consistent trends in dynamic distortion relative to steady-state distortion over different scale sizes. These trends were consistent, when the GE "Method D" Phase 0 Distortion Parameter ("ID") was used and not when gross overall distortion parameters were used.

TABLE OF CONTENTS

LIST OF TABLES

LIST OF ILLUSTRATIONS

LIST OF ILLUSTRATIONS (Continued)

LIST OF ILLUSTRATIONS (Continued)

LIST OF ILLUSTRATIONS (Continued)

LIST OF ILLUSTRATIONS (Concluded)

LIST OF SYMBOLS

M	Free stream Mach number
α	Angle of attack
PSD	Power spectral density
RMS	Root mean square
ADA	Analog distortion analysis
Hz	Frequency $\sim Sec^{-1}$
AT	Average time
R	Duct radius at measurement plane
c	Acoustic velocity $\sim$ 1000 ft/sec
λ	Similarity parameter = $\pi R/AT/c$
f(-3 dB)	$\frac{1}{2}$ power or 0.707 amplitude point of filter
g	Secondary gap area
MFRD	Duct mass flow ratio = secondary + primary
Po	Free stream pressure
Re/ft	Reynold's number per unit length
P_T	Local probe steady-state pressure
P_{RMS}	Local probe root mean square pressure
$P_{FACE\ AVG}$	Average pressure at measurement plane
$P_{FACE\ MAX.}$	Maximum pressure at measurement plane
$P_{FACE\ MIN.}$	Minimum pressure at measurement plane
$P_{RING\ AVG}$	Average pressure in ring of probes
$P_{RING\ MIN.}$	Minimum pressure in ring of probes
η	Recovery $\sim P_{FACE\ AVG}/Po$
$\Delta P/PMX$	$(P_{FACE\ MAX.} - P_{FACE\ MIN.})/P_{FACE\ AVG}$
$\Delta P/PFA$	$(P_{FACE\ AVG} - P_{FACE\ MIN.})/P_{FACE\ AVG}$
$\Delta P/PAV$	$(P_{RING\ AVG} - P_{RING\ MIN.})/P_{FACE\ AVG}$
$\Delta P/PRD$	$(P_{FACE\ AVG} - P_{RING\ AVG})/P_{FACE\ AVG}$
IDC_H	$(\Delta P/PAV_1 + \Delta P/PAV_2)/2$
IDC_T	$(\Delta P/PAV_5 + \Delta P/PAV_4)/2$
IDC	MAX.(IDC_H, IDC_T)
IDR	MAX.$(\Delta P/PRD_5, \Delta P/PRD_1)$
ID	IDR + IDC

LIST OF SYMBOLS (Concluded)

$\Delta(\Delta P/PMX)$	$\Delta P/PMX_{DYNAMIC} - \Delta P/PMX_{STEADY-STATE}$
$\Delta(\Delta P/PAV)$	$\Delta P/PAV_{DYNAMIC} - \Delta P/PAV_{STEADY-STATE}$
ΔIDR	$IDR_{DYNAMIC} - IDR_{STEADY-STATE}$
ΔIDC	$IDC_{DYNAMIC} - IDC_{STEADY-STATE}$
ΔID	$ID_{DYNAMIC} - ID_{STEADY-STATE}$
RID	$ID_{DYNAMIC}/ID_{STEADY-STATE}$
Re	Reynold's number

SECTION I

INTRODUCTION

During the past few years a number of inlet model and inlet/engine tests have been conducted wherein nonsteady pressure distortion characteristics, as well as the usual steady-state pressure distortion characteristics, have been measured. In some cases, significant levels of dynamic distortion have been reported that are nearly double the steady-state levels. In other cases, the increment of dynamic distortion in excess of the steady-state levels was reported to be less. These differences in reported results are attributable, in part, to differences in measurement techniques and data analysis methods. In addition, the effects of model scale size on the relative contributions of dynamic and steady-state distortion levels have not been clearly understood. Consistent trends in the data consequently have not evolved; therefore, a consistent method to project full-scale inlet dynamic distortion levels from scale model data has not yet been developed.

As a result of the considerable testing being done with high-response pressure instrumentation, the measurement techniques have been somewhat standardized. Most significant is the fact that the fluctuating pressure data from these tests, which include between 30 and 48 probes at the distortion measurement plane, are being recorded on what has become an industry standard analog tape system. Constant band width multiplex FM recording systems with 1-inch 14-track tape are in use by virtually all test facilities involved in inlet testing. In-flight inlet test data are also being acquired by these types of systems.

To be able to perform real time distortion analysis on the taped analog data from inlet model and inlet/engine tests, the General Electric Company Aircraft Engine Group developed the Stability Measurements Analysis Laboratory (SMAL). (See Appendix I.) Parallel with the analog analysis capability, improved methods of distortion data analysis for both steady-state and dynamic conditions were developed.

The General Electric "Method D" Distortion Methodology (Appendix II) has been programmed on the digital computer to provide data analysis of inlet pressure on a steady-state or time-variant basis. The combination of an improved distortion methodology for instantaneous as well as steady-state distortion parameter computation, an ability to program the methodology for real time analysis in the SMAL, and "standard" data tapes for virtually all inlet tests with high response pressure measurements has made possible analysis of dynamic distortion data from several inlet tests using consistent analysis methods.

The objectives of these analyses were to assess the trends in dynamic inlet distortion relative to both steady-state distortion levels and to model scale size. Data for analyses were supplied by the AFAPL and AFFDL from the recently completed flight tests of an aircraft and the wind tunnel tests of two different scale geometrically similar models of the inlet of that aircraft. Supplementary data from other inlet model or inlet/engine tests were supplied by General Electric.

SECTION II

SUMMARY

A detailed study of the characteristics of inlet distortion has been conducted. The objective of this study was to assess the trends in the instantaneous dynamic distortion relative to the steady-state distortion levels and to model scale size. To accomplish this task, data were selected from inlet and inlet/engine tests with duct diameters ranging from 3.8 inches to 35.6 inches and steady-state distortion levels ranging from 10% to 30% $\Delta P/PMX$. Data sources were tests of two-dimensional external compression, two-dimensional mixed compression, and axisymmetric mixed compression inlets. Each of these included 30 or more fluctuating/steady-state pressure measurements. Conditions selected were from $M = 0.9$ to $M = 2.5$ and $\alpha = 0°$ to $\alpha = 12°$ for normal and supercritical operating conditions.

Air-Force-supplied data from flight tests of a two-dimensional external compression inlet and wind tunnel tests of two different scale geometrically similar models of that same inlet were carefully selected based on matched steady-state parameters. With these data and other data supplied by GE, a similarity parameter was developed that consistently shows the dynamic distortion from the three scale sizes of the same inlet at closely matched geometric and aerodynamic conditions to have the same trends relative to steady-state distortion over a wide range of average times. These trends were found to be consistent, when the GE "Method D" Phase 0 combined distortion parameter (ID), was used and not when the gross overall distortion parameters ($\Delta P/PMX$ and $\Delta P/PFA$) were used. The internal aerodynamic characteristics were found to have stronger influence on the intensity of dynamic distortion than external aerodynamic conditions.

With the similarity parameter and the combined distortion parameter, data from other types of inlets of various duct diameters were shown to have similar trends in dynamic distortion with respect to steady-state levels at various average times. A method for estimation of peak instantaneous values of ID from scale model steady-state values for use in preliminary studies has been developed on the basis of these data.

SECTION III

DATA SELECTION

1. AIR-FORCE-SUPPLIED DATA

With a goal of detailed distortion analysis of up to 15 data points from the recently completed tests of the full, 0.228, and 0.125 scale sizes of the same inlet (referred to as the DDAS inlet), a search of the supplied data from the three tests was initiated immediately. Consistent with the objectives ("....assessment of trends and dynamic inlet distortion relative to both the steady-state distortion levels and to model scale size"), the criteria used for selection of data points were that (where possible) the same geometric and aerodynamic conditions would exist in each of the three scale sizes. For this initial effort, the search was restricted to aircraft nominal schedule cruise and maneuver operating points rather than atypical extremes in geometric and aerodynamic conditions. A sketch of the inlet is shown as Figure 1.

The comparison of the data point conditions listed in the logs from the tests revealed that the data from these three tests cannot be compared on a constant Reynold's number basis. This is primarily due to the inability of the test facilities to achieve the necessary increase in stagnation pressure for the 0.125 scale model over those values subsequently measured during the full-scale aircraft flight tests. Since the data had been acquired over a range of stagnation pressures for each geometric and aerodynamic test configuration, the criteria of constant free stream total pressure was used to narrow the data selection. However, as much as a factor of 8 difference in Reynold's number results from these criteria. Data were available at M = 0.9 with nearly constant Reynold's number and were selected to determine if any Reynold's number effects were discernable.

The comparison of model test data to full-scale data was further complicated by the fact that, for a given external aerodynamic condition, inlet mass flow was varied in the models by changing the primary flow at constant secondary flow; in the aircraft it was varied by changing the secondary flow (gap area) with the engine holding constant primary flow. In most cases this difficulty was overcome by comparing the specific aerodynamic and geometric conditions for a single full-scale data point with a group of model data points for each scale size.

To further narrow the selection, internal aerodynamic characteristics were matched on a steady-state recovery/maximum distortion level ($\Delta P/PMX$) basis because these parameters utilize the measured data. The primary airflow in the full-scale aircraft was estimated based on engine cycle deck computations for the corrected measured engine rotor speed. The airflow is potentially in error at high Mach number conditions and high angle of attack conditions; therefore, the recovery/airflow technique was not the primary method used for matching the data. It was considered that, with similar maximum distortion levels in the three scale sizes, the objective of scale model

effects on dynamic inlet distortion trends would come closer to being realized.

Once the data point selections were narrowed down with the parameters available, the raw data were processed through the GE Distortion Analysis Program (DAP) to obtain pressure distortion contours. The final data point selection would be the five point sets that had the most similar contour plots to ensure that the steady-state distortion not only agreed in overall level but also agreed in distribution over the distortion measurement plane. The steady-state data for the three scale sizes for the five selected point sets are shown in Figures 2 through 9.

The recovery versus maximum distortion level for the five conditions selected are shown in Figure 2. In each of the two scale models, the next higher and lower recovery points are shown along with the selected points to show the variation of these parameters. For the selected $M = 0.9$ conditions, the 0.228 scale model was not tested at lower recoveries than the points selected.

As a check on the match of the internal aerodynamic characteristics, the recovery versus mass flow ratio for the five conditions is shown in Figure 3. At $M = 1.8$, $\alpha = 10°$, the full-scale aircraft mass flow ratio is much higher than the points selected for the two models even though the recovery and maximum distortion levels agree well. This anomaly could be due, in part, to the effect of estimating the airflow in the aircraft. Also, the presence of only one aircraft point on each plot is due to the aforementioned method of varying the airflow in the aircraft.

The steady-state pressure distortion contours and radial distributions of the "Method D" ring parameters are shown in Figures 4 through 8 for the five selected data point sets. The upper portion of each figure shows the distribution of deviations from the face average pressure on 18 rays and 10 equal area rings for each of the three scale sizes. Contours can be constructed that trace constant levels; but, for simplicity, only the face average contour was drawn with all the positive integers representing the pressures higher than average and the negative integers representing those lower.

The lower portion of each figure shows the radial distribution of the "Method D" parameters for five equal area rings. The $\Delta P/PAV$ is the circumferential distortion for each ring, while the $\Delta P/PRD$ is the radial distortion for each ring. These displays provide more detailed comparisons of the distortion for each of the scale sizes.

The "Method D" distortion parameters are shown in Figure 9 for the selected data point sets. The combined distortion parameter, ID, matches within one point (0.01) between the 0.228 scale and the full-scale data for all points. The 0.125 scale data have consistently higher values of ID for all five conditions.

Based on the steady-state results from the full-scale, 0.228 scale, and 0.125 scale tests of the DDAS inlet, the first 14 data points listed in Table I have been selected for detailed distortion analysis. As discussed later, two additional data points from the tests of the 0.228 scale DDAS inlet were selected. These points will provide the basis for the assessment of trends in dynamic inlet distortion relative to steady-state distortion and to model scale size. To supplement these results, data points from other inlet model and inlet/engine tests have been selected for analysis.

2. GENERAL ELECTRIC SUPPLEMENTAL DATA

To complement the AFAPL-supplied data with additional data for assessment of model scale size effects on dynamic inlet distortion, data were selected from tests of other types of inlets with a similar range of duct diameters. Since all of these sources have different full-scale diameters, the actual model scale size is not a meaningful parameter. The duct radius will be used to compare the data from the various inlet tests on a more consistent basis than model scale size.

One of the GE data sources is a previous test of the identical model used in the 0.228 scale inlet tests described in the previous section. During that test a different primary flow measurement section was used that resulted in a slightly larger distortion measurement plane diameter. A sketch of the Large Scale Inlet (LSI) model is shown in Figure 10. The differences between the LSI and the 0.228 scale models can be seen by comparing Figure 10 to Figure 1. Even though both tests used six rakes, the angular locations were different. The LSI test used six probes per rake and a different centerbody arrangement.

A search of the LSI data was conducted to find similar geometric and aerodynamic conditions to those tested on the 0.228 scale DDAS inlet model. Such sets of data were available at $M = 1.8$ and $\alpha = 1.5°$, and $M = 1.8$ and $\alpha = 10°$. The LSI recovery characteristics for these conditions are shown in Figure 11. However, the LSI recoveries are slightly lower and maximum distortion levels somewhat higher at both conditions (see Figures 2 and 3). The differences in the measurement plane between the two models account for most of the differences in steady-state results as discussed later in this report. However, two points of the LSI data (see Figure 11) were selected for detailed dynamic distortion analysis to determine if these differences seen in the steady-state data would affect the dynamic data results. Also, these two data points will be used to determine the effect on the dynamic distortion of changing angle of attack while holding constant mass flow.

Other GE data sources that were available to supplement the model scale effects data were the 0.21 scale model (ISM) and the full-scale (SIM) testing of an inlet simulator. A sketch of the inlet simulator is shown in Figure 12. The feasibility of this device to match inlet distortion was demonstrated, both steady-state and dynamic, in scale model tests where the identical measurement section from the LSI model was used with the ISM (Reference 1). The later testing of the model in preparation for full-scale inlet simulator/engine testing yielded the data selected here for detailed dynamic distortion analyses. Data from the SIM testing at the same free stream total

pressure, recovery, and flow conditions as the ISM were also selected. Recovery versus the steady-state characteristics of the ISM and SIM are shown in Figure 13 for the two sets of points from each test selected for analysis. Even though the recovery and area ratios were very closely matched, all the distortion parameter levels were slightly different between the two scale sizes.

The final GE sources of data were chosen to provide additional information as to the trends in dynamic inlet distortion relative to steady-state distortion levels. Up to this point, all the data discussed have been from two-dimensional external compression inlets and inlet simulators and have only moderate steady-state distortion levels. Data from mixed compression inlets at normal operating conditions were available that had higher distortion levels.

A small scale model of a two-dimensional mixed-compression inlet provided two of the remaining data points. A sketch of the model is shown in Figure 14. The recovery and steady-state characteristics for the two data points, one supersonic and one subsonic, are shown in Figure 15. These points were selected for detailed dynamic inlet distortion analyses to determine if the higher steady-state distortion levels (approximately 50% greater than the previous selected DDAS inlet data) would affect the dynamic results.

An axisymmetric mixed compression inlet/engine test at M = 2.5 provided the final two data points. A sketch of the inlet/engine configuration is shown in Figure 16. Of the 11 points available from these tests, 2 were selected that had high steady-state distortion levels at similar operating conditions. The difference between the data points is that one point is at a 5° angle of attack and the other point is at a 0° angle of attack. The steady-state distortion and recovery characteristics of these two data points are shown in Figure 17.

As can be seen, the high level of distortion parameter (ID) is made up predominately of radial component in the 0° angle-of-attack case and of circumferential component in the 5° angle-of-attack case. These two points were selected for detailed dynamic inlet distortion analysis to determine if trends in dynamic distortion are affected more by radial or circumferential dominance of the steady-state distortion.

Based upon availability of dynamic inlet distortion data from sources other than those supplied by the AFAPL, the 10 supplementary data points as just discussed were selected for detailed dynamic inlet distortion analyses. These points are also listed in Table I. To assess trends in dynamic inlet distortion relative to both steady-state distortion and model size, the 26 data points summarized in Table I and presented versus duct radius in Figure 18 have been selected primarily by matching steady-state parameters. These data include subsonic and supersonic Mach numbers, cruise and maneuver attitudes, external and mixed compression operation, and moderate and high distortion levels. Also, all of the data points were

selected to be at normal operating primary and secondary mass flow ratios at or slightly above the critical operating point of the respective inlet.

In the process of selection of the data, care has been exercised to ensure that the various data points have something in common with each other. The DDAS inlet and inlet simulator data were chosen to have the best possible chance to be scalable. Also, for each scale size inlet in the AFAPL data, there are data from an inlet of comparable duct diameter for comparison without scaling. Finally, there are data from mixed compression inlets, both two-dimensional and axisymmetric, to compare with the data from the two-dimensional external compression DDAS inlet.

SECTION IV

ANALYSIS OF DYNAMIC DISTORTION

1. EVALUATION OF AIR FORCE DATA

Part of the data selection process not mentioned in the previous section, but certainly as important as the steady-state data matching, was the quality of the analog fluctuating pressure data recorded on magnetic tape. No matter how well the steady-state conditions matched between the three scale sizes in the DDAS inlet test data, the analysis of dynamic inlet distortion would have been impossible with analog data that could not be recovered or calibrated. Therefore, a systematic procedure of checking and comparing the analog data was followed prior to final selection of the 16 DDAS inlet data points.

For each candidate set of data points from the three scale size inlet tests, the analog data tapes were supplied by the Air Force in order that the recoverability of the data could be determined. That is, prior to calibrating and processing the data, signals must be recovered and with the proper polarity. For example, all the data points from one entire flight of the aircraft were immediately eliminated due to all six channels of one track (1/5 of the probes) being unrecoverable. Fortunately, all but a few of the data signals were recoverable for all the test points under consideration. Also there was sufficient information recorded on the tapes to allow identification of the polarity of the signals (i.e. does increasing pressure cause increasing or decreasing voltage?). An increase or decrease step change in pressure to each probe was provided in most cases and is the best check on signal polarity from end to end. Individual wave-form checks for each data point were also performed to eliminate any signals that were either missing or had spurious signal sources, such as common mode voltage or noise spikes, that could affect the dynamic distortion analysis.

To confirm the calibration techniques used on the data once they were recovered, analog RMS and PSD calculations were performed on data from all three scale sizes. These results were compared to RMS and PSD calculations supplied by AFAPL for the same probes from the same data points. In this way end-to-end checks of analog recovery and calibration techniques were performed. Favorable comparison of these results were considered a prerequisite for credibility associated with any new conclusions arising from subsequent analyses of these data.

The results of the end-to-end checks are shown in Figures 19, 20, and 21 for the 0.125 scale, 0.228 scale, and full-scale DDAS inlet data. The data compared were selected from data runs common with those points selected for detailed distortion analysis. The Air-Force-supplied spectral results shown in these figures were determined by digital analysis methods, while the results for this study were determined by analog analysis of generally longer records of data. In the analog results, spikes at discrete frequencies would tend to be at higher amplitude levels and the random data would tend to be at lower levels due to the longer analysis time. The spectra and

P_{RMS} levels shown in Figures 19, 20, and 21 compare very well within the accuracy of these types of analyses. With demonstrated ability to recover and calibrate the data, the detailed analysis could then proceed.

2. ANALOG DISTORTION ANALYSIS

The first step in the detailed dynamic inlet distortion analysis was to process the data points through the Analog Distortion Analysis (ADA) computer in the SMAL (see Appendix I). This computer was programmed to compute continuously the values of the radial parameter IDR, the circumferential parameter IDC, and the Phase 0 combined parameter ID = IDC + IDR. That the computations are within the accuracy expectations for analog data analysis is shown in Appendix I where analog waveforms of several data points are compared to digital computational results.

The main advantage of the analog distortion analysis computer is that the entire analog record of any particular data point can be searched, not only for the maximum peak values of any programmed parameter but also for the number of occurrences of other peak values at nearly the same level. The data can be repeated easily with expanded time scales in the regions of the peaks and with different input filter frequencies to determine the changes in the peaks. Several data points can be processed at relatively low cost to determine trends in the dynamic distortion. A total of 63 analog distortion analyses was performed on some 46 data points in support of this study.

During the selection process of the DDAS inlet data, several of the candidate matched data points from the 0.125 scale and the 0.228 scale models were processed through ADA. This was done with input filtering of 500 Hz on the 0.228 scale data and 1000 Hz on the 0.125 scale data to get an early assessment of trends in the dynamic inlet distortion with model scale size as well as to provide additional input for the final selection. The distortion parameters versus time and their steady-state values for 9 points from each scale size are shown in Figures 22 through 30 with approximately 1/2 second of data either side of the maximum peak of the combined parameter, ID. The time axis was scaled by a factor of two (approximately the ratio of the duct diameters), and the parameter scales were kept the same between the two sets of data to provide a consistent presentation of results. An aid to editing the data comes from displaying the waveforms of the various components of the distortion as can be seen in Figures 24a and 27a. In both cases, an obvious noise spike is seen in the radial parameter; in the second case, the spike caused a peak in the combined parameter (ID) that is larger than the actual maximum peak.

An amazing degree of similarity in the distortion parameter waveforms exists between the data from the two scale sizes for most of the points (see Figures 22, 24, 26, 27, 28, and 30). A plot of the dynamic versus steady-state combined distortion parameter, ID, for these data is presented in Figure 31. With the data selected from matched steady-state conditions and treated with simple acoustic scaling, the points group quite well in both scale sizes around the line representing a ratio of dynamic to steady-state ID (RID) of 1.5.

Five of the 0.228 scale data points were reprocessed without acoustic scaling of the data (i.e., input filtering to 1000 Hz as with the 0.125 scale data). The additional energy input to the dynamic distortion calculations is significant, as can be seen in Figure 32, where the maximum peak value of ID is plotted versus the steady-state value for both the 500 Hz and 1000 Hz analyses. The effect of doubling the frequency content in the dynamic inlet distortion is to increase the peaks so that they cluster around a RID = 1.75 line.

Later processing of the selected data points for the full-scale DDAS inlet tests through the ADA was performed to obtain the effects of filtering the input pressure data. The effects on the distortion parameter waveforms are shown in Figures 33 through 36 for the four data points selected. Presented in these figures are the steady-state values of ID and the 50 Hz, 100 Hz, and 200 Hz filtered waveforms for the same region of time that includes the maximum peak in ID from the 100 Hz results. The relative time of the peak can change as more or less energy is included in the data (see circled peaks in Figures 33 and 35). A summary of the ratio of dynamic to steady-state ID levels, RID, and the increment of dynamic above steady-state ID levels, ΔID, for the maximum peak value of ID for the four data points is shown in Figure 37. The dynamic distortion increases at a greater rate between 50 Hz and 200 Hz than between 200 Hz and 400 Hz indicating that the low frequencies contribute to the dynamic distortion more than the higher frequencies.

Not only were several DDAS inlet data points from the three scale sizes processed, but several LSI and comparable 0.228 scale DDAS inlet model points also were processed through the ADA. Mentioned earlier was the fact that comparable conditions were tested on this model during two separate tests with slightly different instrumentation arrangements. For the $M = 1.8$, $\alpha = 10^\circ$ condition, the distortion characteristics versus recovery are shown on Figure 38. The lowest mass-flow-ratio point for the 0.228 scale DDAS inlet and the highest mass-flow-ratio point for the LSI are two of the original 26 data points selected for detailed distortion analysis. The other two 0.228 scale DDAS inlet points with closed symbols were also selected for detailed analysis to provide the effect of changes in mass flow on dynamic distortion.

Prior to detailed analysis, the basis was determined for the differences in the characteristics of the inlet under apparently identical test conditions during two separate tests. As mentioned earlier, the six rakes used in each test were positioned at different angular locations. The LSI has 60° intervals between rakes with the first rake located at 0°, while the 0.228 DDAS inlet has the same intervals but with the first rake located at 22°. These angles increase in a clockwise direction when looking aft.

Better insight into the differences between the tests in the overall distortion results is achieved when the circumferential and radial breakdowns for each of the four data point pairs are plotted together, as in Figure 39 (a data point pair is points from LSI and 0.228 DDAS inlet at approximately the same mass flow ratio). It is quite interesting to note that the

deviation in rake average pressures from the face average pressure for all 12 rake angles (6 from each test plotted on the same scale) define the same circumferential pattern. Apparently, the top ramp on the inlet causes a very localized low pressure zone at 0° over the outer half of the annulus at this high Mach/high angle-of-attack condition. The fact that the LSI rakes were oriented at 0° causes the LSI measurements to result in consistently lower recovery and higher overall distortion levels at the four mass flow ratios tested. This is demonstrated graphically in the radial distributions of the ΔP/PAV and ΔP/PRD. For each of the four point pairs, the LSI has consistently higher circumferential distortion in the outer half of the annulus due to the lower pressure measured at 0° than at 22°. That the inlet is causing the same pressure distribution in both tests, even though it is measured differently in each test, is proven by the similarity of the rake and ring average pressures when plotted together.

As discussed earlier, these data were used to determine if the differences in the steady-state distortion characteristics, between these two tests of the same inlet, carried over to the dynamic distortion. By processing all eight data points through the ADA with 500 Hz input filtering, an assessment of the increment of dynamic values above steady-state values of IDR, IDC, and ID was obtained. As seen in Figure 40, there is one point (0.01) or less difference in the increases in any of these parameters between the two sets of data points until the inlet exceeds critical operating conditions. These results indicate that, for the subcritical points, the dynamic distortion is spread over a larger circumferential region than the steady-state distortion. However, for the supercritical point, the dynamic distortion as well as the steady-state distortion is concentrated near the top center of the annulus. These results demonstrate the need to optimize rake angles to measure the highest values of steady-state distortion for each particular inlet design.

Along with the use of results for preliminary assessment of trends in dynamic distortion, the ADA waveforms were used to select the analog record time period for digital analysis. For all 18 data points selected (16 DDAS and 2 LSI) from the ADA results for detailed distortion analysis in this study, the following rules were applied:

1. The input to the ADA was filtered at about 1/4 the maximum frequency required in later analyses to be sure that the peaks in the distortion parameters were primarily aerodynamic and not electronic in origin.

2. The entire analog record was processed to determine not only relative time of the maximum peak of the parameter of interest, but also times of peaks in other parameters. Also noted were time periods of high activity in the parameters (i.e., several peaks together) when the maximum peak was relatively isolated from other peaks.

3. Up to five seconds of data including these peaks were digitized at sampling rates proportional to model size for each point and generally 4 to 5 times the analog filter frequency (-3 dB point).

Analog filtering of the fluctuating pressure data was applied to all signals such that the 1/2-power point (-3 dB) was roughly equal to 15,000 divided by the duct diameter in inches. A summary of the specific information pertinent to the digitation of these data points and the other selected data points is contained in Table II.

The above rules for digitation of inlet data are based on spectral considerations from the various inlet or inlet/engine data that have been analyzed for this and related programs. These rules are subject to modification when the response time of a particular application has been specifically determined. However, during inlet model development, these response times are usually not known and dynamic data processing criteria need not be arbitrary.

3. DIGITAL DATA ANALYSIS

The final step in the detailed dynamic inlet distortion analysis was to process the digitized data from the 26 selected points through the General Electric Dynamic Distortion Analysis Program (DDAP). This processing included the computation for each time slice of data, all the "Method D" distortion parameters, as well as the maximum and average gross distortion parameter levels. Other computations that could be performed were a complete DAP output for the time slice of the maximum peak value of the combined distortion parameter ID and plotting of the waveforms of selected parameters over the time period of the analysis.

After the initial digital analysis is performed on the data, one time slice at a time, the question of the effects of reducing the band width of the data always arises. To eliminate the cost and complication of redigitizing the data with different analog filters, digital filters are employed. The simplest of these is the running average. There has been some confusion in the terminology between the frequency corresponding to the averaging time in this type filter and the cutoff or corner frequency of an equivalent analog filter.

We have undertaken to compute the filter characteristics of a digital running average. The formula for the nonrecursive digital filter is:

$$y_i = \sum_{k=M_1}^{M_2} h_k \, x_{i+k}$$

Reference 2 (page 50)

This formula was used to determine the frequency response function of a running average. If M is the number of samples averaged together and the advance rate is one sample between averages, the formula becomes:

$$y_i = \frac{1}{M} \sum_{k=0}^{M-1} x_{i+k}$$

where x_{i+k} are the digital samples averaged together and y_i is the resultant "filtered" sample. The transfer function of the "filter" can be written:

$$H(f) = \frac{1}{M}\sum_{k=0}^{M-1}\left[\cos(2\pi\Delta tkf - j\sin(2\pi\Delta tkf)\right]$$

where Δt is the sample interval and f is the frequency of interest. The modulus is given by:

$$\left|H(f)\right| = \frac{1}{M}\left\{\left[\sum_{k=0}^{M-1}\cos(2\pi\Delta tkf)\right]^2 + \left[\sum_{k=0}^{M-1}\sin(2\pi\Delta tkf)\right]^2\right\}^{\frac{1}{2}}$$

and the phase angle is:

$$\Phi(f) = \tan^{-1}\left\{\left[\sum_{k=0}^{M-1}\sin(2\pi\Delta tkf)\right]\Big/\left[\sum\cos(2\pi\Delta tkf)\right]\right\}$$

A plot of the amplitude and phase for a typical running average is shown in Figure 41. The equivalent analog filter characteristics that most closely match those of the running average are shown in Figure 42.

Several sampling rates and average times were computed to determine the relationship between average time and cutoff frequency. The values of the -3 dB point for these average times are plotted in Figure 43. A straight line was drawn through the data to derive a functional relationship which is closely approximated by the equation:

$$f(-3\ dB) = 0.45/AT$$

where AT is the average time in seconds and f(-3 dB) is the cutoff or corner frequency.

To further demonstrate the equivalence of analog filtering and digital averaging, sample inlet data points have been processed both ways. Two 0.228 DDAS inlet model data points and two full-scale axisymmetric inlet/engine data points were analyzed. A summary of the data setup in these four cases is given in Table III. The comparisons between the calculations of the distortion index, by analog filtering at a low frequency prior to digitizing and by averaging the data that have been digitized with higher frequency filters, are shown in Figures 44, 45, 46, and 47.

Very little difference is seen between the waveforms, particularly at the peak values. We note that the maximum value of the index occurred at two different times in one of the cases, although not at significantly

different levels. These results show with actual data that analog filtering of the data prior to digitizing is equivalent to averaging the data after digitizing provided the relationship in Figure 43 is used.

To process the digital data from the various sources, a parameter was necessary that provided a consistent method for selecting averaging time. The data frequency content, digitation sampling rate, and inlet duct diameter for the sets of data are quite varied in that the various full-scale references are quite different. A parameter was derived from both steady-state and time variant considerations that put these sets of data into a common framework for analysis.

Consider first any pure sinusoidal circumferential distortion at the measurement plane (see Figure 48). Note that each of these classic per rev distortion patterns can be classified with a wave number value, λ. If these were standing waves in an acoustic medium, they would each have a frequency, $f = \lambda c/2\pi r$, where r is the radius and c is the speed of sound. Now let the time variant data be averaged such that waves greater than λ are "filtered" out. The effective filter frequency is related to the average time by the formula from the previous section. Substituting the average time expression into the above and solving for the wave number gives

$$\lambda = (\pi R/AT) \times 10^{-3}$$

where the radius has been set at the outer wall and the speed of sound has been set at 900 fps for convenience. The wave number then becomes an averaging time parameter in that the values of AT are proportional to the duct radius; and, for integer values of λ, the data are averaged (filtered) to the frequency corresponding to an n/rev standing wave circumferential distortion.

All data points were processed at four values of λ. The number of samples averaged for the various digitation rates and duct diameters were chosen so that the average times would produce values of λ of approximately 0.5, 1.0, 2.0, and 5.0. A reasonable spread in the average time was desired and four values were selected to better define the trends in dynamic inlet distortion. A complete list of the average times and equivalent analog filter cutoff frequencies for the four values of λ is given in Table IV for all the data sources. The record length processed for each data point is also given. In most cases, the data were processed for two separate time periods of the record length listed in Table IV. Both of these time periods occurred within the five seconds of digitized data. Based on the available ADA results or a search by digital methods of the five seconds of digital data, the two time periods were chosen to include the maximum peak values of at least ID, IDC, and $\Delta P/PMX$, if not all the distortion parameters.

SECTION V

CHARACTERISTICS OF DYNAMIC DISTORTION

1. PARAMETER CHOICE EFFECTS

In realizing the goal of assessing trends in dynamic inlet distortion relative to steady-state distortion levels, one of the objectives was to determine the differences in the results using gross distortion level measurements compared with those using "Method D" parameters. Comparisons were made between the relative changes in the gross distortion parameters $\Delta P/PMX$ and $\Delta P/PFA$ and the changes in the distortion parameters IDC, IDR, and ID, to determine if these changes were consistent when fluctuating pressures were considered along with steady-state pressures.

Of course, both the frequency content of fluctuating pressures and the model size will also influence the results. That is, dynamic distortion data including fluctuations up to 500 Hz in a full-scale inlet and up to 500 Hz in a 0.25 scale model of that inlet will undoubtedly exhibit different trends relative to their respective steady-state distortion levels. Also, the same data considered to 125 Hz in both scale sizes will potentially have different trends than the 500 Hz results.

Under the assumption that acoustic scaling of the fluctuating pressures between scale sizes is adequate, the averaging time parameter (λ) also can be used as a similarity parameter for data scaling. Considering the data from the three sizes of the DDAS inlet at a constant value of λ should enable assessment of trends in the various distortion parameters independent of model size for that particular frequency content of fluctuating pressure. To be consistent in frequency content with the ADA results, the results for the five distortion parameters presented are for the $\lambda \approx 1.0$ average time (see Table IV).

The dynamic distortion at $\lambda \approx 1.0$ versus the steady-state distortion for the five point sets selected from the DDAS inlet data are shown in Figures 49 through 53. In each figure are plotted the maximum peak values for each of the five distortion parameters that occurred within the record lengths processed for each of the three model sizes.

The constant ratio lines are drawn on each figure through the data point with the lowest ratio of dynamic to steady-state values for each parameter and serve as a handy reference. The results are quite consistent between the gross distortion parameters and the combined distortion parameter for this value of λ. The distortion component parameters, IDC and IDR, are not quite as consistent. However, they are useful for obtaining an indication of the nature of the dynamic distortion. Large increases in either component parameter indicate that the instantaneous distortion pattern has increased more in that component than in the other.

The assumption of acoustic scaling appears valid for these data. The gross distortion parameters and the combined distortion parameter measured in either scale model had the same increase as the full-scale for the supersonic data. The 0.125 scale model had significantly more dynamic distortion in these three parameters than either the 0.228 scale model or full-scale inlet in both subsonic cases.

Now that initial trends in the dynamic inlet distortion for the DDAS inlet and confidence in the use of λ as a similarity parameter have been established, the other inlet data that have been analyzed will be compared. The first set of supplemental data of interest is from the LSI (Figure 54).

As seen in the preliminary analog analysis of the LSI data, the dynamic distortion is not as severe in comparison to the steady-state distortion as the 0.228 scale DDAS inlet data (see Figures 49 and 50). The ratios are slightly smaller due to the fact that the steady-state distortion levels measured in the LSI were higher than in the 0.228 DDAS inlet model. As with the DDAS inlet data, the gross distortion parameters and the combined distortion parameter have the same trend in the ratio of the dynamic to steady-state distortion.

The next set of supplemental data is from tests of the 0.21 scale model and full-scale inlet simulator. Since the model was of nearly the same diameter as the LSI and the 0.228 scale DDAS inlet, the data from these three models can be compared directly without concern for scaling. Also, the validity of the similarity parameter, λ, can be tested when the model data are compared with the full-scale data. The maximum peak values of the five parameters for $\lambda \approx 1$ are plotted versus the steady-state values for the two data point sets in Figures 55 and 56.

In these data a consistency exists between ratios of the gross distortion parameters and the combined distortion parameter for the low recovery point only. Two other very significant features for these data are noted. The first is that use of the similarity parameter consistently provides the same ratio of dynamic to steady-state distortion in both sizes for both point sets, at least in the combined distortion parameter, ID, if not in the gross distortion parameters.

The second and most important point is that for $\lambda \approx 1.0$ the ratio of dynamic to steady-state distortion, seen in Figures 55 and 56, is much higher in the inlet simulator than in the inlet data seen in Figures 49 through 54. Bear in mind, however, that the inlet being simulated when these data (Figures 55 and 56) were generated was not either the LSI or DDAS inlet even though both the inlet simulator and DDAS inlet had about the same steady-state values for the distortion parameters. The total data spectrum discussed thus far shows that for $\lambda \approx 1.0$ the potential increase in dynamic distortion over the steady-state values can range from RID = 1.3 to RID = 2.0.

The remaining two sets of supplemental data are from mixed-compression inlets and are characterized by higher steady-state values for the various distortion parameters. The two-dimensional inlet has a duct diameter close

to that of the 0.125 scale DDAS inlet and can be compared directly without scaling. Data from that model for a subsonic maneuver and a supersonic cruise point are shown in Figure 57 with the maximum peak value of the five parameters plotted versus their respective steady-state values.

There is little consistency between the gross distortion parameter, $\Delta P/PMX$, and combined distortion parameter, ID, with respect to the ratio of dynamic to steady-state values. However, the gross distortion parameter, $\Delta P/PFA$, compares well with the combined distortion parameter, ID. The ratio of dynamic to steady-state values of $\Delta P/PMX$ is higher for the subsonic point and lower for the supersonic point than the similar ratio of ID. In the previous discussion a large range in RID for two separate configurations was noted, and now a range of RID = 1.4 to RID = 1.7 is seen here for the same inlet.

The last two supplemental data points are from the axisymmetric mixed-compression inlet/engine test at M = 2.5. Both the 0° and 5° angle-of-attack points have similar steady-state distortion levels to the two-dimensional mixed-compression inlet. The dynamic versus steady-state distortion values for both points are shown in Figure 58.

The gross distortion parameter, $\Delta P/PFA$, and the combined distortion parameter, ID, have the same ratio of dynamic to steady-state values for the $\alpha = 5°$ condition, but not for the $\alpha = 0°$ condition. As previously noted, the steady-state distortion patterns are predominately radial for the $\alpha = 0°$ point and circumferential for the $\alpha = 5°$ point. However, when the dynamic distortion is computed, the increase in radial components for both conditions has the same ratio to the steady-state value, but the circumferential component increases much more dramatically at $\alpha = 0°$ than at $\alpha = 5°$. This increase in circumferential component at $\alpha = 0°$ causes the combined distortion parameter, ID, to double; while at $\alpha = 5°$, the RID is of the same order as the two-dimensional mixed-compression inlet. Here again in one inlet a ratio of dynamic to steady-state distortion ranging from RID = 1.5 to RID = 2.0 is possible.

Data for 24 points from several inlets have been presented for a $\lambda \approx 1$ scaled average time. The ratio of dynamic to steady-state distortion as measured by the combined distortion parameter, ID, has ranged from RID = 1.3 to RID = 2.0. Scaling of the data between all the inlet sizes has been accomplished by use of the similarity parameter, λ. There is consistency between the ratio of dynamic to steady-state values of the gross distortion parameter, $\Delta P/PFA$, and the combined distortion parameter, ID. This is due in part to the fact that ID is an average minus minimum parameter. It remains to be seen if changes in the average times significantly affect any of these preliminary findings.

2. ANALYSIS AVERAGE TIME EFFECTS

As previously mentioned, all the data points selected for detailed distortion analysis were processed through the DDAP at four average times

corresponding to values of $\lambda \approx 0.5$, 1.0, 2.0, and 5.0 (see Table IV). To continue the study of trends in the dynamic inlet distortion as measured by gross distortion parameters and "Method D" parameters, the average time results are presented in terms of the increments of the dynamic above the steady-state values for each of the five parameters. The first set of data presented is from the three sizes of the DDAS inlet.

The average time effects on the increments of the dynamic above the steady-state values of the five parameters are shown in Figures 59 through 63. As the average time is decreased (λ and frequency content increase), there is considerably less consistency between scale sizes when the results are plotted in terms of the gross distortion parameters, $\Delta P/PMX$ and $\Delta P/PFA$, than in terms of the combined distortion parameter, ID. This is particularly true for the 0.228 scale data. This effect is caused in part by the frequency response limitations of the instrumentation and data processing systems rather than anything aerodynamic. Spurious noise from electronic sources or instrumentation resonances tend to input spikes into the fluctuating pressure signals. Since both $\Delta P/PMX$ and $\Delta P/PFA$ are dependent on single probes, these "electronic" sources can cause wide variations in these parameters when higher frequency content is included in the data.

Two significant trends in these data should be noted. The similarity parameter, λ, and the combined distortion parameter, ID, adequately describe the trends in the dynamic inlet distortion relative to both the steady-state distortion levels and to model size. The 0.228 scale and full-scale data exhibit the same trend in the ΔID in all five data point sets. In all but two of the five cases, the 0.125 scale and full-scale data also compare well. These comparisons also exist for $\Delta(\Delta P/PMX)$ and $\Delta(\Delta P/PFA)$ at values of λ less than or equal to 1.0.

The second important trend is the rate of change of ID over the range of λ used in the analysis. In all three model sizes, the increase in increment of ID between $\lambda = 0.5$ and $\lambda = 2.0$ is nearly double the increase between $\lambda = 2.0$ and $\lambda = 5.0$.

This "filtering" effect is due to the natural distribution of fluctuating pressure energy over the frequency spectrum for these types of inlets. The spectra shown in Figures 19 - 21 for the DDAS inlet are characterized by a triangular shape with the spectral density level one decade lower at frequencies corresponding to $\lambda \approx 5$ than at the low frequency limit. Previous work (Reference 3) with inlet fluctuating pressures that exhibit similar spectral shapes has shown that 95% of the available energy was contained in this low frequency bandwidth. That is, all the energy above the "one decade down point" only contributes 5% more to the integrated RMS levels. With this rough description of how the spectral shape of the fluctuating pressure data affects the energy levels with various filter bandwidths or average times, it is plain to see how the rate of change of the increment of dynamic distortion over steady-state distortion changes rapidly with decreasing values of λ below $\lambda \approx 2$.

A plot of the increments in the five distortion parameters over the same range of average times for the LSI (Figure 64) shows the same general trends as the DDAS inlet. That is, the shape of the distortion parameter curves with λ are consistent between the LSI and the DDAS inlet data. There is, however, an apparent inconsistency in the LSI data that deserves explanation.

With few exceptions the DDAS inlet data exhibited the same trends in both the ratio and increment of dynamic distortion over steady-state distortion relatively independent of flight conditions. The LSI data in Figure 54 have the same trends in the ratio of dynamic to steady-state distortion parameters as the DDAS inlet. However, the increment of dynamic distortion over steady-state distortion, while having the same shape with average time, is appreciably greater at 10° than at 1.5° angle of attack. The primary reason for these apparent inconsistencies is that at $M = 1.8$ at both angles of attack, the DDAS inlet data were selected at matched conditions with nearly constant corrected flow while the LSI data were selected at conditions of nearly constant mass flow. This resulted in a much higher corrected flow for the LSI data at a 10° angle of attack than at a 1.5° angle of attack.

While on the subject of flow effects, it is worthwhile to compare the dynamic distortion at the three flows for the 0.228 scale DDAS inlet data shown with the closed symbols in Figure 38. Detailed distortion analysis was performed on these three data points to determine if trends in the dynamic distortion established at matched flow conditions changed significantly at increased inlet operating flows.

In this case at $M = 1.8$, $\alpha = 10°$, the lower flow point (1) was one of the points used to compare with the full-scale and the 0.125 scale models. Also note that this is a subcritical operating point. The next higher flow point (3) has the same steady-state recovery and distortion characteristics and is also a subcritical point. The highest flow point (4) is "around the corner" such that the inlet is operating supercritical and, as a result, has lower recovery and higher distortion levels than both points 1 and 3. With this background, the maximum peak values of the five distortion parameters for a $\lambda \approx 1.0$ average time versus their respective steady-state values are presented for these three data points in Figure 65.

The trends in the dynamic distortion levels for both points 1 and 3 are virtually the same in all five parameters and consistent with the other DDAS inlet data. However, the ratio of dynamic to steady-state distortion for point 4 is higher than points 1 and 3 in the gross distortion parameters as well as in the combined distortion parameter. These effects of corrected flow change are even more pronounced when presented in terms of increments in the dynamic distortion levels above the steady-state distortion levels as functions of average time parameter.

The increased corrected flow between points 1 and 3 causes a slight increase in the increments in all the parameters versus λ as shown in Figure 66. A much larger increase in the increments occurs when the inlet goes

supercritical as a result of the mass flow change than when it remains subcritical. Therefore, the effect on dynamic distortion due to corrected flow change can be large. This effect depends more upon whether the inlet goes supercritical than upon the amount of flow change. This stands to reason, since the shock system for the external compression inlet is taken inside, and potentially will produce larger pressure fluctuation amplitudes due to its increased strength. Further, the diffuser is "effectively" shortened, thus decreasing the length available for attentuation.

The trend of increased dynamic distortion levels relative to steady-state levels during supercritical operation may explain why the inlet simulator has such high ratios of dynamic distortion to steady-state distortion compared to the DDAS inlet data. The inlet simulator is deliberately run supercritical to generate shock-induced pressure fluctuations without benefit of an external compression process. Data already presented (Figures 55 and 56) show that the ratio of dynamic to steady-state values of ID for all four points from the model and full-scale inlet simulator was no less than 2.0 while the same ratio for most of the DDAS inlet data was as little as 1.3. This trend of higher values for the simulator than for the inlet is seen in the increment of dynamic distortion levels above steady-state distortion levels plotted versus the average time parameter (Figures 67 and 68).

The inlet simulator data are consistent between the two sizes for all values of λ only in the combined distortion parameter, ID. This is further substantiation that the similarity parameter, λ, and the combined distortion parameter, ID, are sufficient to describe the trends in dynamic distortion relative to both the steady-state distortion levels and to model size. Even though the dynamic distortion levels are higher for the inlet simulator data than for the DDAS inlet data, the use of λ and ID will scale the distortion data. This was true for both sets of data when points with matched steady-state distortion levels and patterns were selected from tests with similar aerodynamic and geometric conditions between the model sizes.

Additional full-scale DDAS inlet data points were processed on the analog distortion analyzer (ADA) to establish the effect of supercritical operation on the intensity of dynamic distortion. Full-scale data were selected for this portion of the study to rule out model size effects and to demonstrate the significance of the dynamic distortion in the actual inlet/engine environment. Three consecutive data points were chosen that were taken by increasing the secondary flow while at constant engine flow from two separate flights but at nearly the same conditions. The data were at $M = 1.8$ cruise and have similar recovery characteristics to the data shown in Figure 3.

The ratio of dynamic to steady-state ID values for $\lambda \approx 1.0$ are presented in Figure 69 versus a recovery loss parameter $(1-\eta)$. This presentation was chosen to show the strong dependency on one-dimensional duct aerodynamics exhibited by the dynamic distortion. Shown for reference in Figure 69 are the full-scale inlet simulator data from Figures 55 and 56.

It should be noted that the intensity of the dynamic distortion covers the range of RID $\approx$ 1.3 to RID $\approx$ 2.0 for the model scale data as well as for the full-scale data (see Figures 49-56). These data points had all geometric and aerodynamic conditions matched except Reynold's number, which was as much as a factor of 8 different (between 0.125 scale and full-scale DDAS inlet data). However, no significant difficulty in scaling the data was noted for the two different configurations (DDAS inlet and SIM) analyzed. These trends seem to indicate that the dynamic distortion is much more dependent upon the duct internal aerodynamics than the external aerodynamics of the inlets. This may not be true, however, if smaller models or lower Reynold's numbers were tested.

The trends in the increments for the five distortion parameters measured on the mixed compression inlets are shown in Figures 70 and 71. Even though the ratio of dynamic to steady-state distortion for both of these inlets was in the same range as the external compression inlet data at $\lambda \approx 1.0$, the increments in the parameters will be higher due to the 25% to 50% higher steady-state distortion levels in the mixed compression inlet data. Therefore, a change in scales was necessary for the presentation of changes in increments of the five distortion parameters as a function of average time.

The two-dimensional mixed-compression inlet data average time effects are shown in Figure 70, and the results for the axisymmetric mixed-compression inlet/engine data are shown in Figure 71. Both sets of data show similar effects with average time in the increment of the dynamic above the steady-state level of ID. This trend is the same in nature as the external compression inlets but has a significantly different shape. That is, the increment in ID goes through a much larger change between values of $\lambda = 0.5$ and $\lambda = 2.0$ for matched operating conditions in the mixed-compression inlet than in the external-compression inlet. This is probably a reflection of the fact that the distortion levels are 25% to 50% higher in the mixed-compression inlet data.

From all appearances in the data, the small scale two-dimensional mixed-compression inlet is operating supercritical for the subsonic maneuver condition. This observation is based upon the fact that the data point is located on the vertical part of the recovery/mass flow ratio curve (Figure 16) and that the changes in the increment of dynamic above steady-state distortion levels with average time are similar to those in the supersonic data known to be from supercritical conditions.

The incremental changes in the distortion parameters with average time for the axisymmetric mixed-compression inlet also exhibit trends similar to the external-compression inlet under supercritical operating conditions. The primary difference, between the trends in dynamic distortion for the axisymmetric mixed-compression inlet data and the other inlet data analyzed, is the significantly higher levels in the incremental changes in the distortion parameters. This is due, in part, to the nature of the flow through an axisymmetric inlet. For a 0° angle of attack, the steady-state distortion is dominated by radial distortion and for a 5° angle of attack, the primary distortion is circumferential, as discussed earlier (Figure 18).

However, when dynamic distortion is considered, even at a relatively low frequency ($\lambda \approx 1.0$), the nature of the distortion changes drastically. We saw earlier that for $\lambda \approx 1.0$, the increase in the radial component of dynamic distortion over its steady-state levels was similar for both angle-of-attack conditions (Figure 58). However, for the same average times, the circumferential distortion increased by a factor of 13 at a 0° angle of attack while it increased by a factor of only 1.7 at a 5° angle of attack. The inability of the distortion to maintain similar ratios of circumferential-to-radial components in the dynamic distortion as in the steady-state distortion can cause a considerable change in the dynamic distortion data trends for an axisymmetric inlet as compared to a two-dimensional inlet.

The most consistent parameter for presentation of the effects of average time on dynamic inlet distortion has been the combined distortion parameter, ID. The average time has been consistently treated by including it in the similarity parameter, λ, so that the data from the various inlet sizes can be scaled. The results of average time effects on the data are summarized below.

- For a value of $\lambda \approx 1.0$ (equivalent to 4 millisecond average time and 111 Hz analog filtering on the full-scale DDAS inlet data), the ratio of dynamic to steady-state values of ID was 1.3 to 1.5 for normal operating conditions for all the inlets selected. The value increases to as much as 2.2 when the inlets are operated supercritical.

- For values of $\lambda = 0.5$ to $\lambda = 2.0$, the increment in ID between the dynamic distortion and the steady-state distortion increases from values of 0.01 to 0.02 to values of 0.03 to 0.04 for the DDAS inlet under normal operating conditions. The increment in ID for these data was only another 0.01 for the range of $\lambda = 2.0$ to $\lambda = 5.0$. For supercritical operation of the DDAS inlet and the inlet simulator, the increment in ID can increase from 0.04 to 0.07 over the range of $\lambda = 0.5$ to $\lambda = 2.0$.

- For values of $\lambda = 0.5$ to $\lambda = 2.0$, the increment in ID for supersonic operation of both mixed-compression inlets, increases from 0.06 to 0.11 under normal operating conditions. The axisymmetric inlet at $\alpha = 0°$ increased the increment in ID from 0.10 to 0.17 over this range of λ.

3. PARAMETER COMBINATION EFFECTS

During the development of the General Electric "Method D" distortion methodology, a high degree of flexibility in computation of the distortion parameter, ID, was implemented. The primary objective of this was to develop a methodology that not only standardized distortion measurements in inlets, but also included engine sensitivity effects. That is, if an engine was predominately sensitive to circumferential distortion but not sensitive to radial distortion, the components of ID could be weighted by appropriate factors. Therefore, as shown in Appendix II, the "Method D" distortion methodology has several functions and factors that can be used to weight various components of the distortion.

Another objective of the current study was to establish if varying the way in which these weighting or sensitivity factors are used to compute ID has significant effects on the trends in dynamic distortion relative to steady-state distortion. Of course, there is an infinity of variations, but the first and simplest thing is to consider only the circumferential component of distortion. That is, assume that the radial sensitivity is zero. The results of these assumptions are seen by comparing the IDC plots to the ID plots in Figures 49 through 71.

If the radial sensitivity factor were zero, the ratio of dynamic to steady-state values of IDC follow the trends in ID, but with higher values. At $\lambda \approx 1.0$ the range in ratios of dynamic to steady-state IDC are 1.5 to 1.7 for normal operation and 2.5 to 3.5 for supercritical operation. The effect on the dynamic increment of IDC above the steady-state value of varying average time is more consistent with the trends in ID. For all the data points, the increment in IDC at each value of λ is virtually the same as the increment in ID. This implies that the greatest contribution to dynamic distortion as measured by the combined distortion parameter, ID, comes from increases in the circumferential component. This was pointed out earlier to be very dramatic in the case of the axisymmetric mixed-compression inlet at $\alpha = 0°$.

The real test of the dynamic distortion parameter variations with average time was performed with both sets of the mixed-compression inlet data. A set of sensitivity factors which depend on flight conditions that had been derived for each applicable engine were used in computing values of ID for the dynamic distortion data (see Appendix II). The same values of λ were used with the Phase I ID as with the Phase 0 ID results shown in Figures 70 and 71.

The incremental increase in ID from steady-state to dynamic levels for each value of λ were normalized by the increment at $\lambda \approx 1.0$ (ΔID_B). This produced the results shown in Figures 71 and 72 that compare average time effects on ID as computed for the same data with two quite different formulations of the combined distortion parameter. Significantly, there is little difference in the trends in ID, whether Phase 0 or Phase I, as average time is varied. There is, however, considerable difference in the value of the increment itself due to the different weighting factors used in the computation of the respective ID values.

In summary, the trends in dynamic inlet distortion relative to steady-state distortion values and model size are not significantly altered by use of different formuli for ID. However, it is not possible with the small sampling of data analyzed for this study to predict the absolute dynamic levels of any other formulation of ID than Phase 0.

SECTION VI

CONCLUSIONS

Several significant conclusions pertinent to the trends in dynamic inlet distortion have resulted from detailed analyses of unsteady pressure data selected from various scale model inlet and full-scale inlet/engine tests.

The conclusions from this study have to do primarily with the trends in dynamic inlet distortion data. However, conclusions concerning the adequacy of the test data from the various sources and the analysis methods and parameters utilized in this study are important and, thus, are also presented.

1. ADEQUACY OF CURRENT DATA

- Scalable dynamic inlet distortion data can be recovered from the three scale size tests of the DDAS inlet.
  - Similar geometric and aerodynamic conditions were tested.
  - Reynold's number not matched but effects seen to be small.
  - Very few of the 30 probes provided bad data.
  - Frequency response was sufficient to define dynamic distortion.
  - "Standard" methods of recording dynamic data were used.
  - Recovery and calibration instructions for dynamic data were available.
- Consistent dynamic inlet distortion results were obtained from other available inlet test data.
  - Model and full-scale inlet simulator data confirmed scaling.
  - Thirty or more probes were used in each test.
  - Other supercritical data confirmed increased corrected flow effects.
  - Rake orientation was seen to affect steady-state data.

2. ANALYSIS METHODS AND PARAMETERS

- Analog distortion computers can be invaluable in the analysis of dynamic inlet distortion.
  - Low cost computation of distortion parameters for entire data record.

- High visibility dynamic data editing is a fringe benefit.
- Preliminary data trends are readily available.
- Data are easily reprocessed for filtering effects.
- Time region for detailed digital analysis is readily identified.

■ Analog filtering can be made equivalent to digital averaging.

- Frequency response of five-pole linear phase filter matches averaging.
- Analog filter -3 dB point is 0.45 times reciprocal of average time.

■ "Method D" combined distortion parameter showed consistent trends for all inlet sizes and average times evaluated. The gross distortion parameters did not show nearly so consistent trends.

- Noise spikes affect single probe parameter at short average times.
- Dynamic to steady-state ratios generally agree for similar conditions.

■ A new similarity parameter (λ) was developed that provides a basis for use of consistent average times for various inlet sizes.

- Acoustic scaling is applicable for dynamic distortion.
- Wave theory concepts can be used to relate duct radius to average times.
- Dynamic inlet distortion is scalable with use of λ.
- Consistent trends from different inlets result when λ is used.

3. DYNAMIC DISTORTION SEVERITY

■ For DDAS inlet normal operating conditions, the results indicated that the ratio of dynamic to steady-state distortion using Method D parameters is 1.3 to 1.4.

- These results are for $\lambda \approx 1.0$ and Phase 0 Method D.
- All three scale sizes yield the same range of 1.3 to 1.4.
- Both supersonic and subsonic conditions produce this result.
- Both cruise and maneuver conditions produce this result.

- For normal operating conditions with mixed-compression inlets the ratio of dynamic to steady-state distortion is 1.4 to 1.5.
  - These results are for $\lambda \approx 1.0$ and Phase O Method D.
  - Both a two-dimensional and an axisymmetric inlet were examined.
  - Subsonic and supersonic maneuver conditions were included.
- For supercritical operation of the DDAS inlet, inlet simulators, and mixed-compression inlets, the results indicated that the ratio of dynamic to steady-state distortion using Method D parameters is 1.5 to 2.4.
  - These results are for $\lambda \approx 1.0$ and Phase O Method D.
  - Both supersonic and subsonic conditions produce this result.
  - These results include the well-known increase in steady-state distortion.
  - These results show stronger dependency on duct Mach number than Reynold's number.
- For changes in average time from $\lambda \approx 0.5$ to $\lambda \approx 2.0$, the data indicated that the increment of dynamic over steady-state values of the Method D parameters can double.
  - This is consistent with the nature of fluctuating pressure energy.
  - The full-scale DDAS and small scale 2DMC results show this trend.
  - All other data analyzed, except $\alpha = 0°$ ASMC, increased at least 50%.

4. SCALING DYNAMIC DISTORTION

- Dynamic inlet distortion from three different size DDAS inlet models and two different size inlet simulators was the same when scaled using the similarity parameter, λ, and the Phase O Method D parameters and:
  - Geometric and aerodynamic conditions were closely matched.
  - Recovery and mass flow were similar.
  - Instrumentation quantity and location were similar.
  - The product of frequency band and radius was similar.

- Ratios of dynamic to steady-state distortion from different inlets of various sizes were in the same range.
  - Different ranges result from normal and supercritical conditions.
  - Phase O Method D was used for the ratios given.
  - The similarity parameter, λ, was used for average time.
  - Digitation rates and filters were consistent with λ.

5. ESTIMATING DYNAMIC DISTORTION

- Model scale dynamic data can be used to estimate full-scale dynamic inlet distortion levels for assessment of inlet development progress.
  - Select the value of λ for the full-scale application.
  - Compute the model scale average time.
  - Compute the analog filter frequency, f.
  - Digitize the data at a rate of three to five times f.
- Model scale steady-state data can be used in the absence of adequate dynamic distortion data to approximate full-scale dynamic inlet distortion very early in the inlet development program.
  - Multiply the steady-state Method D Phase O parameters by 1.5.
  - If supercritical, multiply the steady-state parameters by 2.0.

The above conclusions and rules of thumb are based on trends established in this study and are subject to change as more data are subsequently analyzed and reported.

SECTION VII

RECOMMENDATIONS

Based on this study of dynamic inlet distortion, there are several recommendations. Some of these have to do with additional analysis using current data. The remainder have to do with the acquisition of dynamic data from future inlet model tests.

1. FURTHER ANALYSIS USING CURRENT DATA

- The full-scale DDAS and model scale DDAS inlet data should be further analyzed to more clearly define effects of Reynold's number and supercritical operation on dynamic distortion levels relative to steady-state distortion levels and to provide a broader base for the scaling hypothesis.

- Dynamic data from other full-scale and model scale tests should be similarly analyzed to further substantiate, expand, and/or modify the results of this study.

- Additional analysis using the techniques and parameters developed here should be undertaken to establish the degree of improvement realized in estimating dynamic inlet distortion from steady-state model data with the addition of a limited number of dynamic probes.

2. CONSISTENT FUTURE DATA

- The similarity parameter, λ, and the Method D Phase O distortion parameters should be employed in the analysis of scale model test data for estimation of full-scale dynamic inlet distortion.

- The analog techniques used in this study should be employed to ensure that high quality taped data with the maximum values of distortion are selected for analysis. Comparable rules for equivalency of analog filtering and digital averaging should be developed if different equipment/techniques are used.

- Equivalent digital methods including the developed rules for digitation should be employed in future analysis of dynamic inlet distortion to ensure consistent results between the various sources of data.

- Reference to dynamic inlet distortion results should be made in terms of measurement plane diameter. Diameters of 3.8 to 4.0 inches or larger should be used within reasonable blockage limits to more closely simulate full-scale Reynold's numbers. A benefit from these criteria could be standard diameters to facilitate multiple test usage of the very costly dynamic probe/rake hardware.

- Analog distortion computers used on-line during inlet model testing can help to assure the quality of the dynamic data, to determine preliminary trends in the dynamic distortion, and to optimize the inlet test data in terms of operating conditions.

- Standard procedures for data acquisition, logging, and documentation should be employed during all inlet model tests to facilitate exchange of data for dynamic distortion analysis.

APPENDIX I

STABILITY MEASUREMENTS ANALYSIS LABORATORY

Inlet/engine interface plane time dependent pressure distortion data are processed in the General Electric Stability Measurements Analysis Laboratory (SMAL) shown in Figure 74. The FM multiplexed signals recorded from the pressure transducers at the distortion measurement plane are recovered from the analog tapes in the SMAL. By using the tape speed reduction technique, the actual frequency content in the data can be reduced up to 16 times to facilitate data analysis.

The 30 signals from the DDAS inlet data were demodulated with the discriminators, AC coupled, and then sent through variable band-width low-pass filters (not shown) to the analog distortion analyzer (ADA). The steady-state pressures were summed with these signals, and the resultant absolute pressures versus time were processed through the Phase 0 "Method D" ADA program shown in block diagram form in Figure 75. The "Method D" parameters along with time code information were presented on the chart recorder for the entire recorded record. The data were filtered for each scale size at the $\lambda \approx 1$ frequency for peak determination. The region of the peak was then reprocessed with expanded time scales and with different input filter frequencies.

To check out the ADA computation of the "Method D" parameters, two of the axisymmetric mixed-compression inlet data points were processed. The 30-probe data had previously been digitized and processed at a $\lambda \approx 1$ average time so the CALCOMP waveforms were available for comparison. The analog waveforms for IDR, IDC, and ID from the ADA are shown with reduced size versions of the DDAP waveforms in Figures 76 and 77. The two points were selected to emphasize the accuracy in computation of both the radial and circumferential distortion components.

Setup and calibration for a given set of data is the most time consuming part of ADA operation in the SMAL. After a one- to two-hour setup period for each data tape, the data points can be processed at a rate of 15 minutes each. Depending upon whether the points to be processed are on the same tape, or (in the case of the three scale sizes of the DDAS inlet) on separate tapes, ADA processing time can be 15 minutes to 2 hours per point.

APPENDIX II

GENERAL ELECTRIC "METHOD D" DISTORTION METHODOLOGY

The General Electric Distortion Methodology, "Method D," was developed to provide a more general way to translate inlet/engine flow field distortion into descriptive indices for assessment of engine tolerance to that distortion. This methodology is based on extensive empirical analysis of engine and compression component distortion test data (Reference 4). The basic element used to describe the flow field distortion is the spatial total-pressure distribution for both steady-state and time-dependent data. The pressure distribution is separated by the methodology into circumferential and radial components at both the inner and outer regions of the flow. These components are then weighted by sensitivity factors and summed together with a superposition factor to obtain the combined distortion index.

The index, ID, is based on five radial elements or rings in centers of equal areas and is determined from the following:

$$ID = B \times K_c \times IDC + K_R \times IDR$$

$$IDC = \text{Larger of } (IDC_H,\ IDC_T)$$

$$IDR = \text{Larger of } (K_H \times IDR_H/K_R,\ K_T \times IDR_T/K_R)$$

$$IDC_H = (IDC_1 + IDC_2)/2$$

$$IDC_T = (IDC_5 + IDC_4)/2$$

$$IDR_H = \Delta P/PRD_1 + \alpha_H \times \Delta P/PRD_2$$

$$IDR_T = \Delta P/PRD_5 + \alpha_T \times \Delta P/PRD_4$$

$$IDC_r = S_r \times E_r \times M_r \times \Delta P/PAV_r$$

$$\Delta P/PAV_r = (P_{RING\ AV} - P_{RING\ MIN.})_r/P_{FACE\ AV} \qquad r = 1,2,3,4,5$$

$$\Delta P/PRD_r = (P_{FACE\ AV} - P_{RING\ AV})_r/P_{FACE\ AV} \qquad r = 1,2,3,4,5$$

The following terms, factors, and subscripts are used in the above formulations:

Terms

$P_{FACE\ AVG}$ = Face area averaged total pressure

$P_{RING\ AVG}$ = Ring area averaged total pressure

$P_{RING\ MIN.}$ = Ring minimum total pressure within largest low pressure area

Factors

B = Superposition factor

K_C = Circumferential stability usage factor

K_R = Radial stability usage factor; which is either K_T for tip or K_H for hub, depending upon IDR selection.

α_H = Hub radial extent factor

α_T = Tip radial extent factor

S = Pattern shape factor

E = Circumferential extent factor

M = Multiple low pressure areas factor

Subscripts

C = Circumferential

R = Radial

H = Hub or inner region

T = Tip or outer region

r = Methodology ring

1 = Ring 1 (centered at 10% area)

2 = Ring 2 (centered at 30% area)

3 = Ring 3 (centered at 50% area)

4 = Ring 4 (centered at 70% area)

5 = Ring 5 (centered at 90% area)

The "Method D" methodology as developed is very flexible and two of its formulations have been used in this study. The simplest formulation or Phase 0 has been used throughout to develop the relationships between dynamic and steady-state distortion. The Phase 0 "Method D" is arrived at by setting the various factors to either 1.0 or 0.0 as follows:

$$S = E = M = B = K_C = K_R = 1.0$$

$$\alpha_H = \alpha_T = 0.0$$

The values of ID are then similar to other widely used distortion parameters.

The other formulation used is referred to in Figures 72 and 73 as Phase I. For the axisymmetric mixed-compression inlet data, a full set of values for all the factors were employed. For the two-dimensional mixed-compression inlet data, a set of B, K_C, and K_R values dependent upon the Mach number and altitude were used with the other factors set to 1.0 or 0.0 as follows:

$$S = E = M = 1.0$$

$$\alpha_H = \alpha_T = 0.0$$

With the appropriate values for K_C, K_R, and B, the values of ID are then indicative of stall-free operation if they are less than 1.0 according to the following definition:

$$ID = \frac{\text{Stability Margin Loss Due to Distortion}}{\text{Stability Margin Available for Distortion}}$$

The steady-state values of the "Method D" parameters and the gross distortion parameters, $\Delta P/PFA$ and $\Delta P/PMX$, are computed by the General Electric Distortion Analysis Program (DAP). The input to this program is the radial and angular location of the probes, radii of the duct walls, pressure values for the probes, and values for the various factors (when Phase 0 is desired the factor values are preset).

The program then produces five pages of output. The first page contains the matrix of input pressures and all the computed "Method D" parameters and indices. For those cases that the probe radii do not lie in centers of equal area regions, the second page has the matrix of pressures interpolated to the five methodology rings and all the computed "Method D" parameters and indices. The third page has a matrix of deviations of the probe pressure from the face average for the input pressures. The fourth page is a spatial pattern of the distortion made by printing the percent local deviation from the face average pressure at 180 elements (10 equal area rings and 18 rays). To provide a further breakdown of the pressure distortion pattern, three profile plots appear on the fifth page. The deviation of the rake average pressures from the face average pressure versus angular location, the deviation of ring average pressures from the face average pressure versus radial location, and the ring circumferential distortion versus radial location are the three plots.

The dynamic or instantaneous values for the various "Method D" parameters and the gross distortion parameters, ΔP/PFA and ΔP/PMX, are computed by the General Electric Dynamic Distortion Analysis Program (DDAP). The input to this program is the same as to the DAP except that the pressures are in the form of digitized values on magnetic tape, one time slice through all the probes at a time. Of course, several other parameters relevant to the time sliced data and digital averaging must also be supplied. Since several output options are available, these parameters values must also be input.

The program computes, for each time slice of data, all the "Method D" parameters and indices for up to 5000 time slices. While passing through the data, the time of the maximum values for ID, IDC, IDR, ΔP/PFA, and ΔP/PMX are stored. A summary of these values and the time of occurrence of the maximum for each parameter is provided as a minimum output.

Optional output is a full DAP printout for the time slice in which the maximum value of ID occurred. Other options are a printed summary of the "Method D" parameters for each time slice, a full DAP printout for each time slice including the patterns, or CALCOMP plots of any selected parameters versus time.

Table I. Selected Data Point Steady-State Parameters.

Source	Dia (inches)	Type	Point	M	α	η	$\Delta P/PMX$	$\Delta P/PAV$	ID
0.125 DDAS	3.795	2DEC	1420.5	1.804	10.2	0.873	0.154	0.064	0.099
			1413.3	1.804	1.5	0.913	0.126	0.077	0.080
			1396.4	1.600	1.5	0.952	0.103	0.072	0.072
			1044.2	0.899	5.1	0.959	0.118	0.075	0.073
			1122.2	0.889	5.1	0.966	0.114	0.080	0.081
0.228 DDAS	6.92	2DEC	123.4	1.785	10.0	0.874	0.145	0.058	0.081
			203.2	1.790	1.5	0.892	0.135	0.072	0.073
			192.2	1.600	1.5	0.944	0.097	0.060	0.064
			598.1	0.899	5.0	0.974	0.091	0.064	0.064
			669.1	0.900	5.0	0.971	0.099	0.069	0.071
1.0 DDAS	30.37	2DEC	2912.20	1.772	11.1	0.868	0.141	0.063	0.071
			816.17	1.817	2.3	0.880	0.126	0.070	0.069
			2815.10	1.589	2.2	0.950	0.101	0.064	0.067
			2014.01	0.956	4.7	0.962	0.094	0.074	0.071
0.228 DDAS	6.92	2DEC	123.1	1.785	10.0	0.858	0.170	0.086	0.101
			123.2	1.785	10.0	0.873	0.162	0.068	0.082
LSI	7.50	2DEC	1113	1.800	1.34	0.925	0.117	0.075	0.077
			1126	1.800	9.83	0.852	0.196	0.114	0.125
ISM	7.50	2D	1089	>1.0	---	0.870	0.116	0.038	0.056
			1012	>1.0	---	0.790	0.126	0.055	0.058
SIM	35.60	2D	260	>1.0	---	0.860	0.101	0.044	0.046
			263	>1.0	---	0.790	0.077	0.036	0.037
0.10 Scale	4.5	2DMC	70.4	2.200	-1.59	0.854	0.192	0.088	0.110
			368.4	0.849	12.07	0.834	0.212	0.117	0.122
Full-Scale	16.2	ASMC	154	2.499	0	0.799	0.197	0.105	0.111
			162	2.580	5.0	0.769	0.357	0.115	0.144

Table II. Digitized Data Points.

Source	Point	-3 dB (Hz)	Rate (sec^{-1})	Time (sec)
0.125 DDAS	1420.5	4000	20,000	4.5
	1413.3	↓	↓	5.0
	1396.4			5.0
	1044.2			5.0
	1122.2			5.0
0.228 DDAS	123.4	2000	10,000	5.0
	203.2	↓	↓	5.0
	192.2			5.0
	669.1			5.0
	598.1			5.0
1.0 DDAS	2912.20	500	2500	2.0
	816.17	↓	↓	5.0
	2815.10			5.0
	2014.01			3.0
0.228 DDAS	123.2	2000	10,000	5.0
	123.1	↓	↓	5.0
LSI	1113	2000	10,000	5.0
	1126	↓	↓	5.0
ISM	1089	2000	10,000	5.0
	1012	↓	↓	6.0
SIM	260	500	2500	5.0
	263	↓	↓	5.0
2DMC	70.4	4000	8000	5.0
	368.4	↓	↓	5.0
ASMC	154	2000	8000	5.5
	162	↓	↓	5.5

Table III. Data Points for Analog Filter Vs. Digital Average.

Source	Point	-3 dB (Hz)	SR	SA	YAT
0.228 DDAS	123.2	500	3333/sec	---	---
	123.2	2000	10000/sec	9	1111/sec
	660.3	500	2500/sec	---	---
	660.3	2000	10000/sec	9	1111/sec
Axisymmetric Mixed Compr.	148	250	4000/sec	---	---
	148	2000	8000/sec	14	571/sec
	82	250	4000/sec	---	---
	82	2000	8000/sec		571/sec

Table IV. DDAP Digital Runs.

Source	Pass	Save	AT ($\times 10^{-3}$ sec)	-3 dB (Hz)	λ*	Record Length (sec)
0.125 DDAS	1	2	0.1	4400	4.97	0.080
	2	5	0.25	1780	1.99	
R = 0.158'	3	10	0.5	890	0.99	
	4	20	1.0	445	0.50	
0.228 DDAS	1	2	0.2	2200	4.58	0.160
	2	5	0.5	890	1.83	
R = 0.292'	3	10	1.0	445	0.92	
	4	20	2.0	223	0.46	
1.0 DDAS	1	2	0.8	550	4.97	0.600
	2	5	2.0	223	1.99	
R = 1.27'	3	10	4.0	111	0.99	
	4	20	8.0	56	0.50	
Inlet	1	2	0.8	550	5.81	0.600
SIM	2	6	2.4	184	1.94	
R = 1.48'	3	12	4.8	92	0.97	
	4	25	10.0	46	0.46	
Inlet	1	2	0.2	2200	4.91	0.160
SIM Model	2	5	0.5	890	1.96	
R = 0.313'	3	10	1.0	445	0.98	
	4	20	2.0	223	0.49	
2D Mixed	1	1	0.125	4000	4.72	0.080
Comp.	2	2	0.25	1780	2.36	
R = 0.188'	3	5	0.625	720	0.94	
	4	10	1.25	360	0.47	
Axisymmetric	1	4	0.5	890	4.24	0.250
Mixed	2	9	1.125	392	1.88	
Compression	3	18	2.25	196	0.94	
R = 0.675'	4	36	4.5	98	0.47	
Large	1	2	0.2	2200	4.91	0.160
Scale	2	5	0.5	890	1.96	
Inlet	3	10	1.0	445	0.98	
R = 0.313'	4	20	2.0	223	0.49	

*$\lambda = (\pi R/AT) \times 10^{-3}$

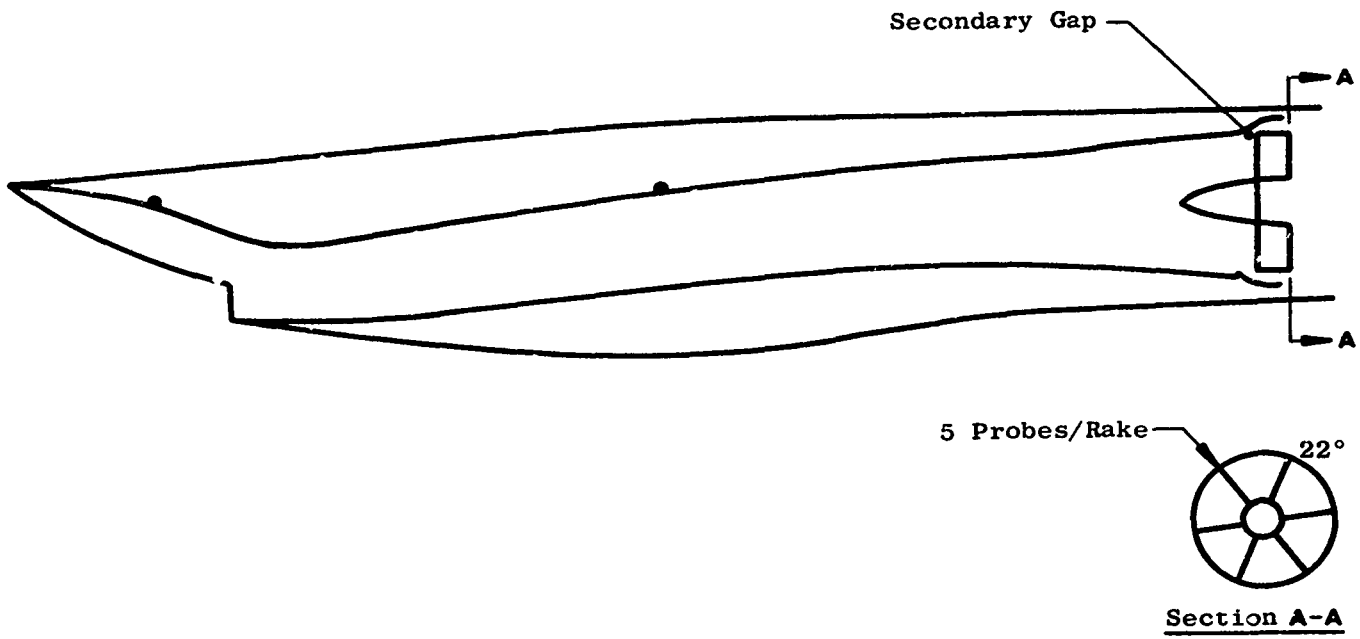

Figure 1. Sketch of Distortion Data Analysis Study (DDAS) Inlet.

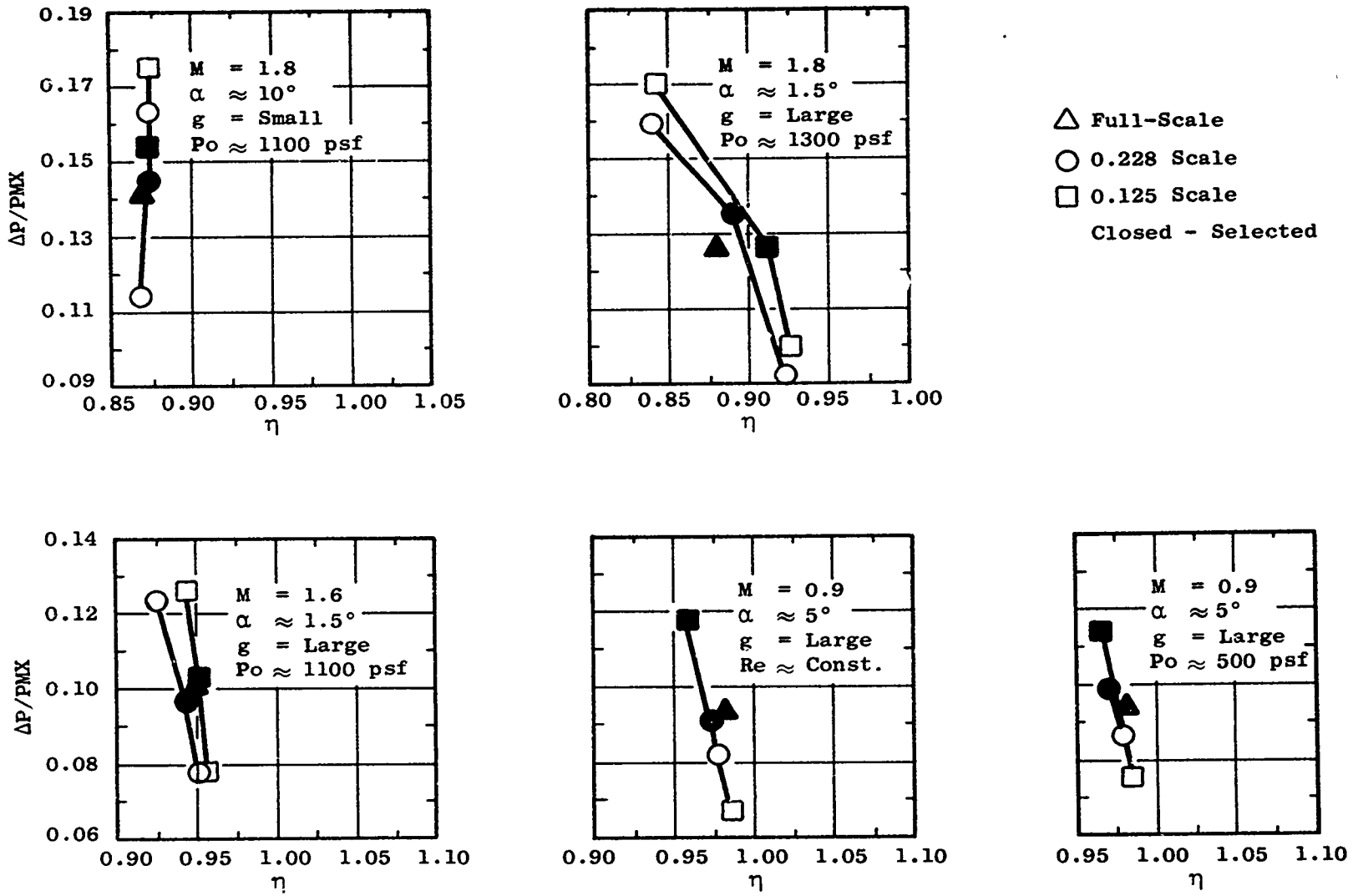

Figure 2. Maximum Distortion Vs. Recovery for DDAS Inlet.

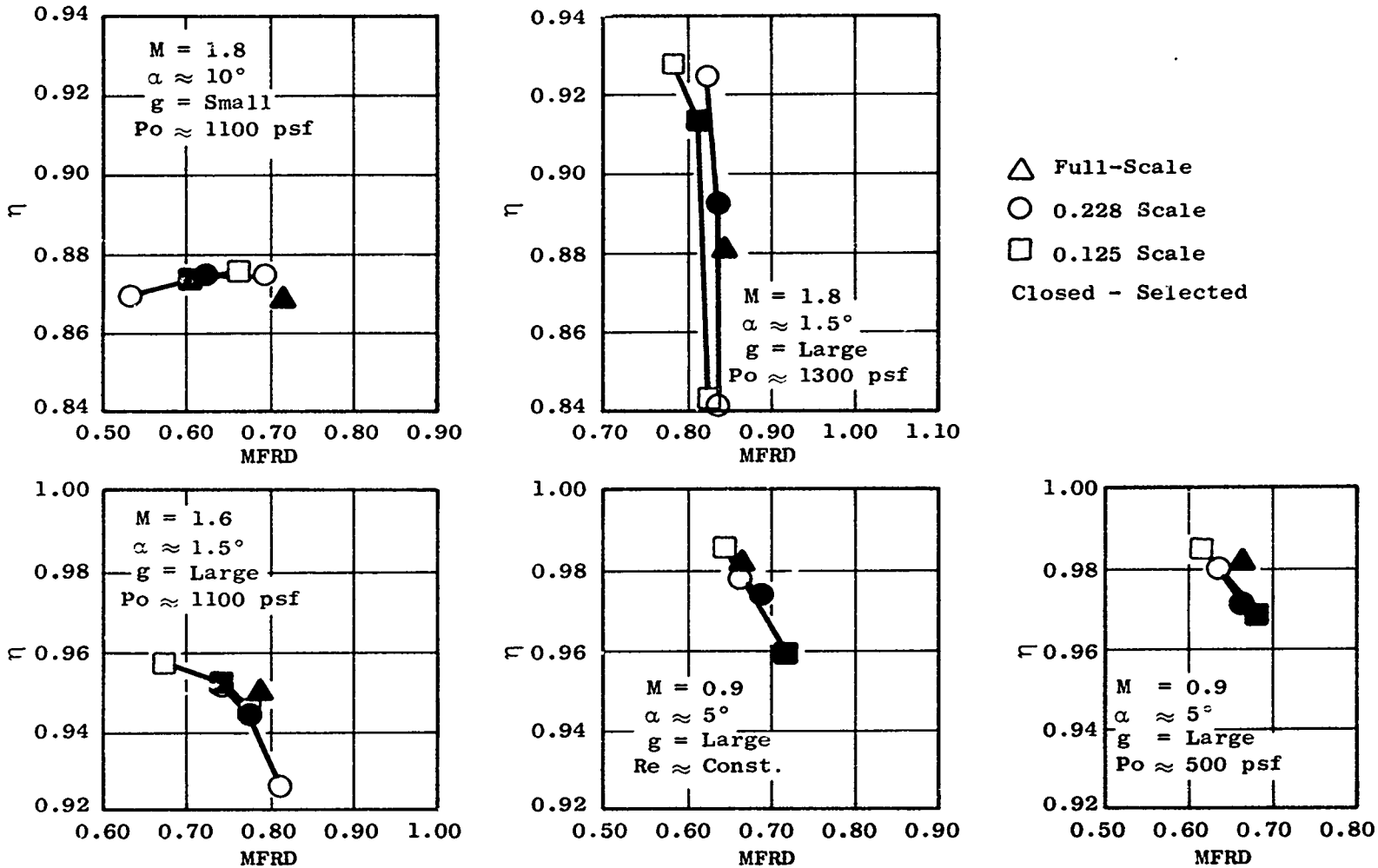

Figure 3. Recovery Vs. Mass Flow for DDAS Inlet.

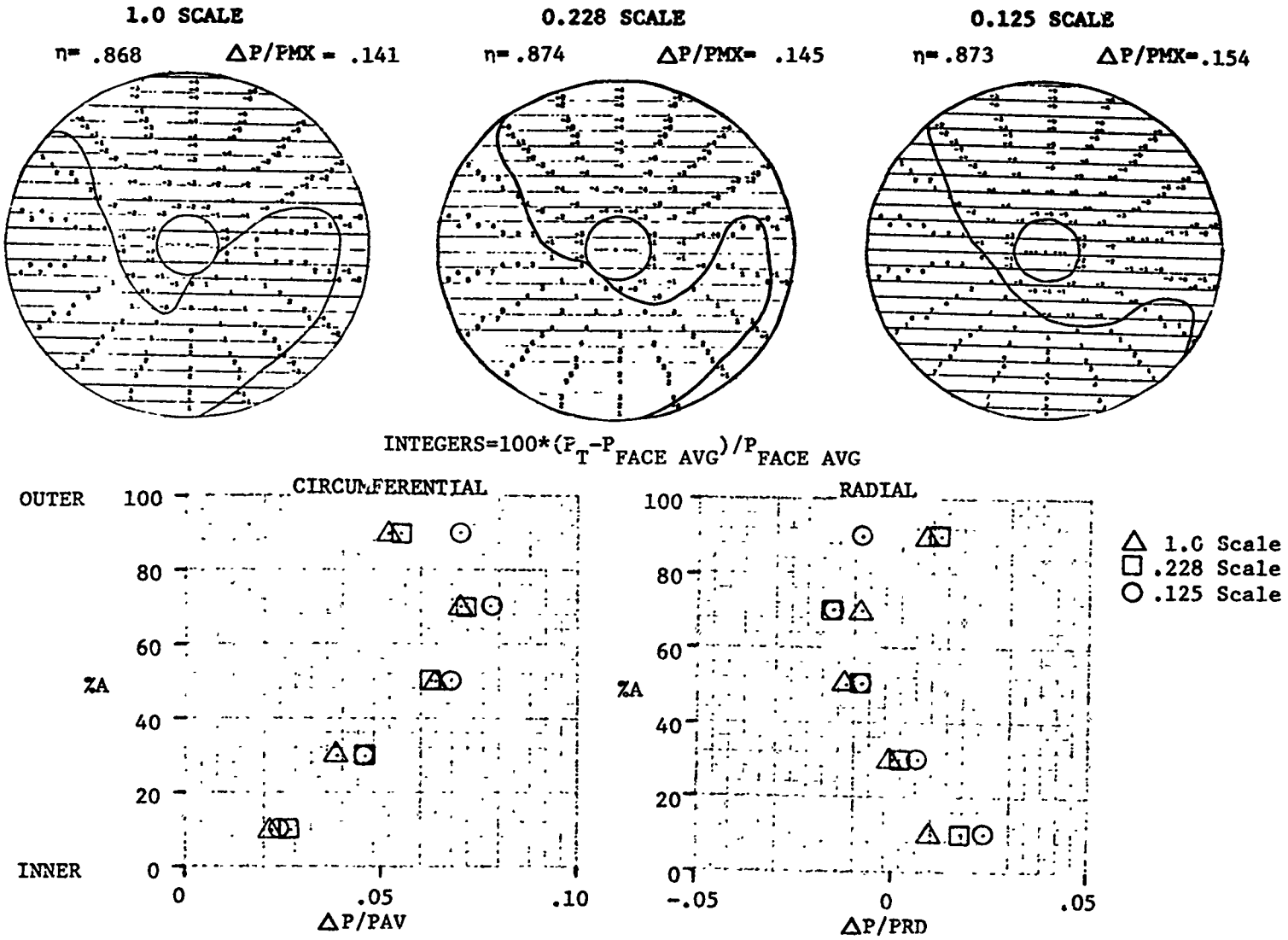

Figure 4. Steady-State Distortion Patterns and Profiles for DDAS Inlet, M = 1.8, $\alpha \approx 10°$, Po ≈ 1100 psf, Small Gap.

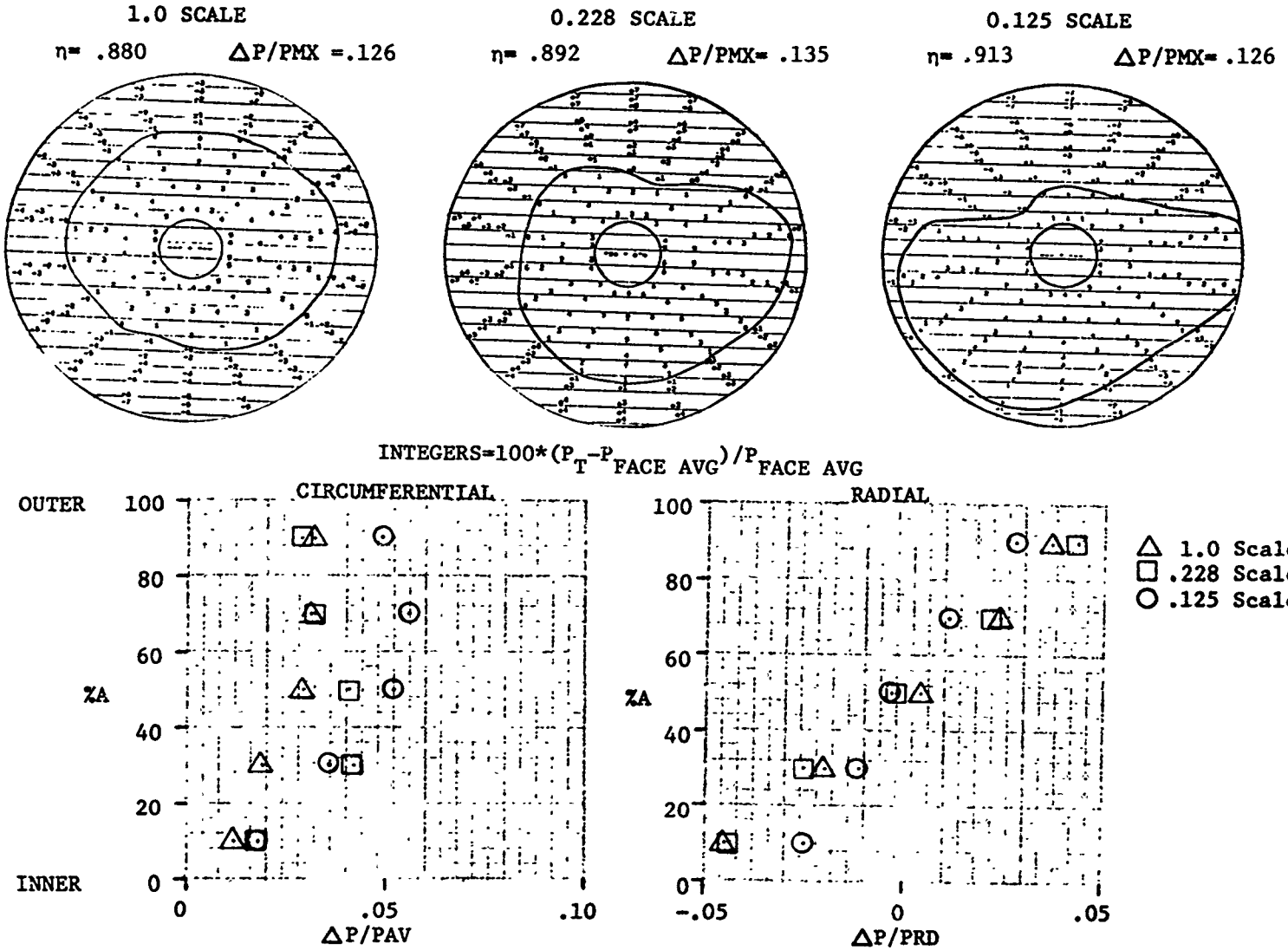

Figure 5. Steady-State Distortion Patterns and Profiles for DDAS Inlet, M = 1.8, $\alpha \approx 1.5°$, Po ≈ 1300 psf, Large Gap.

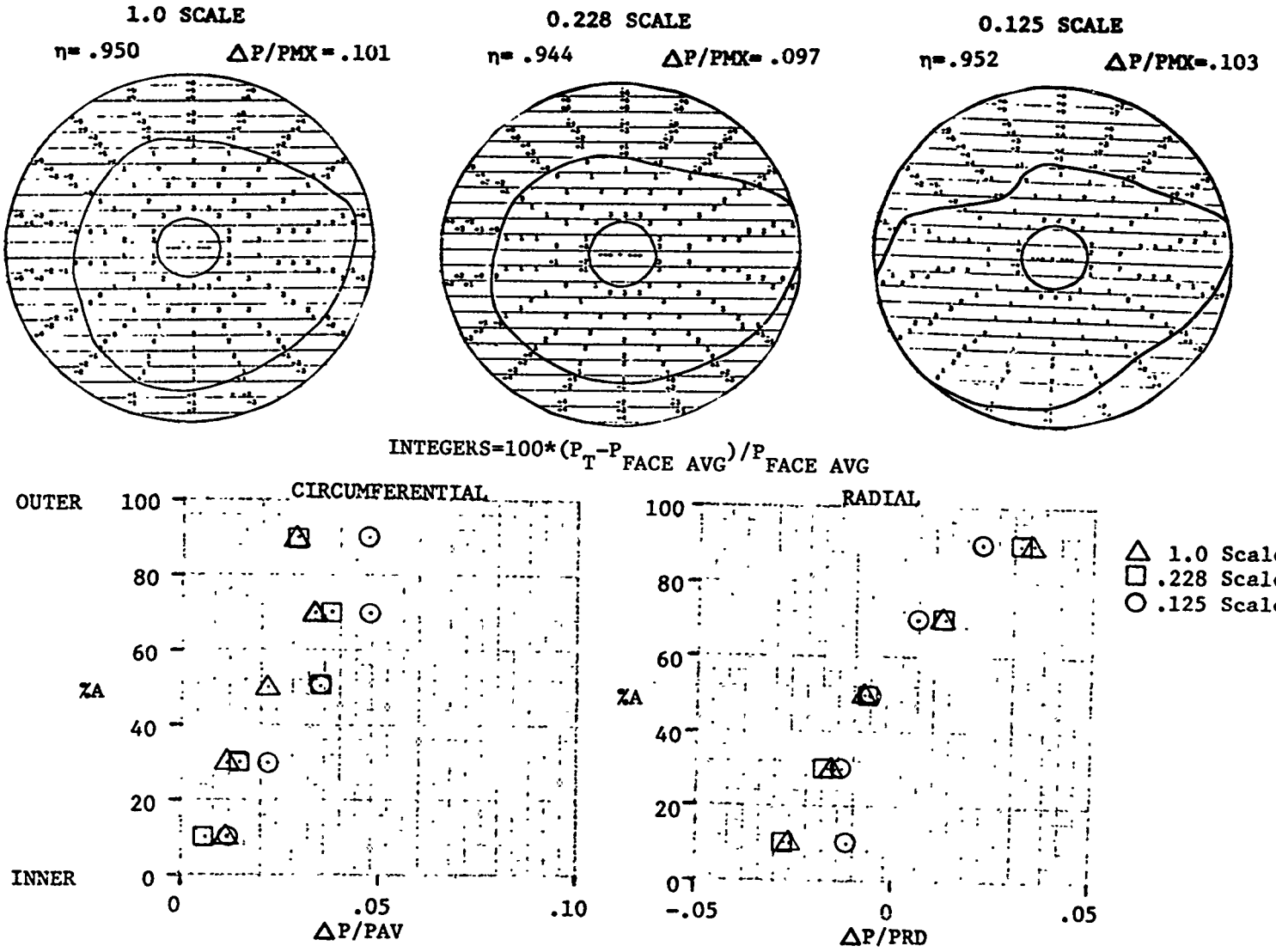

Figure 6. Steady-State Distortion Patterns and Profiles for DDAS Inlet, M = 1.6, $\alpha \approx 1.5°$, Po ≈ 1100 psf, Large Gap.

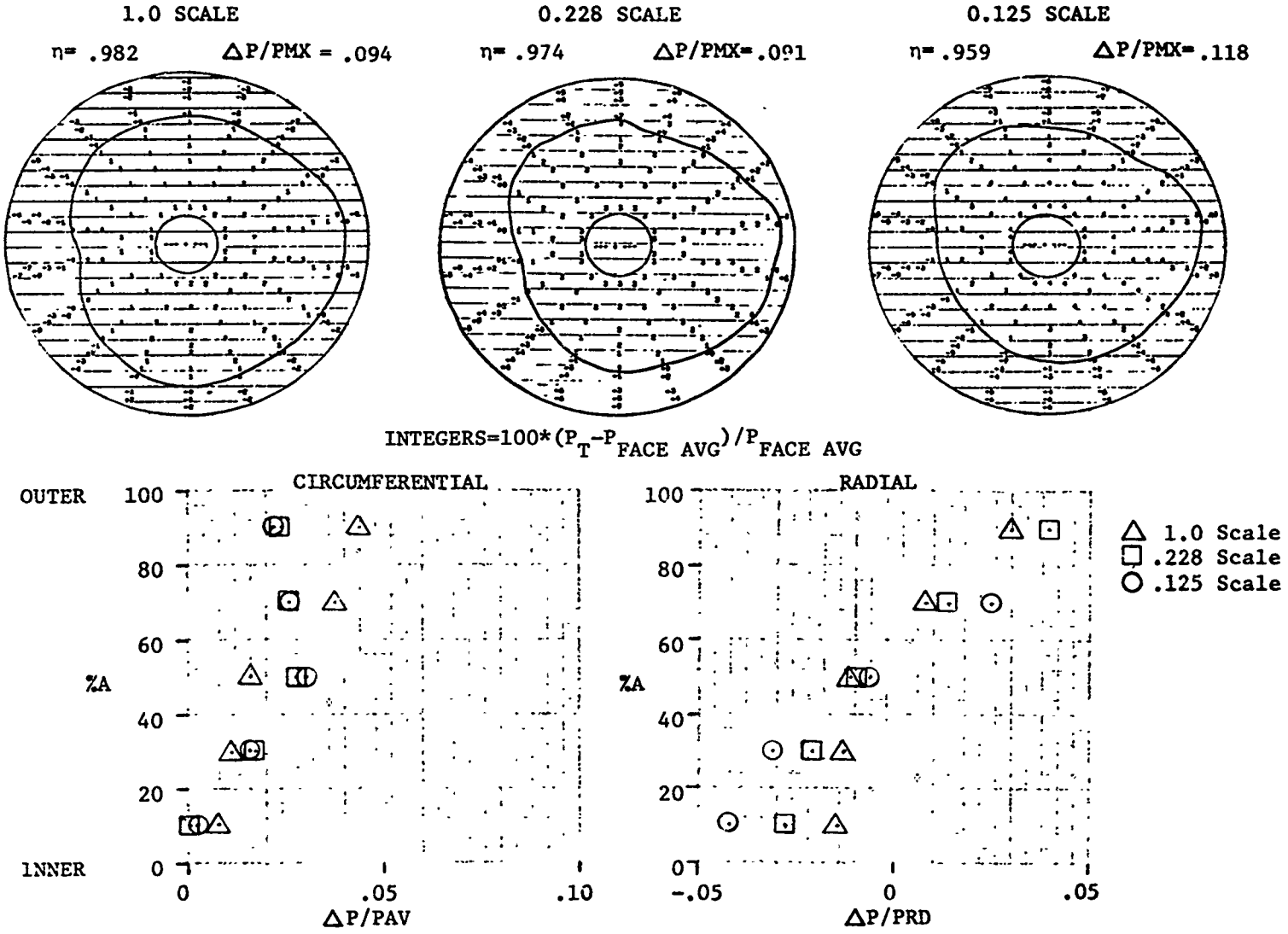

Figure 7. Steady-State Distortion Patterns and Profiles for DDAS Inlet, M = 0.9, $\alpha \approx 5°$, Re ≈ Constant, Large Gap.

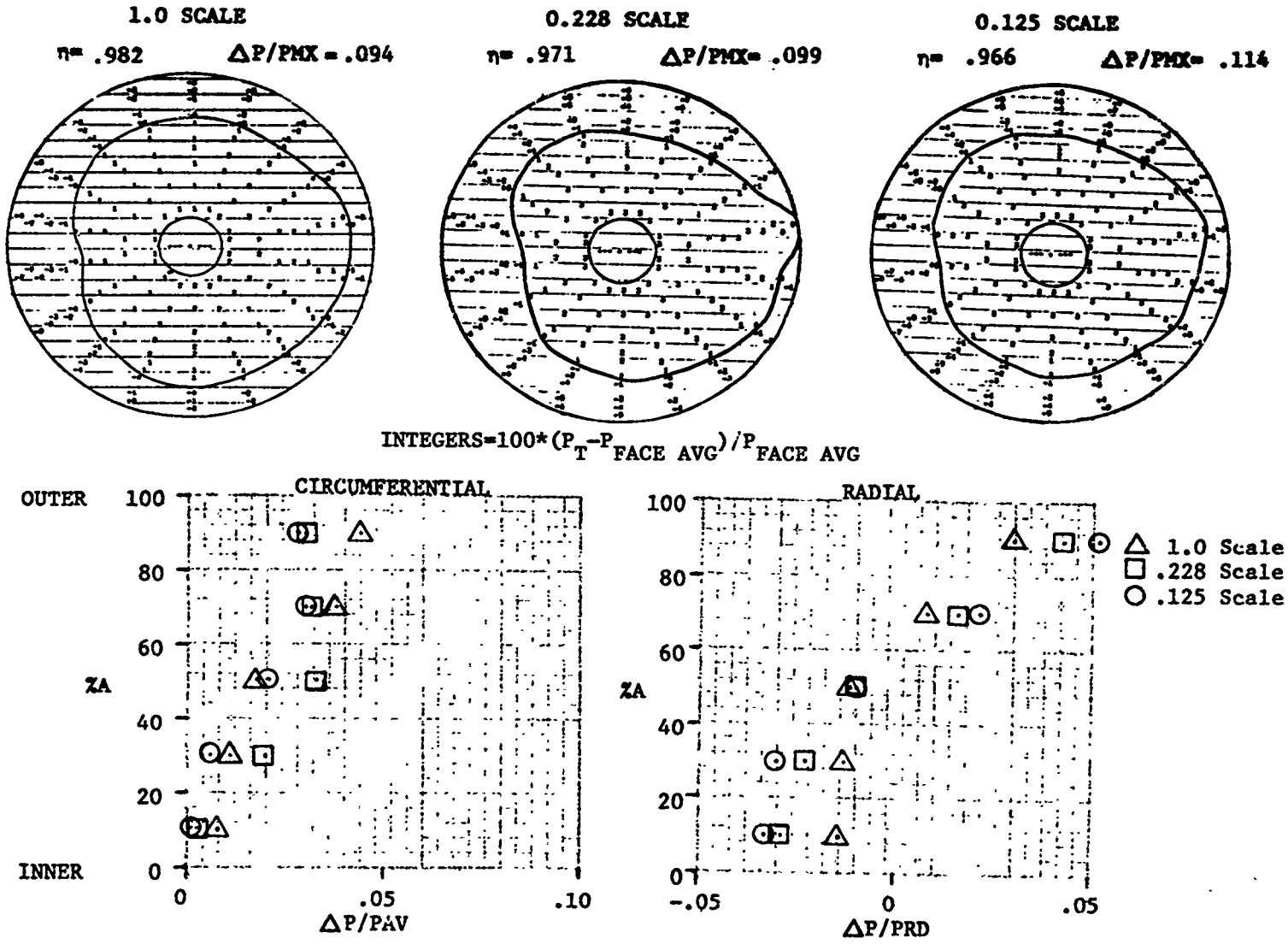

Figure 8. Steady-State Distortion Patterns and Profiles for DDAS Inlet, M = 0.9, $\alpha \approx 5°$, Po ≈ 500 psf, Large Gap.

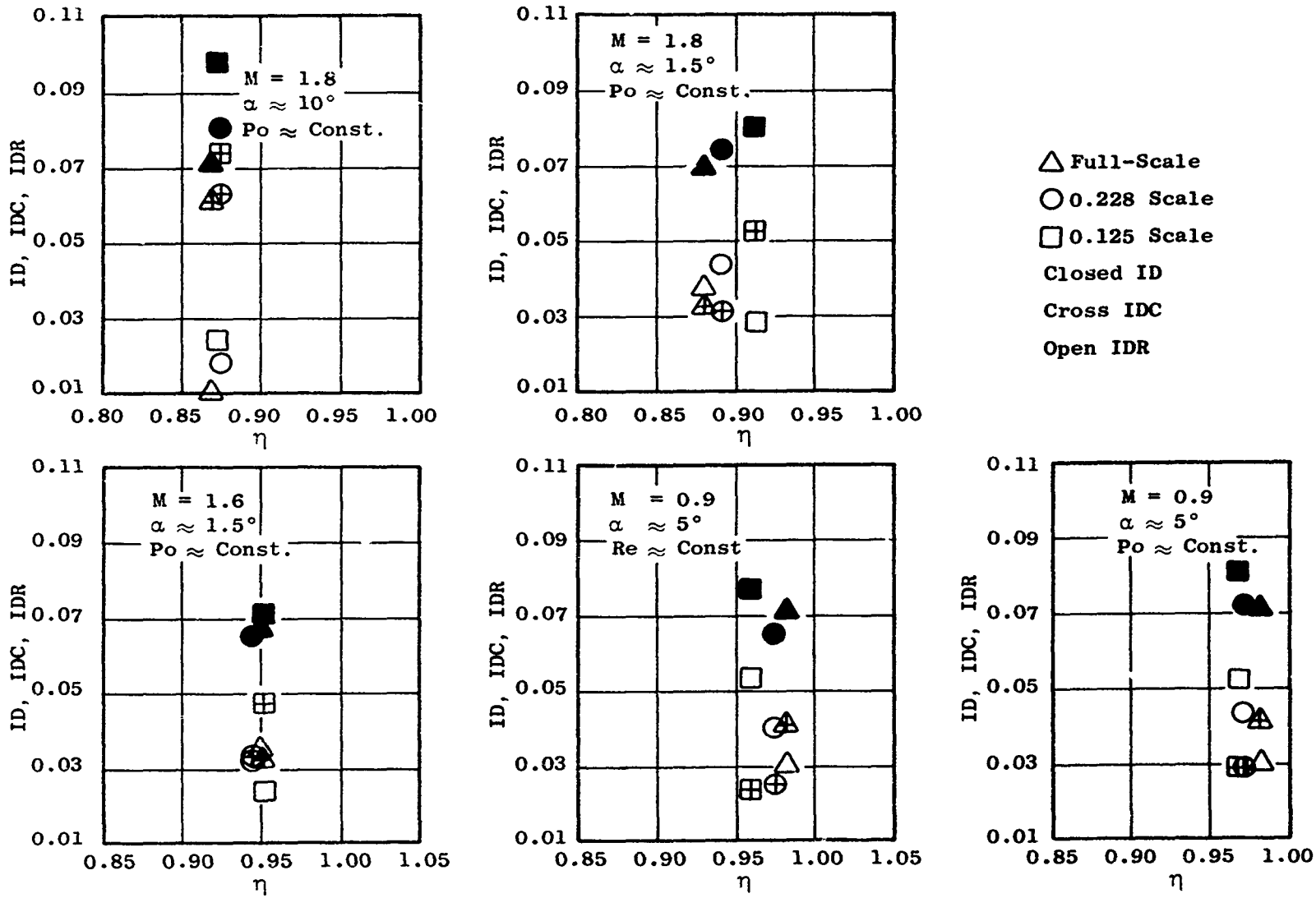

Figure 9. Distortion Parameters Vs. Recovery for DDAS Inlet.

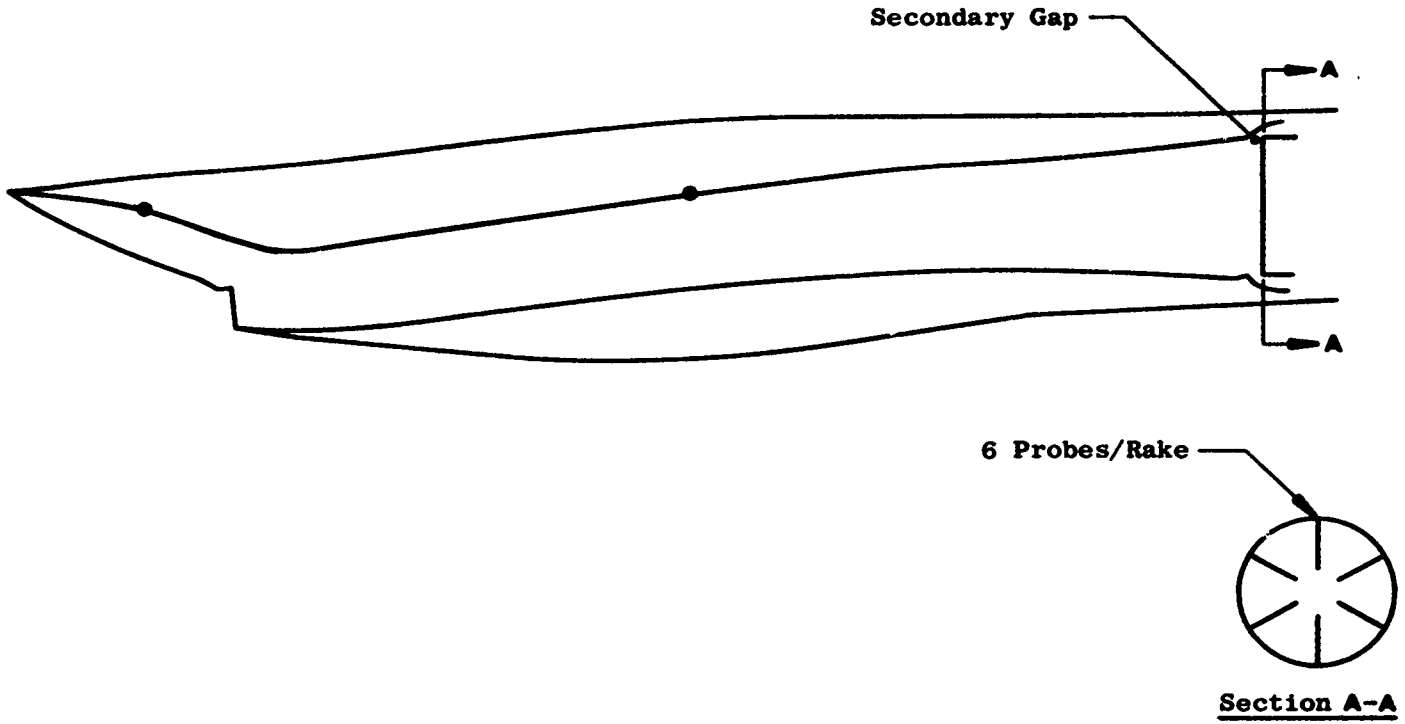

Figure 10. Sketch of Large Scale Inlet (LSI).

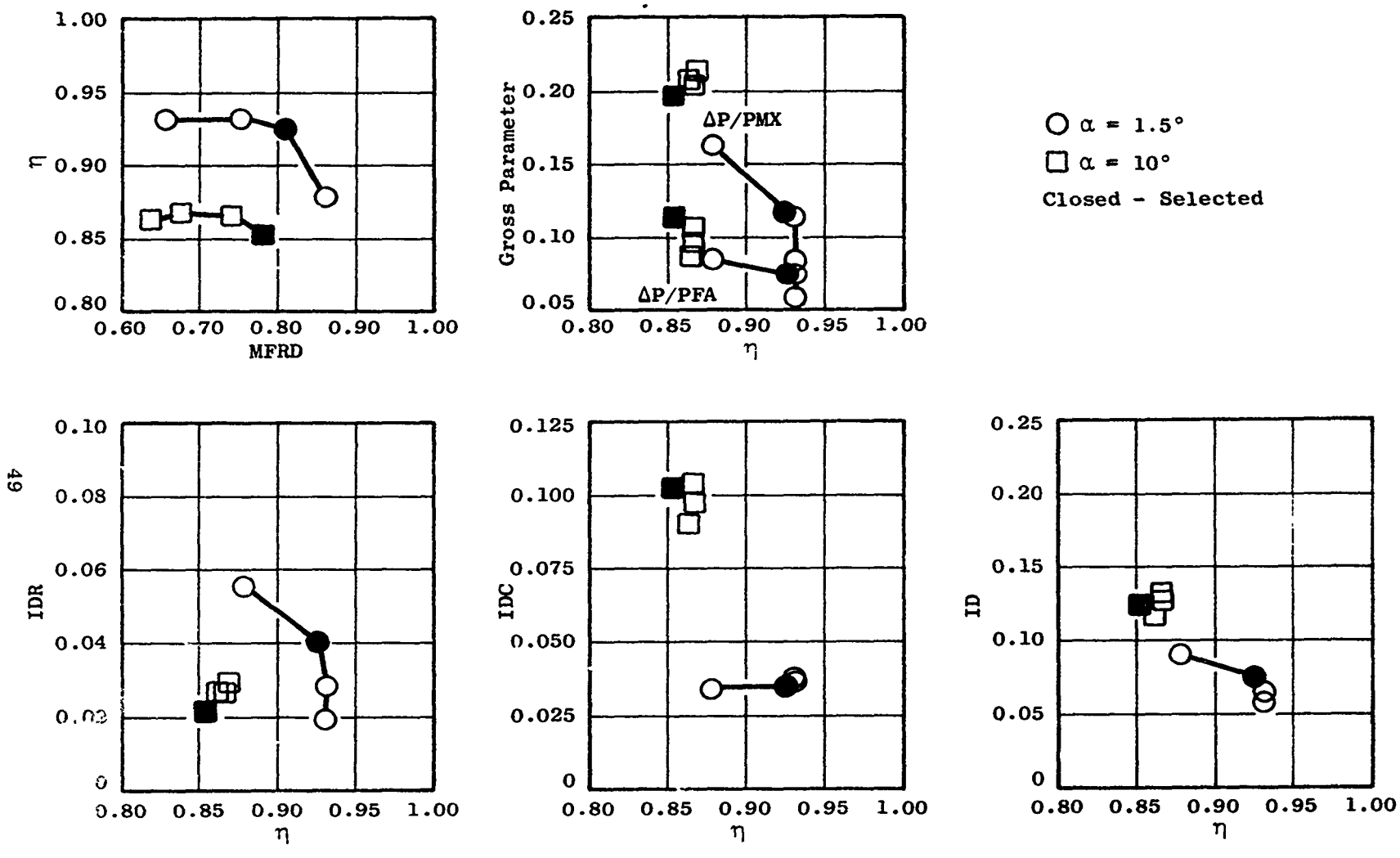

Figure 11. Recovery and Distortion Characteristics for LSI, M = 1.8, Small Gap.

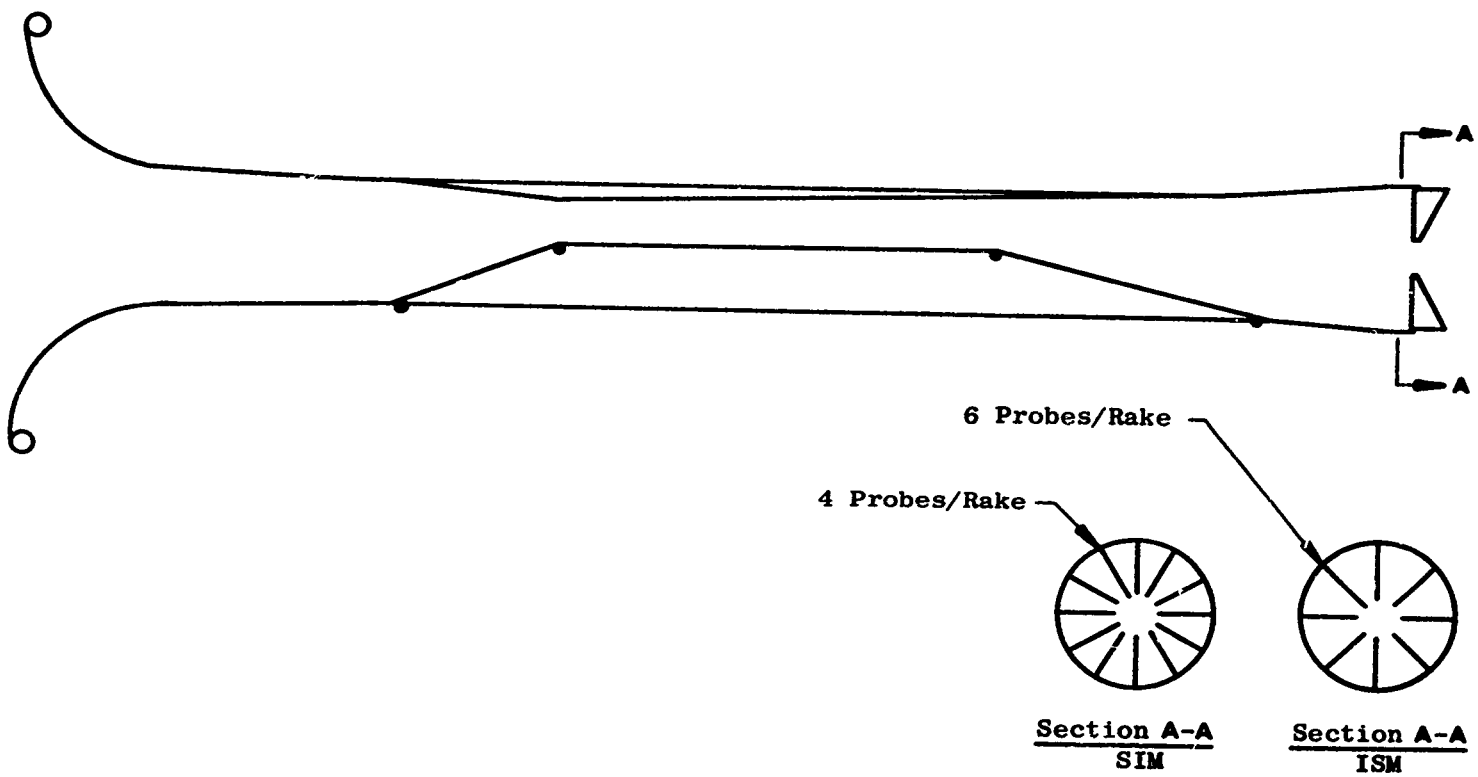

Figure 12. Sketch of Inlet Simulator (SIM and ISM).

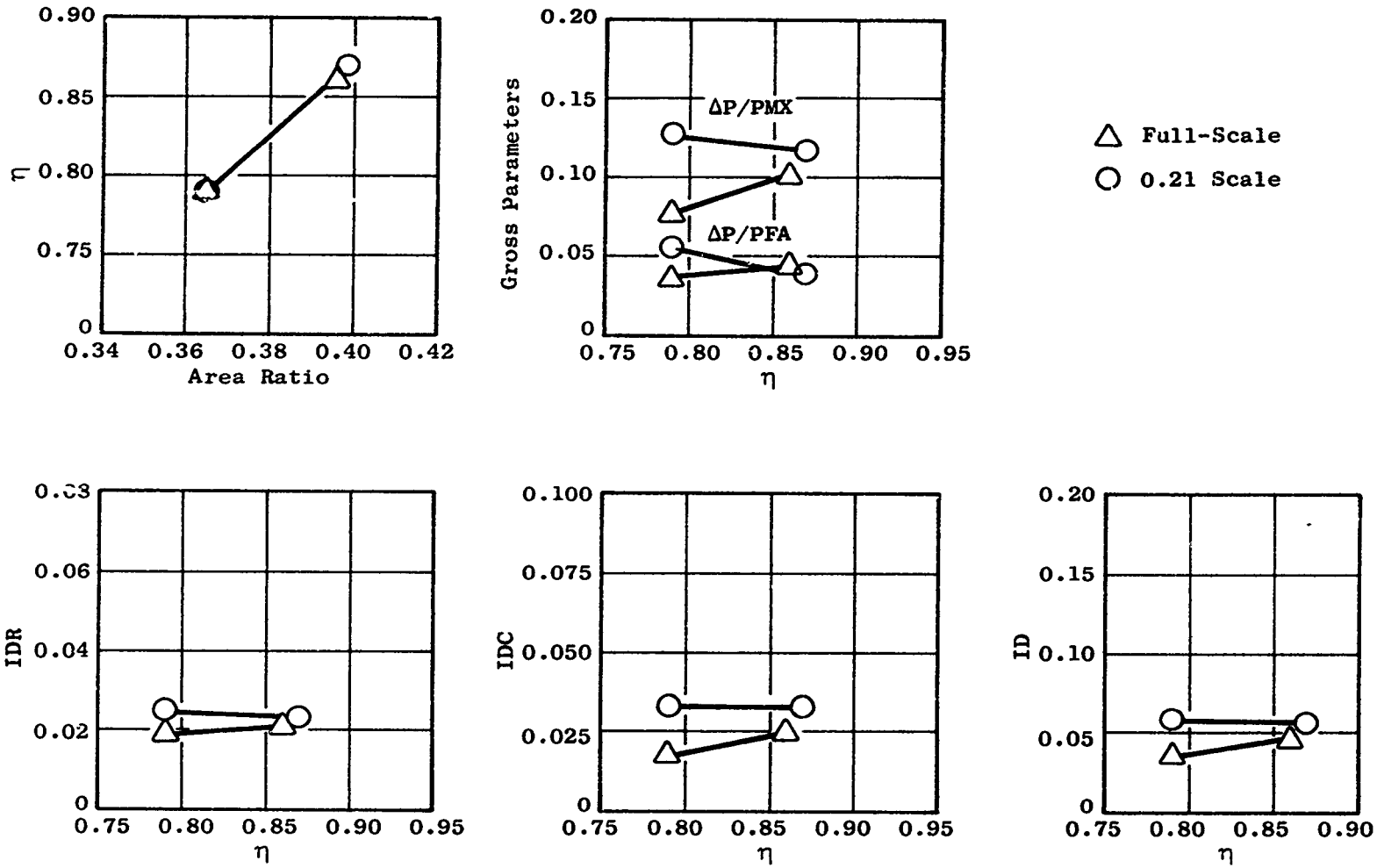

Figure 13. Recovery and Distortion Characteristics for Inlet Simulator.

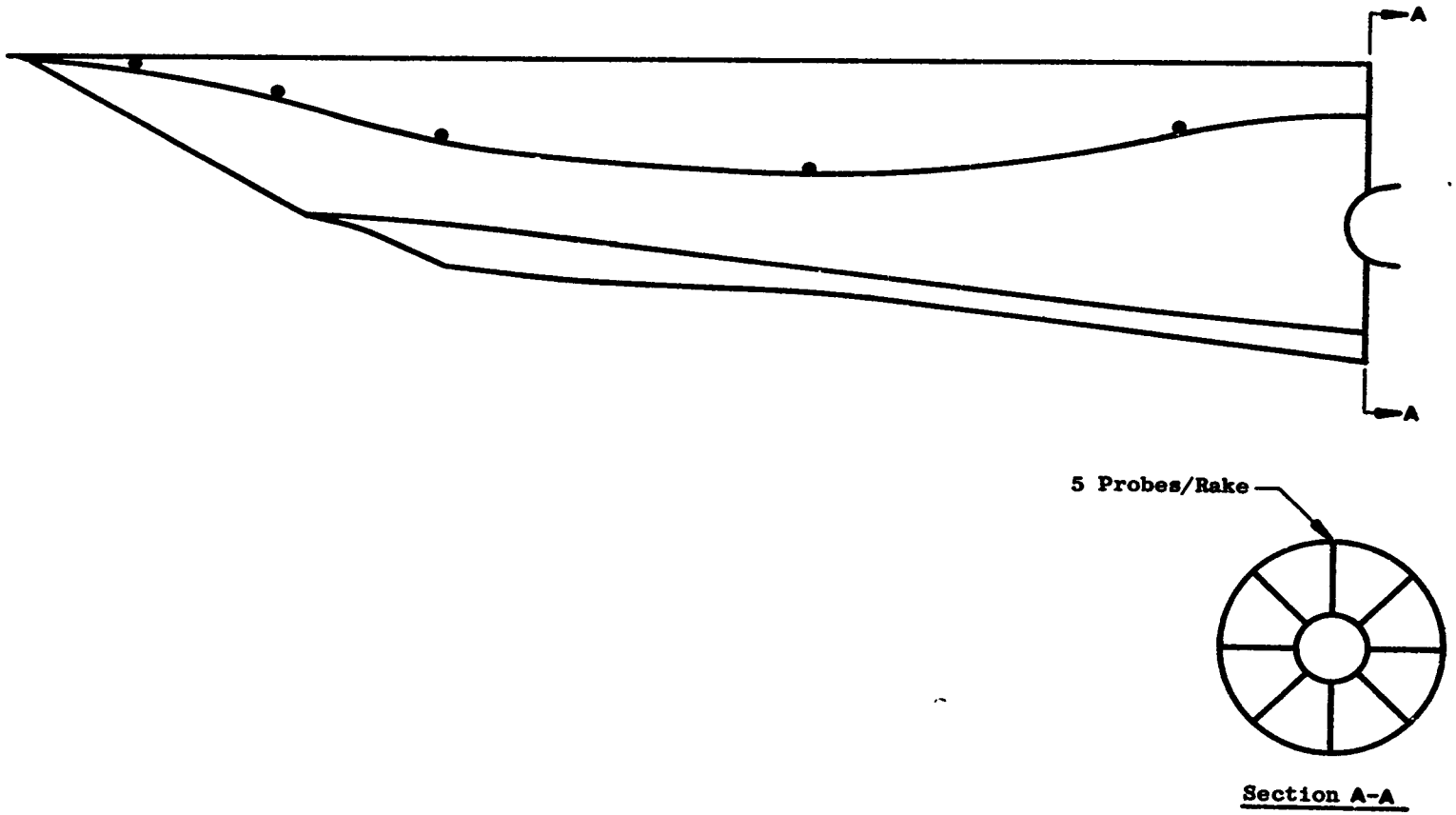

Figure 14. Sketch of Two-Dimensional Mixed Compression Inlet (2DMC).

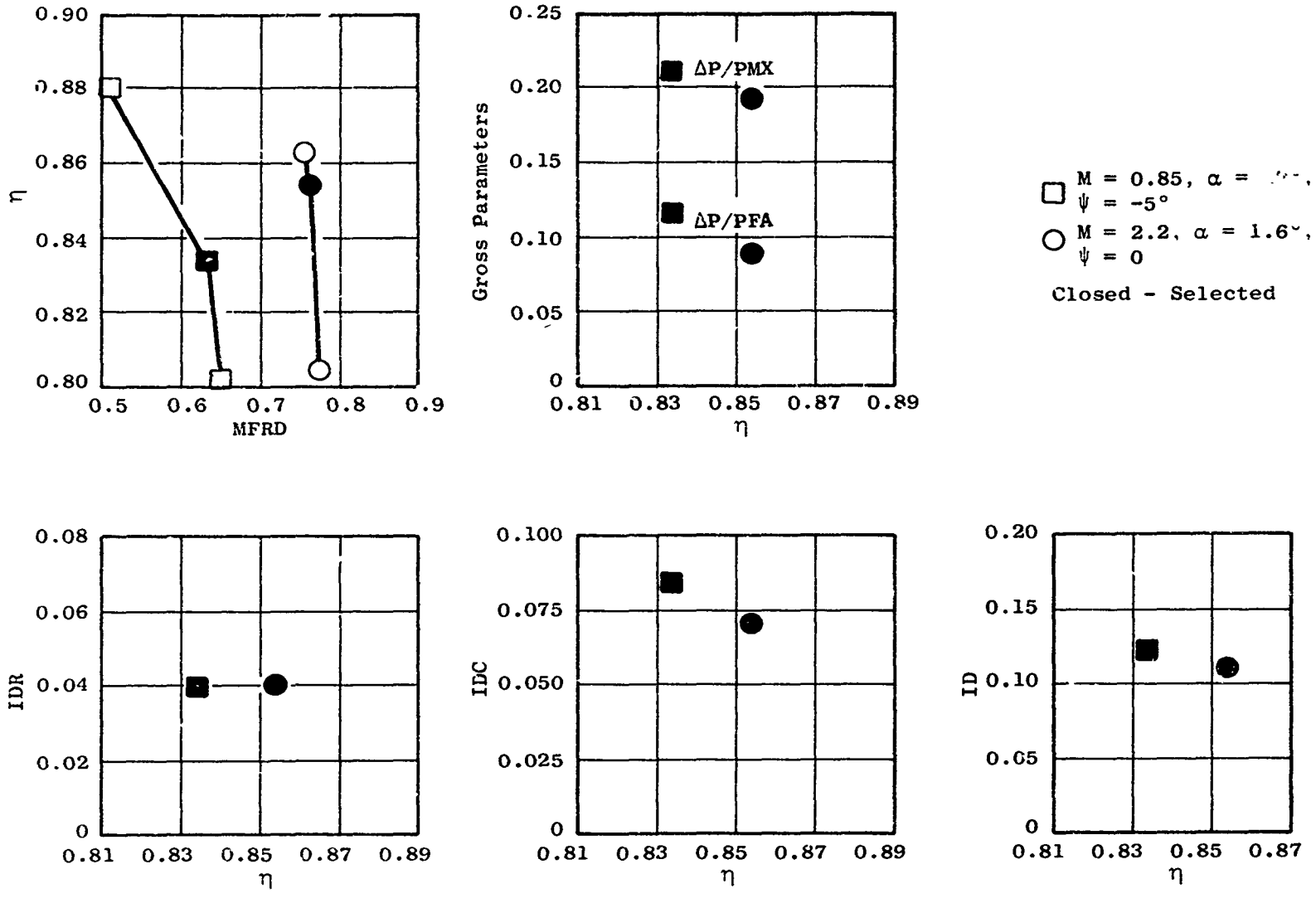

Figure 15. Recovery and Distortion Characteristics for 2DMC Inlet.

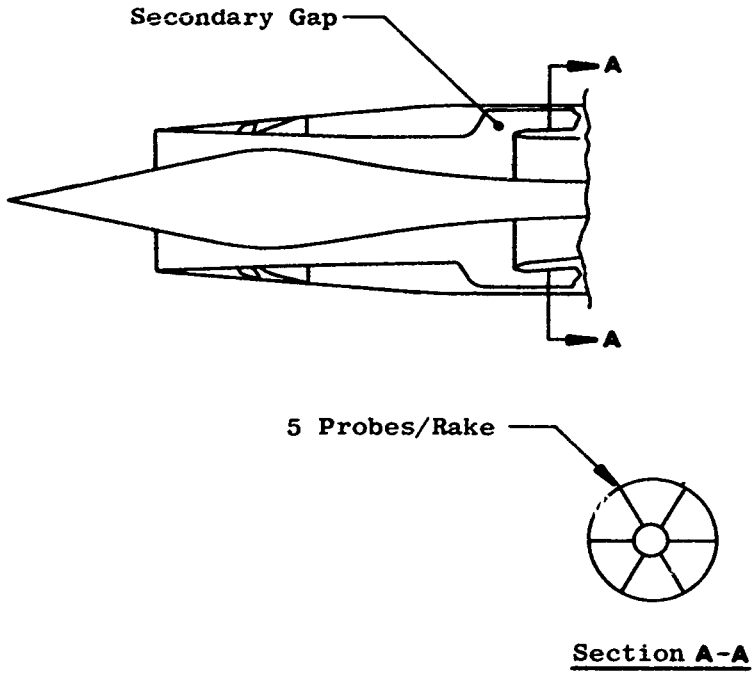

Figure 16. Sketch of Axisymmetric Mixed Compression Inlet (ASMC).

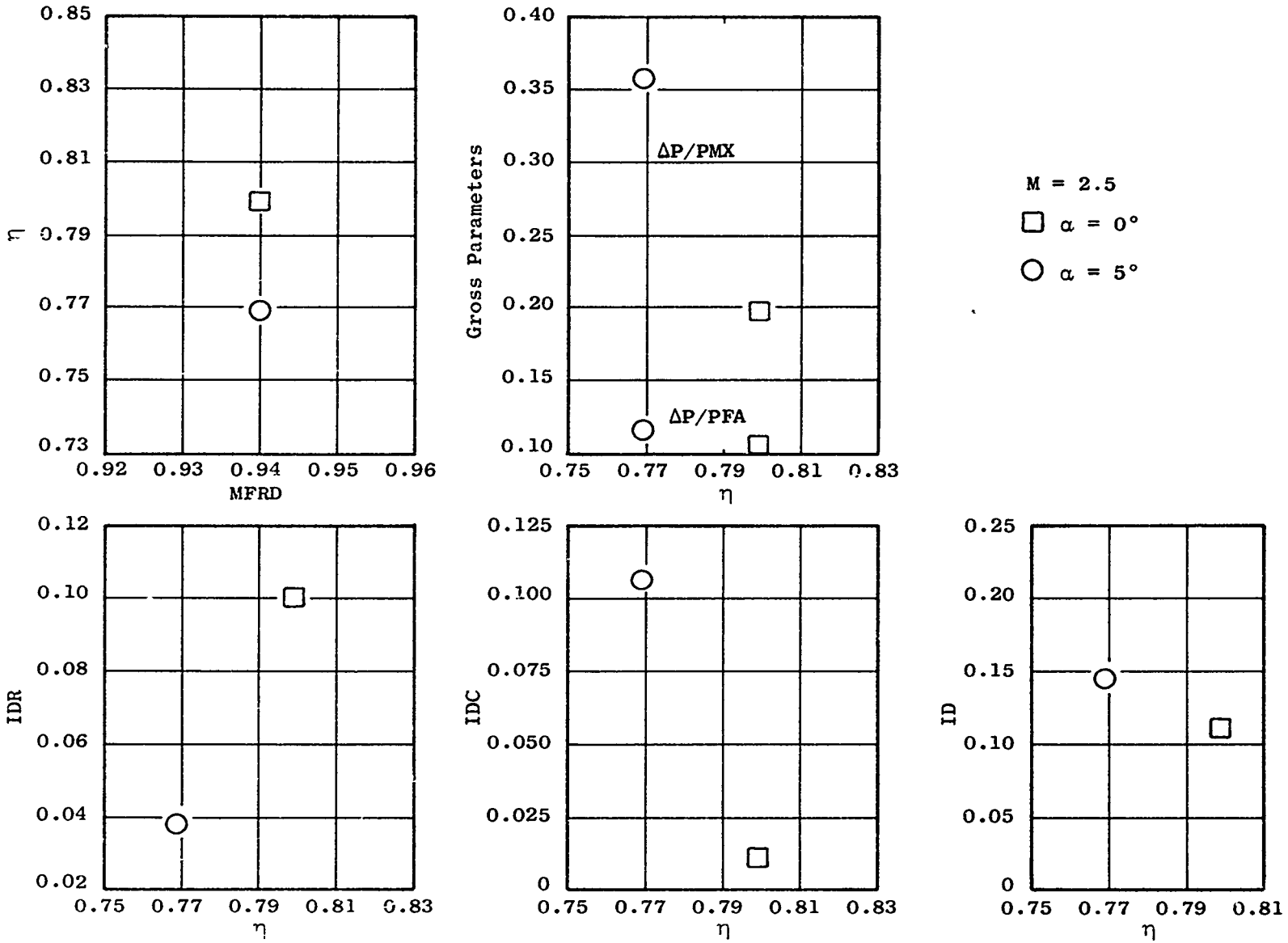

Figure 17. Recovery and Distortion Characteristics for ASMC Inlet.

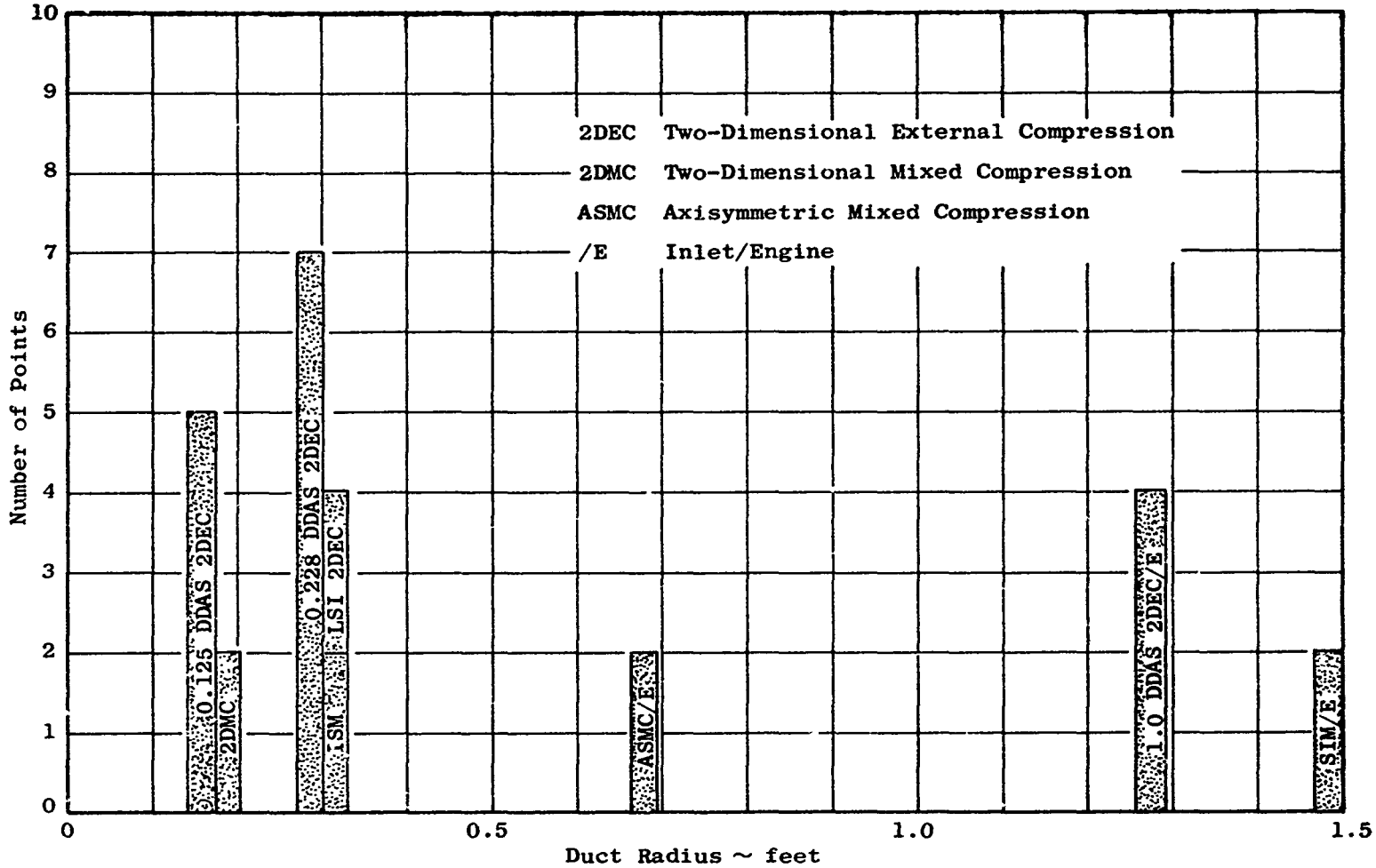

Figure 18. Selected Data Points from AFAPL and GE Sources Vs. Duct Radius.

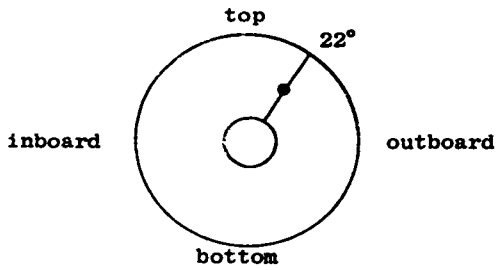

Engine Face Looking Aft

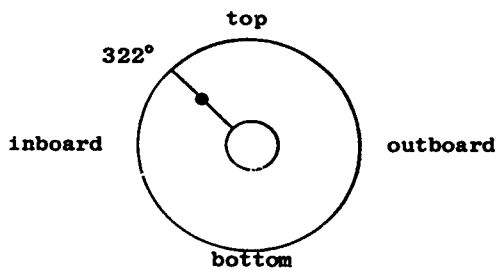

Engine Face Looking Aft

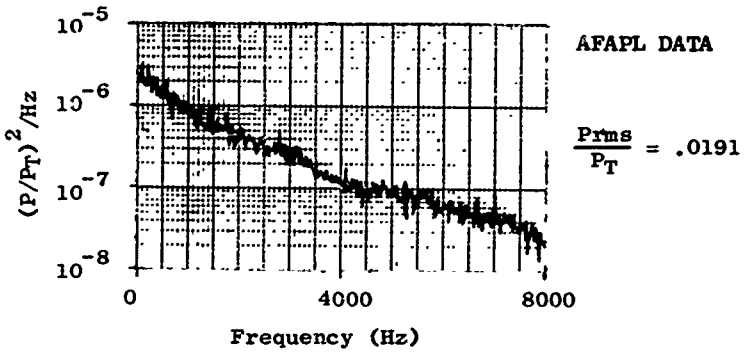

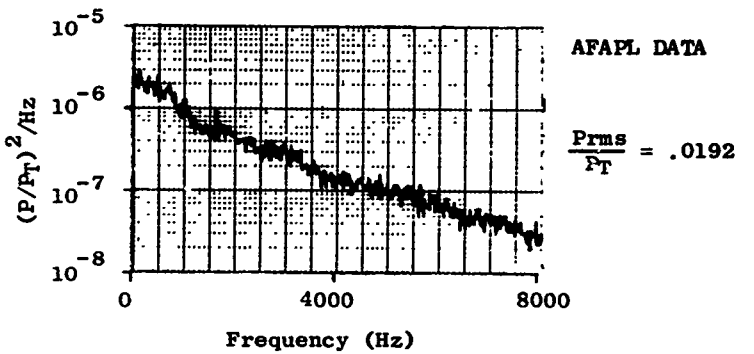

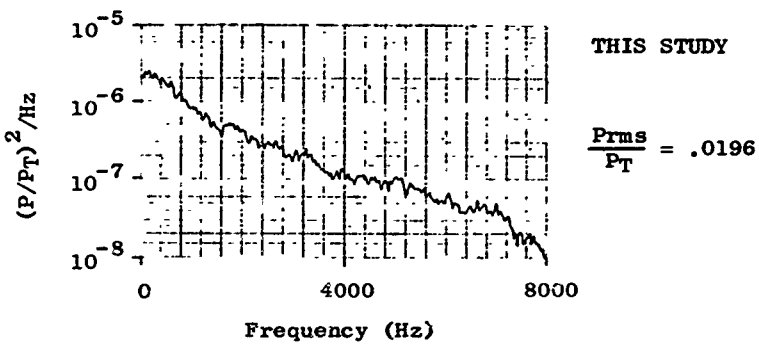

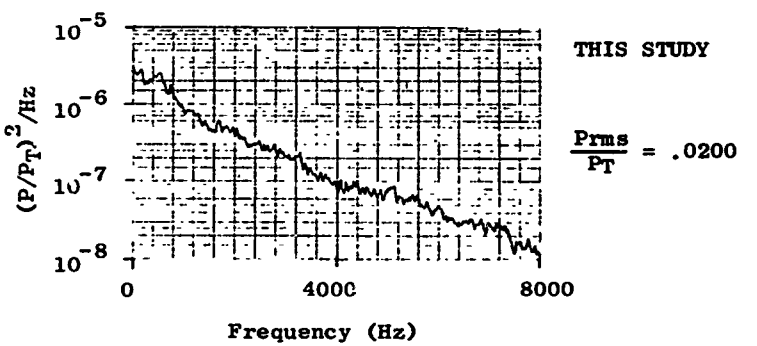

a) M = 0.0, α = 0.0, Ring 3, 22° and 322°

Figure 19. End-to-End Check 0.125 Scale DDAS Inlet Data.

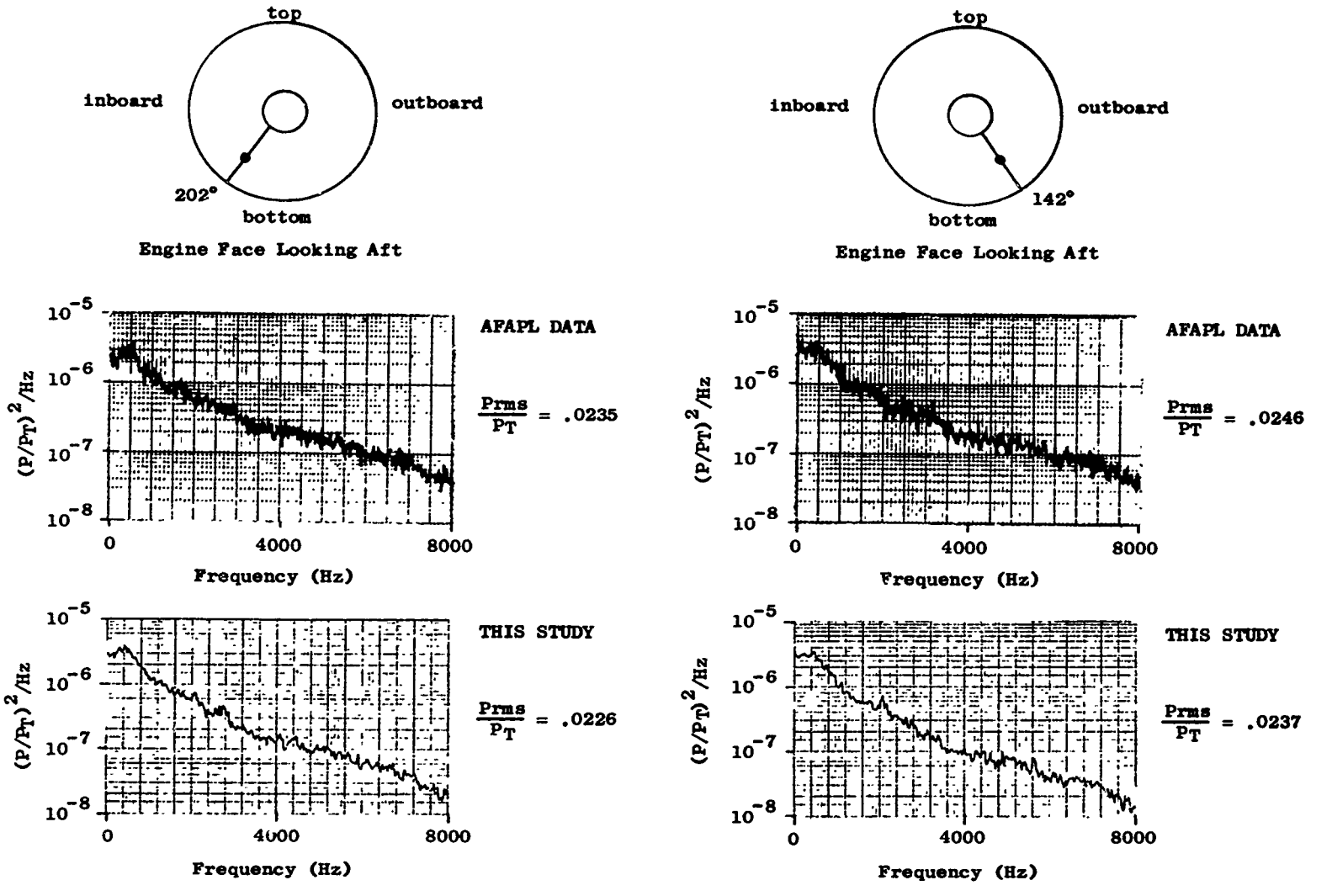

b) M = 0.0, α = 0.0, Ring 3, 142° and 202°

Figure 19. End-to-End Check 0.125 Scale DDAS Inlet Data (Concluded).

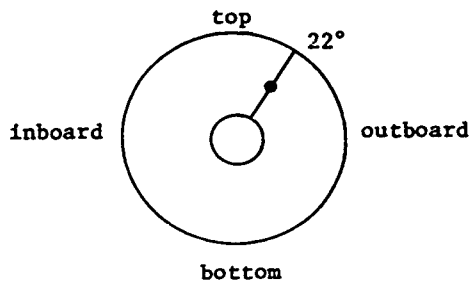

Engine Face Looking Aft

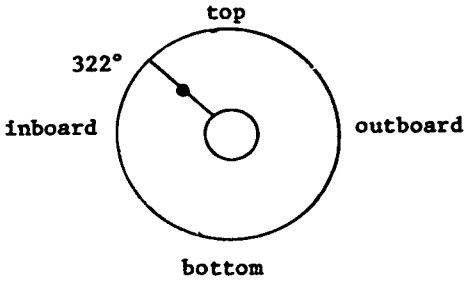

Engine Face Looking Aft

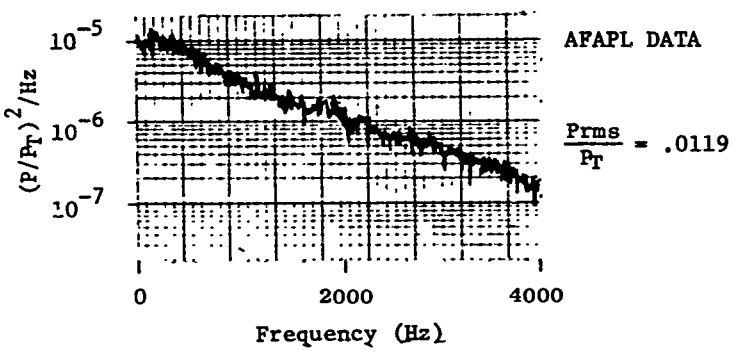

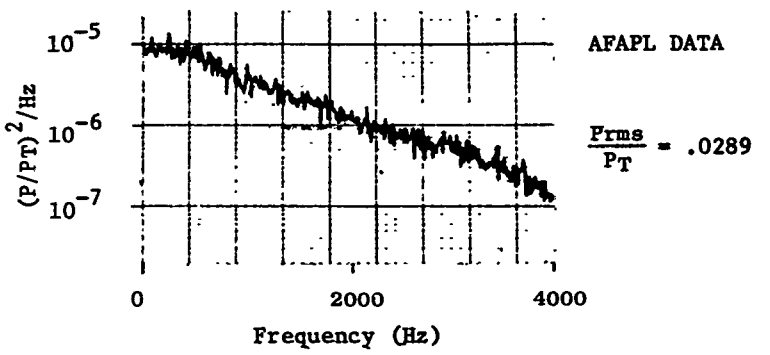

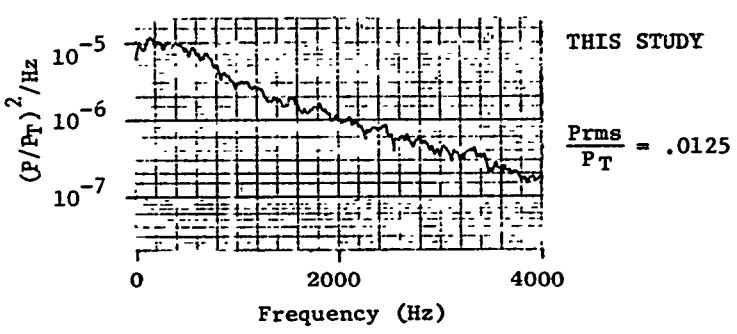

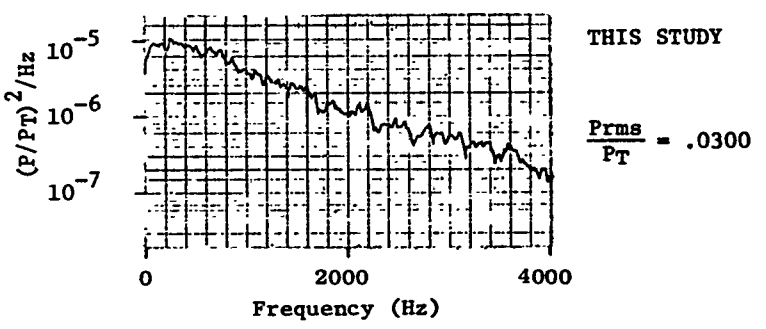

a) M = 1.8, α = 1.5°, Ring 3, 72° and 322°

Figure 20. End-to-End Check 0.228 Scale DDAS Inlet Data.

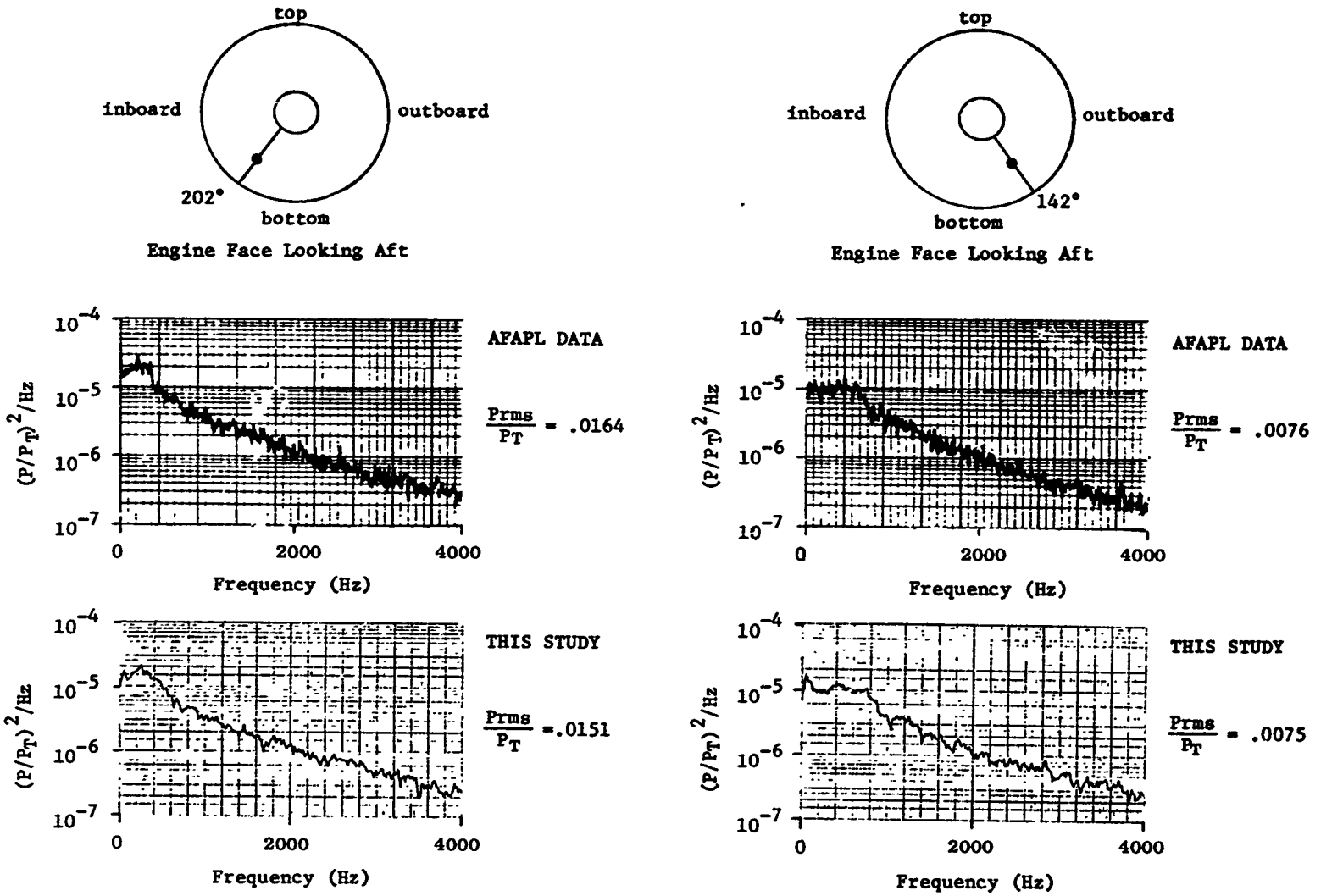

b) M = 1.8, α = 1.5°, Ring 3, 142° and 202°

Figure 20. End-to-End Check 0.228 Scale IDAS Inlet Data (Concluded).

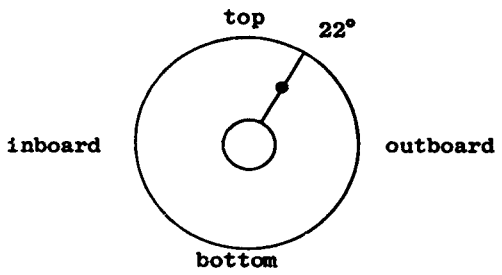

Engine Face Looking Aft

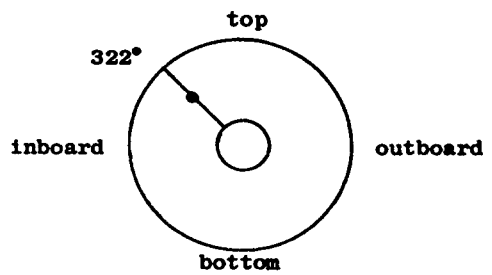

Engine Face Looking Aft

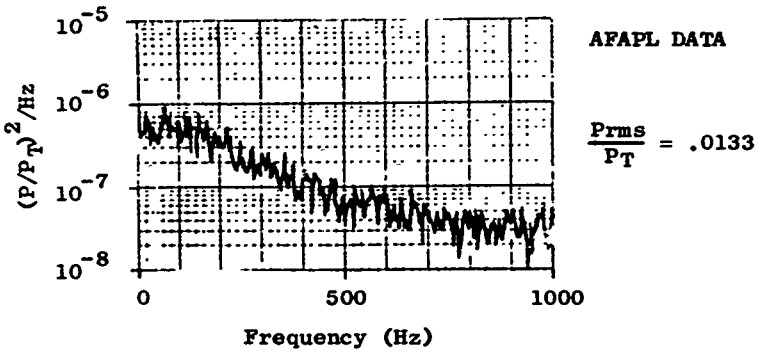

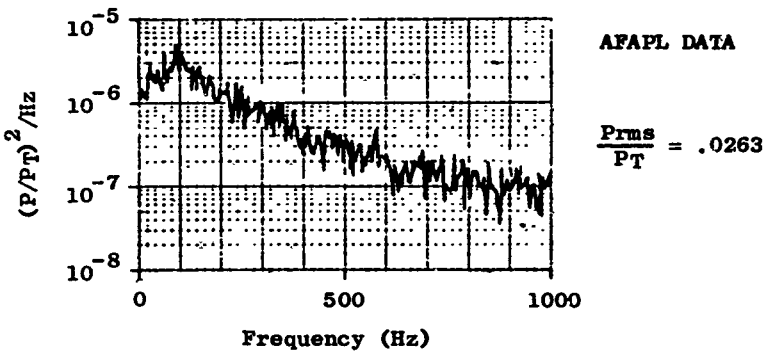

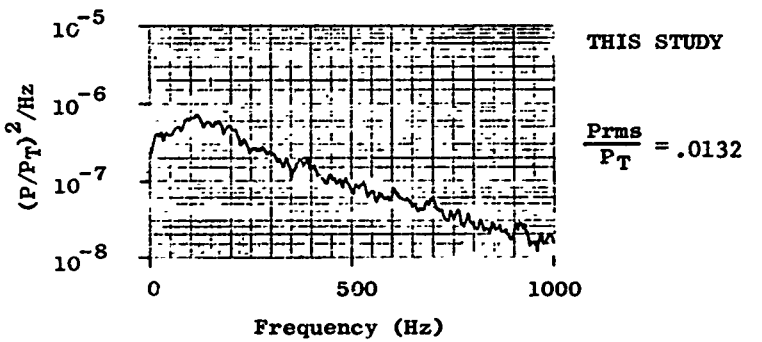

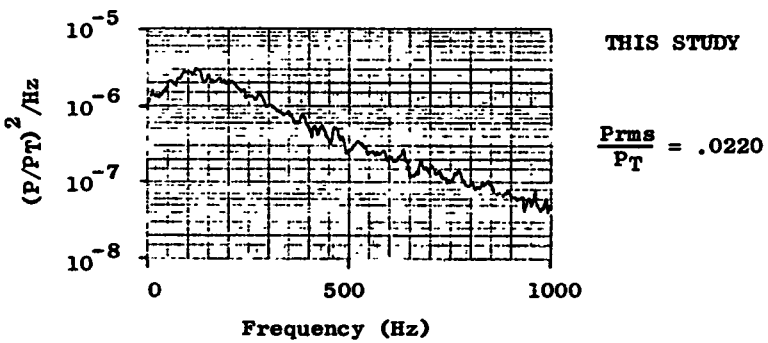

a) M = 1.8, α = 11°, Ring 3, 22° and 322°

Figure 21. End-to-End Full-Scale DDAS Inlet Data.

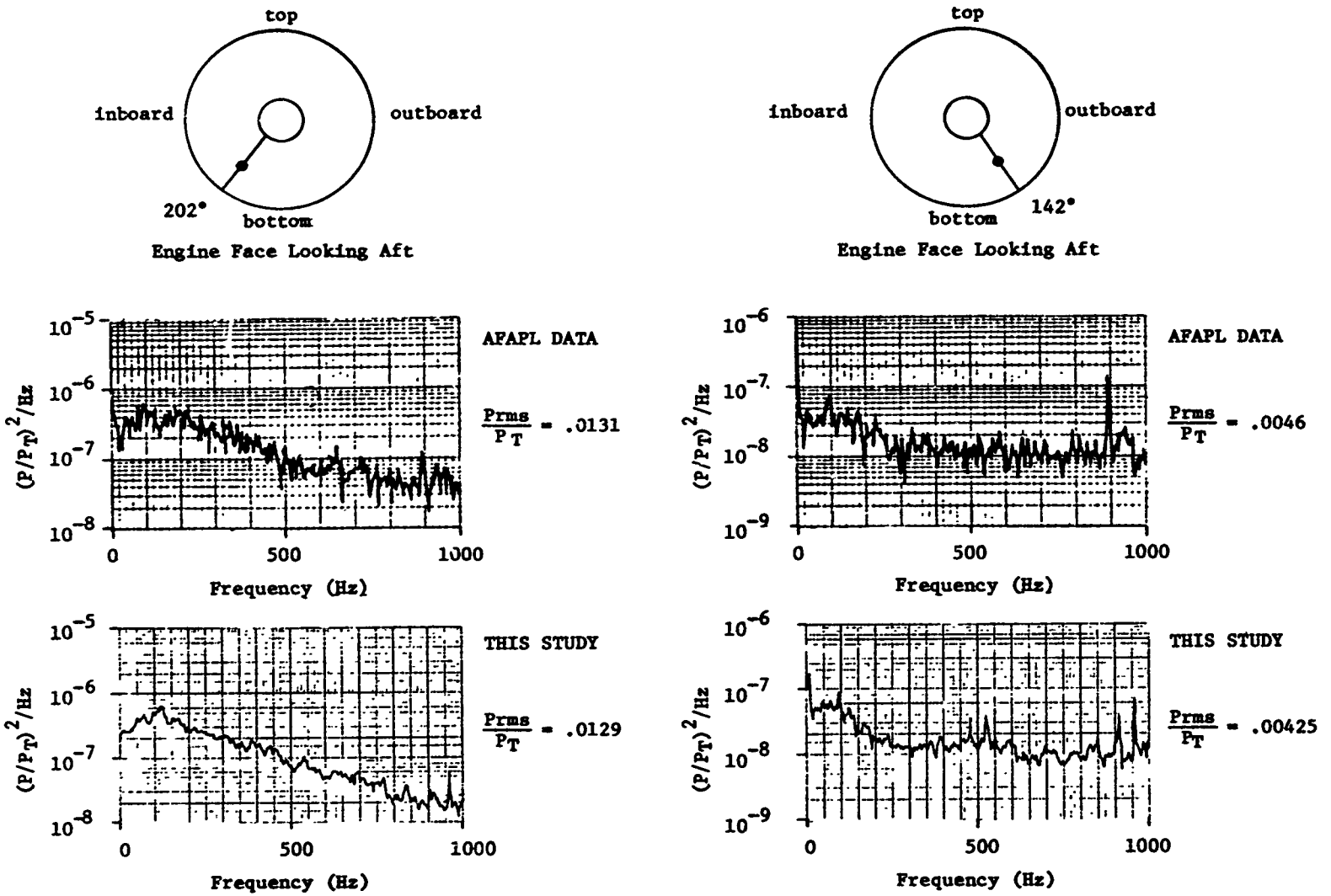

b) M = 1.8, α = 11°, Ring 3, 142° and 202°

Figure 21. End-to-End Full-Scale DDAS Inlet Data (Concluded).

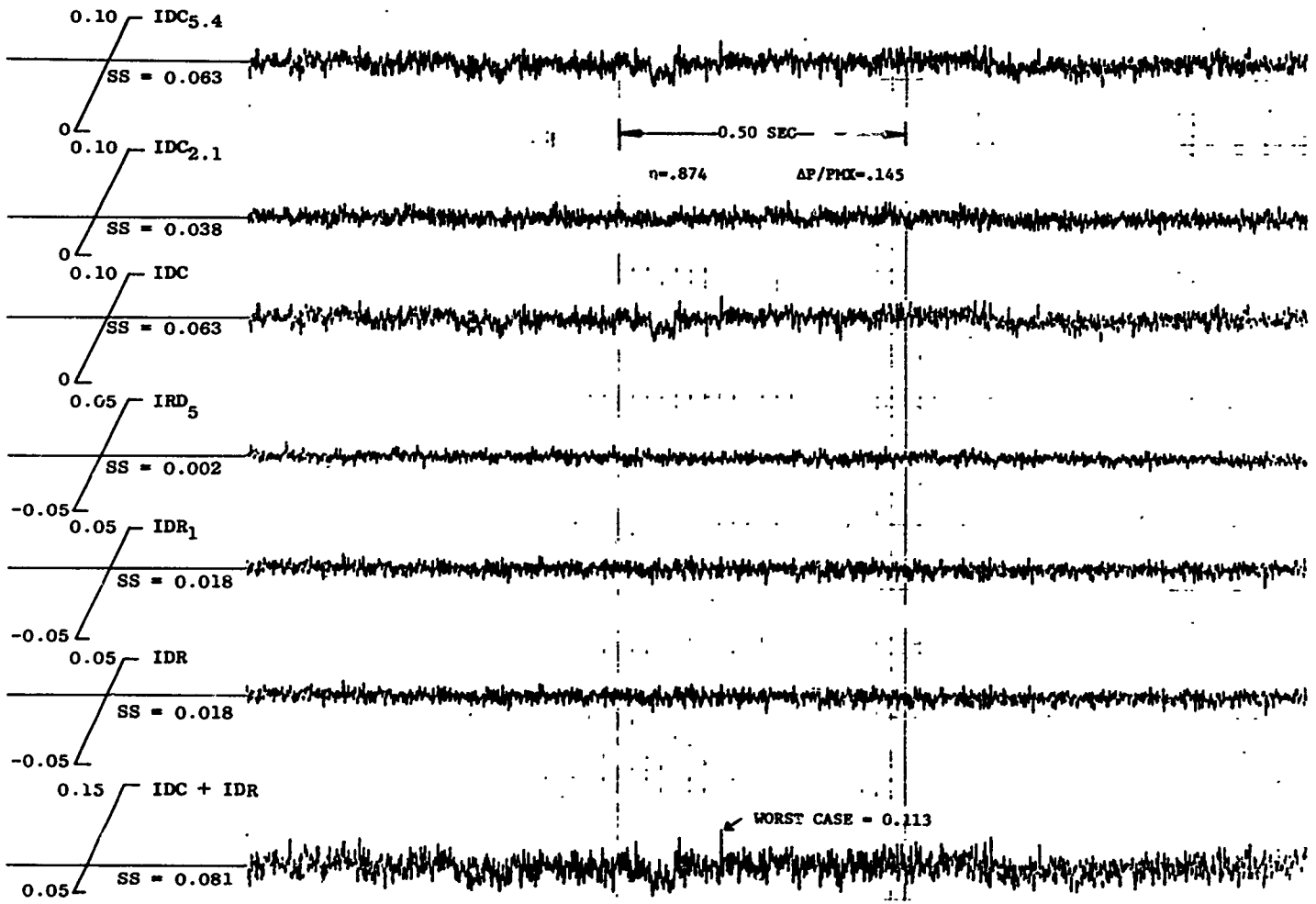

a) 0.228 Scale DDAS Inlet, 0-500 Hz

Figure 22. Distortion Vs. Time, M = 1.8, $\alpha \approx 10°$, Po ≈ 1100 psf, Small Gap.

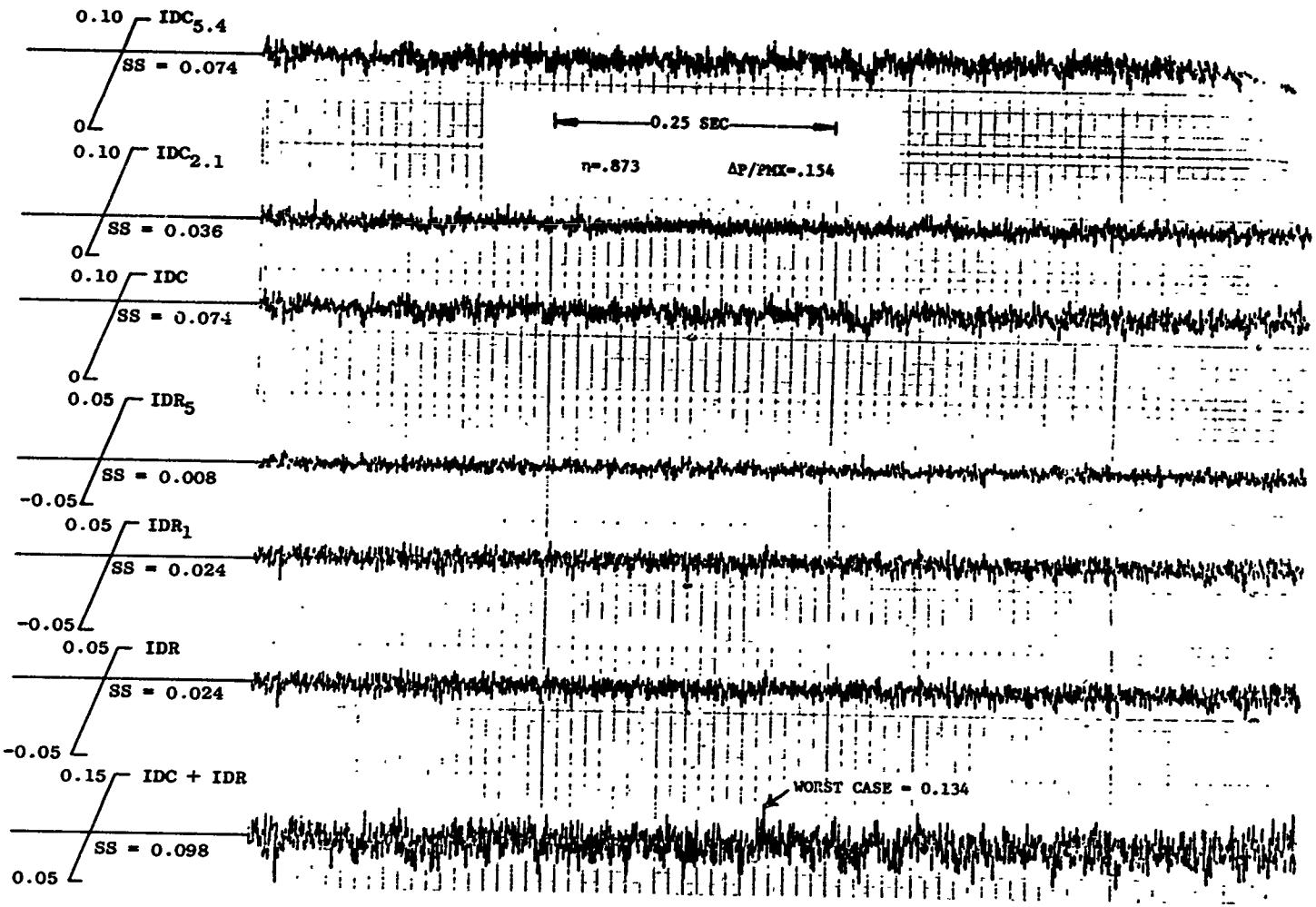

b) 0.125 Scale DDAS Inlet, 0-1000 Hz

Figure 22. Distortion Vs. Time, M = 1.8, $\alpha \approx 10°$, Po $\approx$ 1100 psf, Small Gap (Concluded).

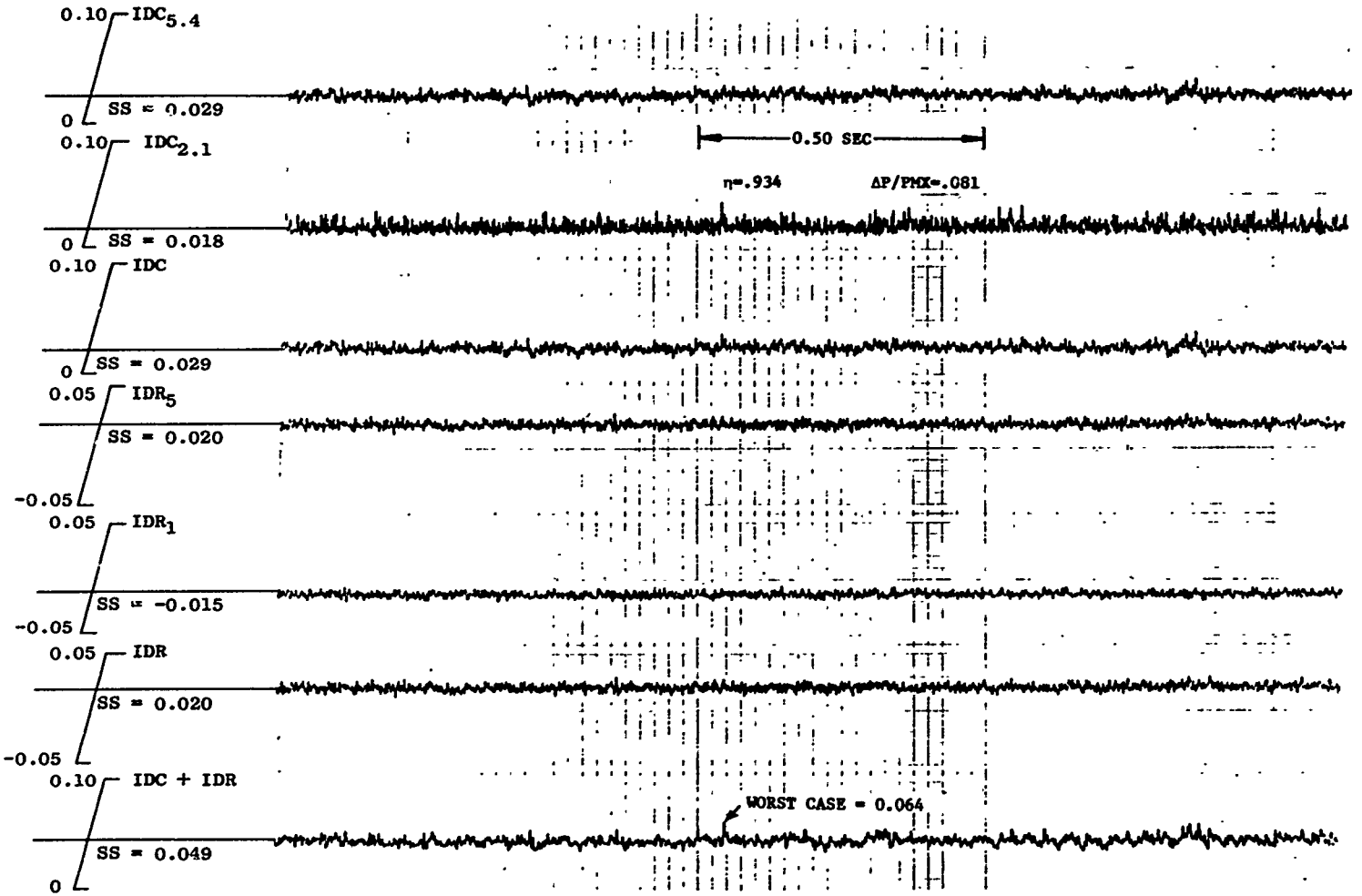

a) 0.22% Scale DDAS Inlet, 0-500 Hz

Figure 23. Distortion Vs. Time, M = 1.8, $\alpha \approx 1.5°$, Po $\approx$ 1300 psf, Small Gap.

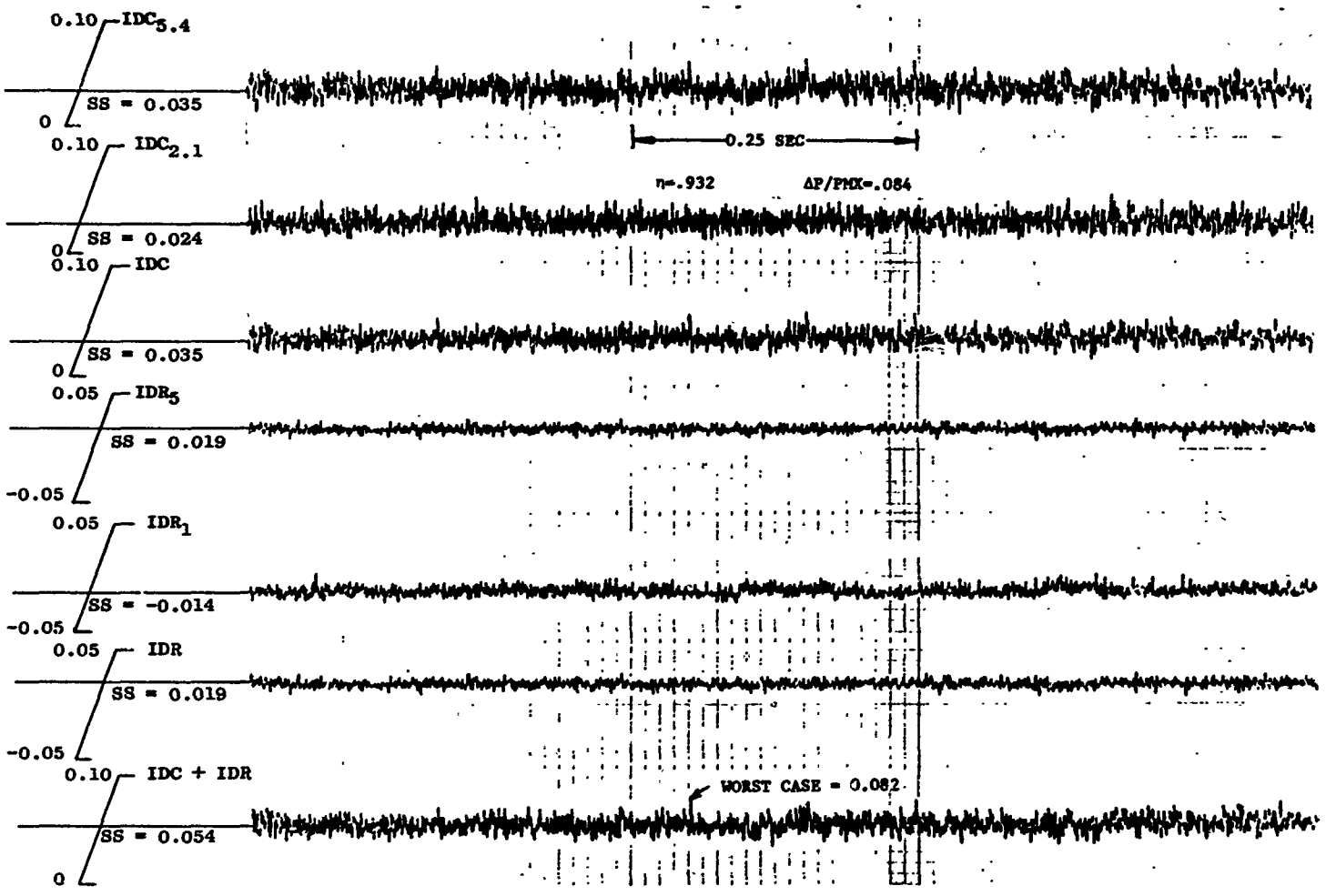

b) 0.125 Scale DDAS Inlet, 0-1000 Hz

Figure 23. Distortion Vs. Time, M = 1.8, $\alpha \approx 1.5°$, Po $\approx$ 1300 psf, Small Gap (Concluded).

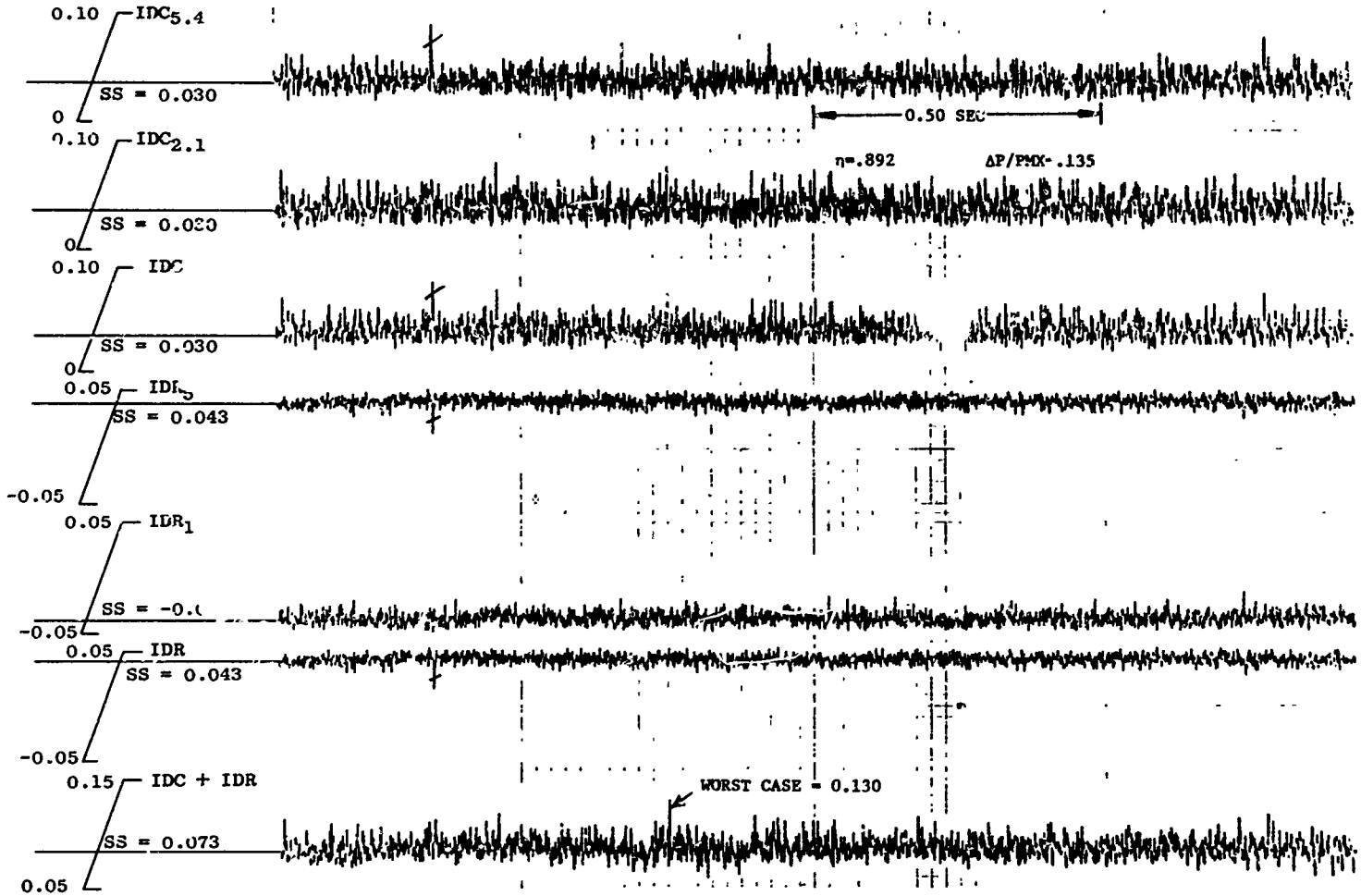

a) 0.228 Scale DDAS Inlet, 0-500 Hz.

Figure 24. Distortion Vs. Time, M = 1.8, $\alpha \approx 1.5°$, Po $\approx$ 1300 psf, Large Gap.

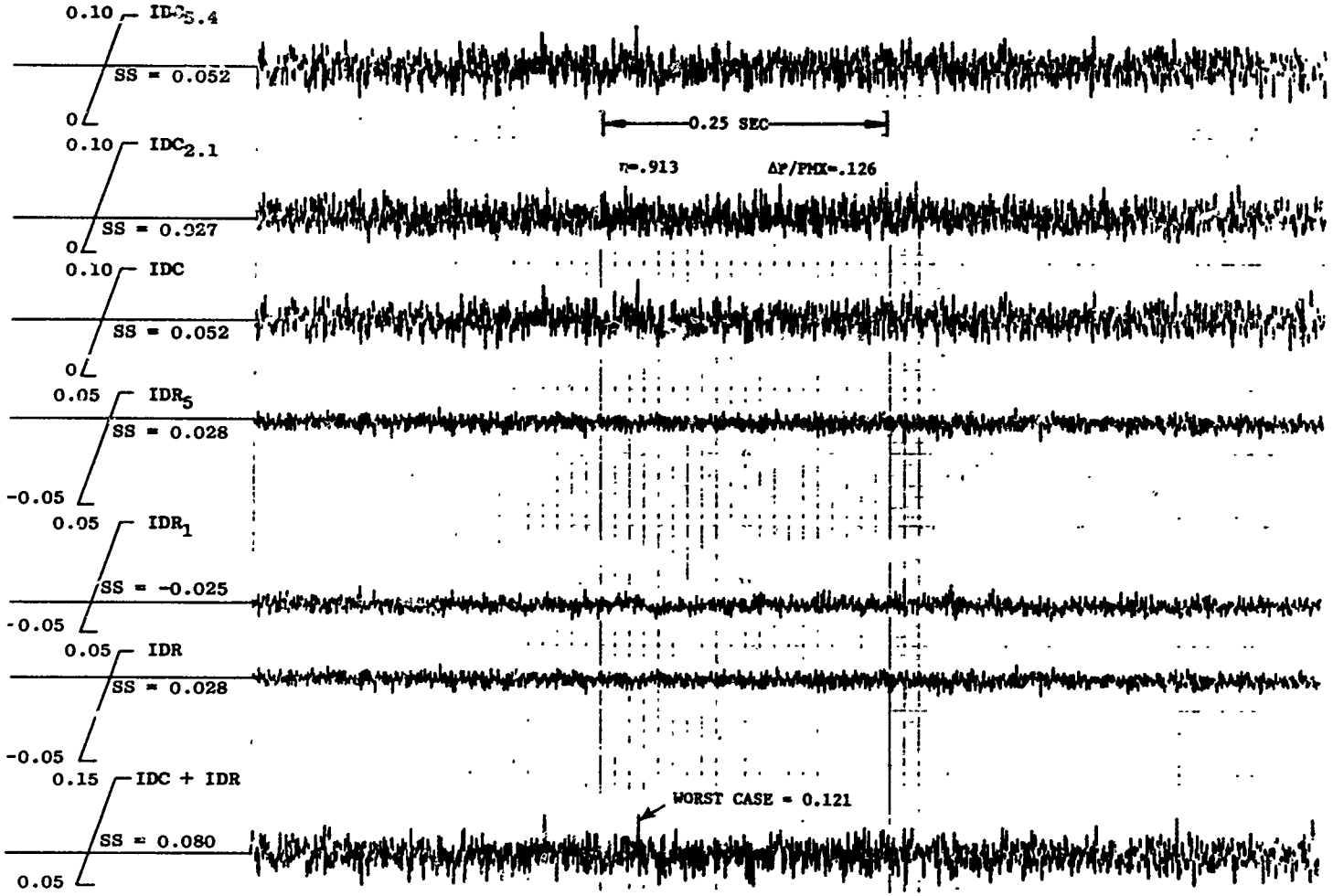

b) 0.125 Scale DDAS Inlet, 0-1000 Hz

Figure 24. Distortion Vs. Time, M = 1.8, $\alpha \approx 1.5°$, Po $\approx$ 1300 psf, Large Gap (Concluded).

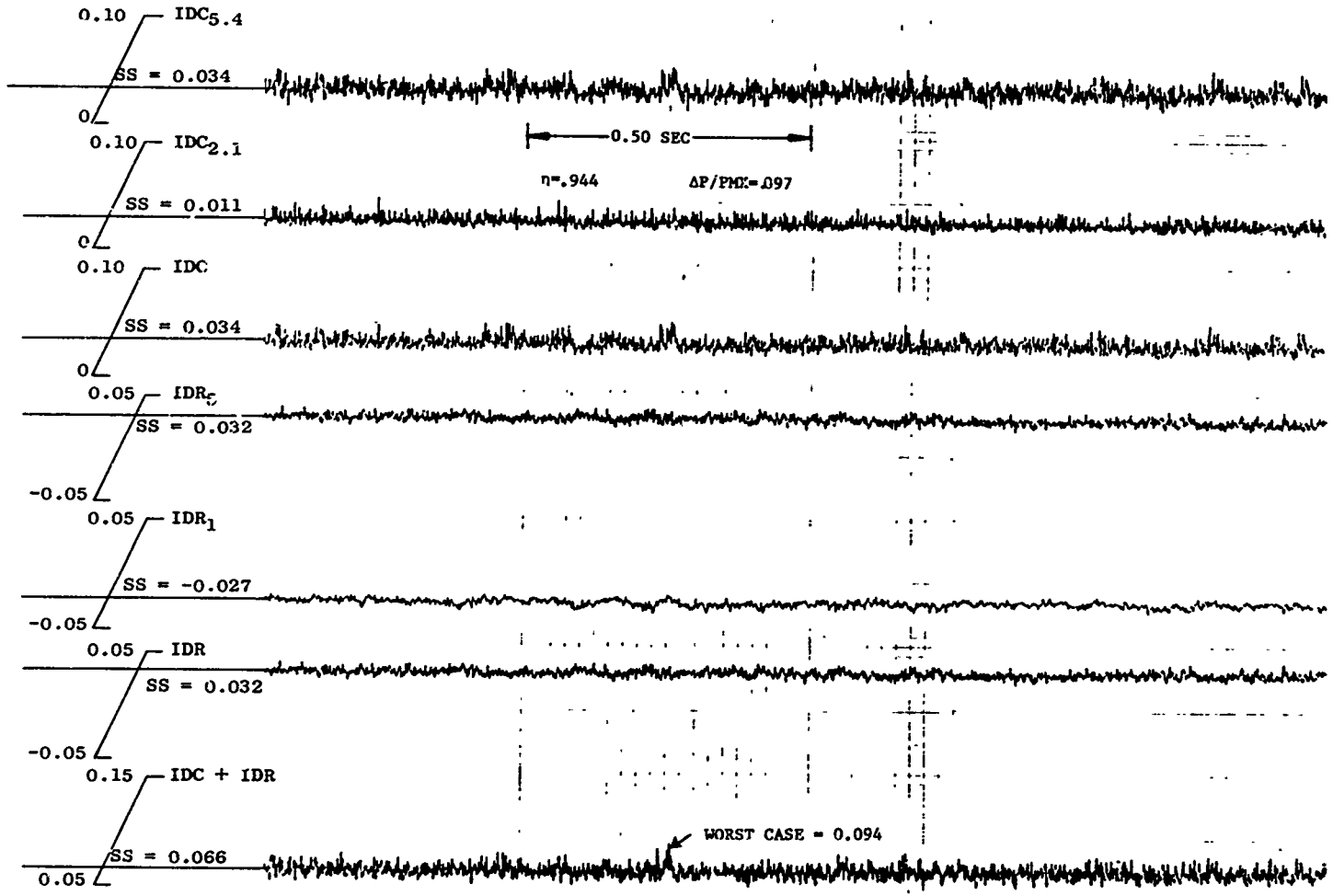

a) 0.228 Scale DDAS Inlet, 0-500 Hz

Figure 25. Distortion Vs. Time, M = 1.6, $\alpha \approx 1.5°$, Po $\approx$ 1100 psf, Large Gap.

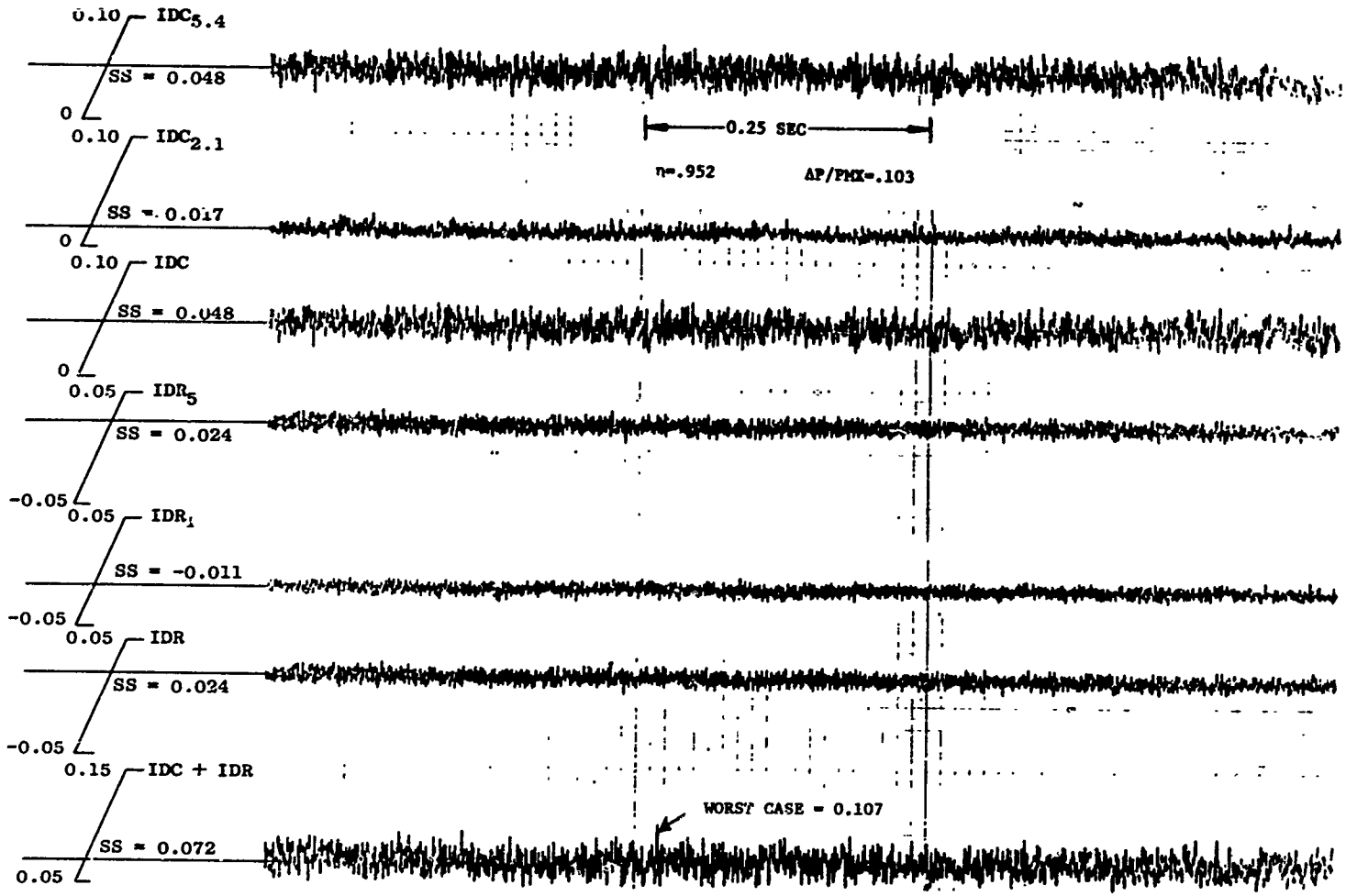

b) 0.125 Scale DDAS Inlet, 0-1000 Hz

Figure 25. Distortion Vs. Time, M = 1.6, $\alpha \approx 1.5°$, Po $\approx$ 1100 psf, Large Gap (Concluded).

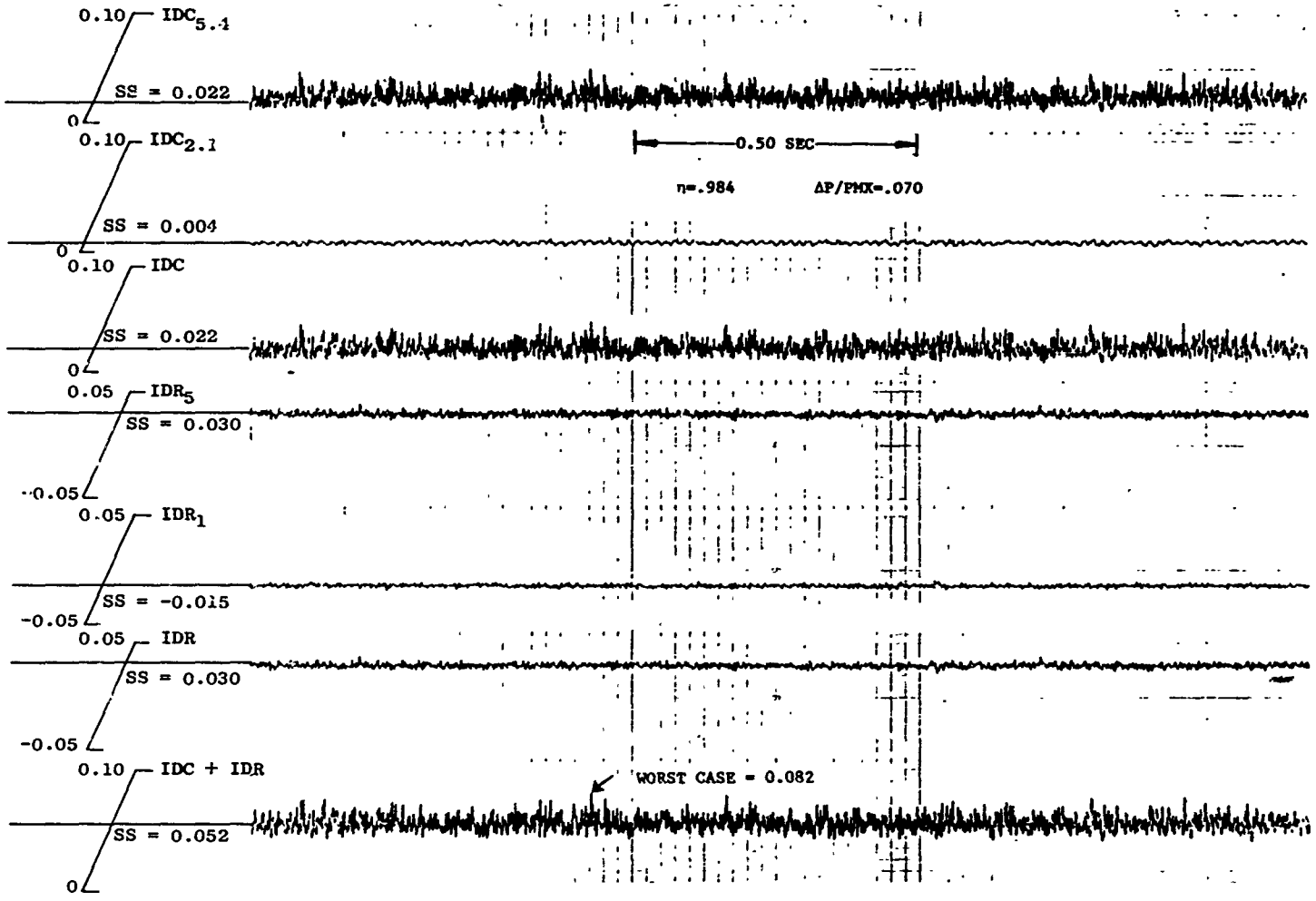

a) 0.228 Scale DDAS Inlet, 0-500 Hz

Figure 26. Distortion Vs. Time, M - 1.2, $\alpha \approx 7°$, Po $\approx$ 1700 psf, Large Gap.

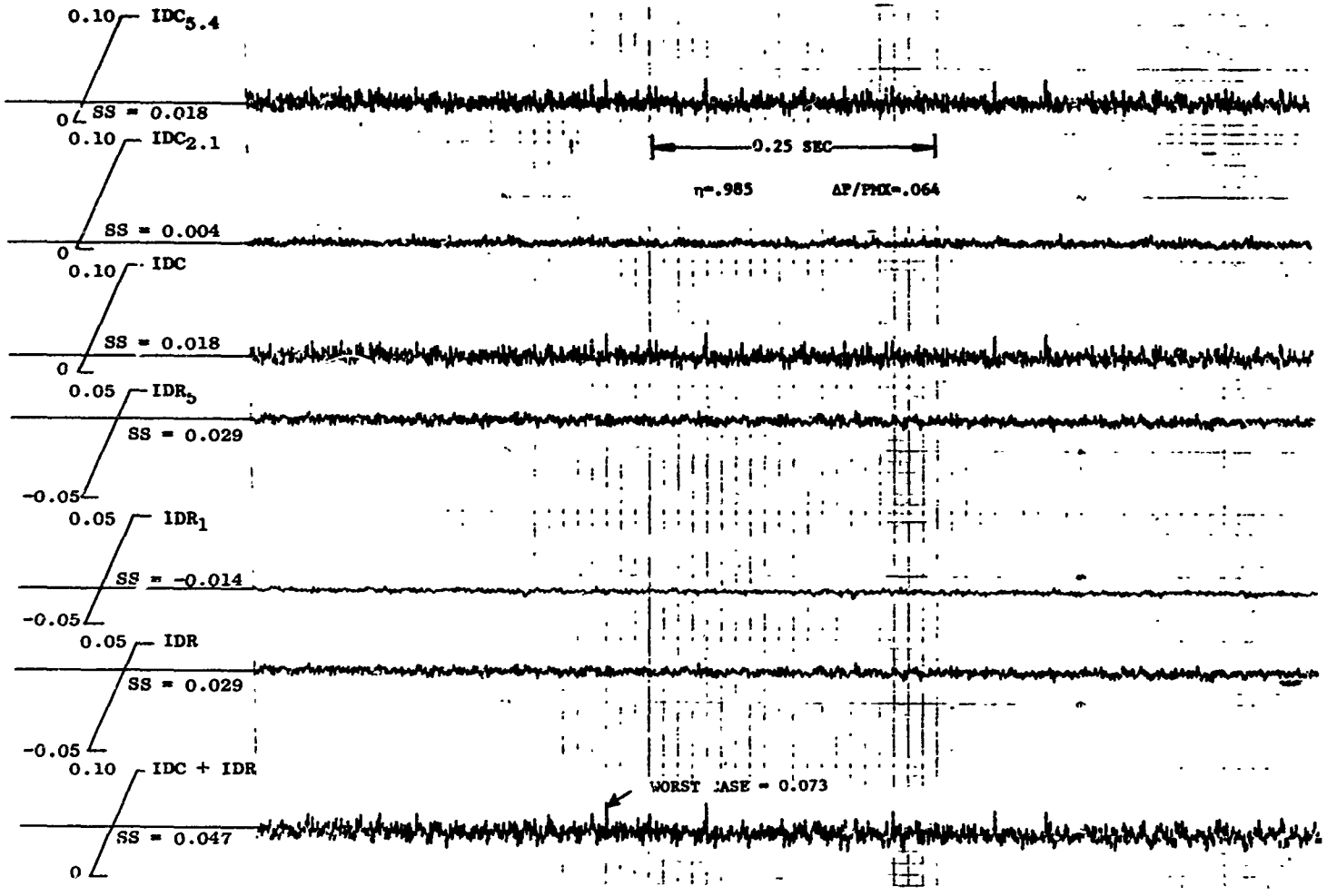

b) 0.125 Scale DDAS Inlet, 0-1000 Hz

Figure 26. Distortion Vs. Time, M = 1.2, $\alpha \approx 7°$, Po $\approx$ 1700 psf, Large Gap (Concluded).

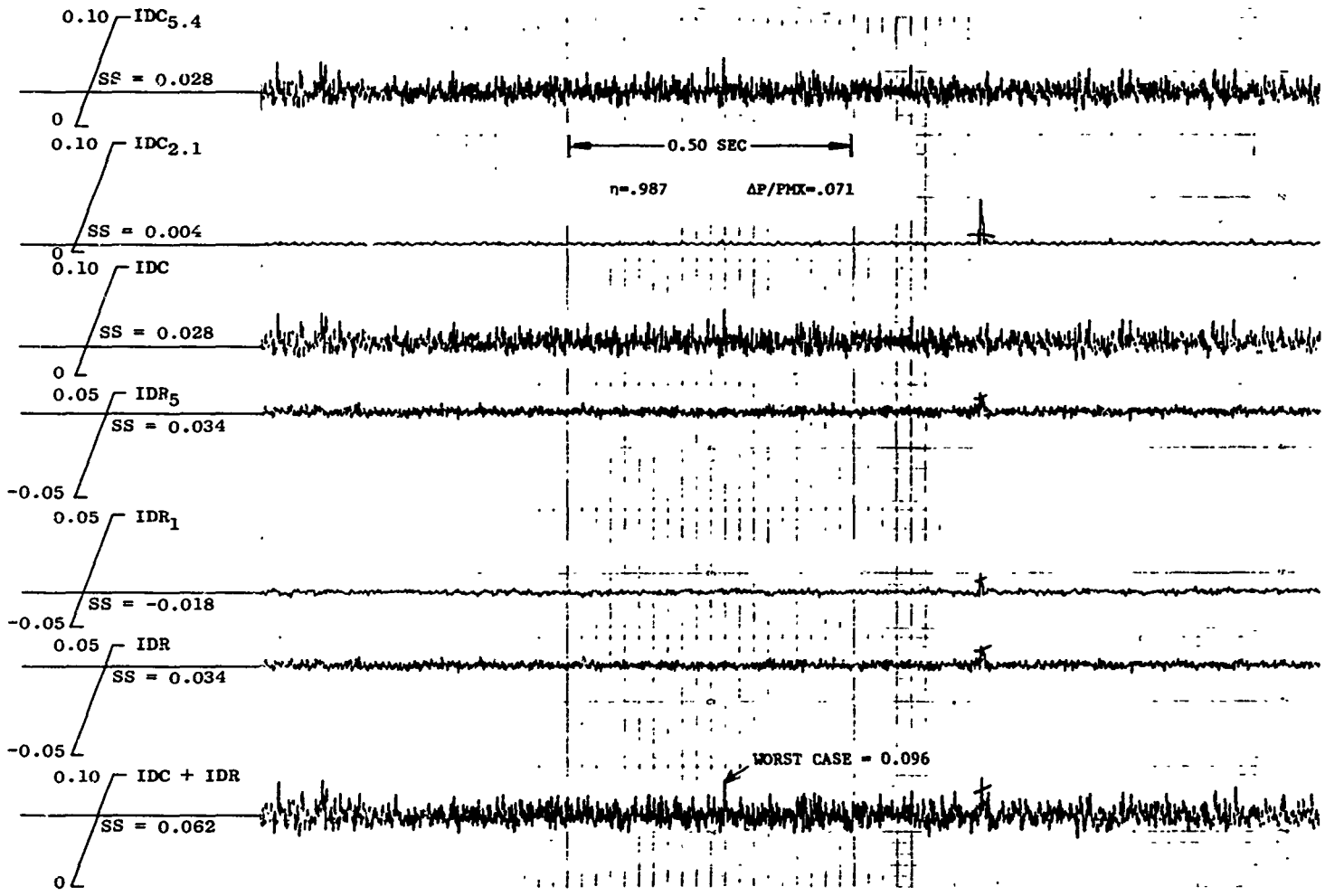

a) 0.228 Scale DDAS Inlet, 0-500 Hz

Figure 27. Distortion Vs. Time, M = 0.9, $\alpha \approx 1.5°$, Po $\approx$ 2200 psf, Large Gap.

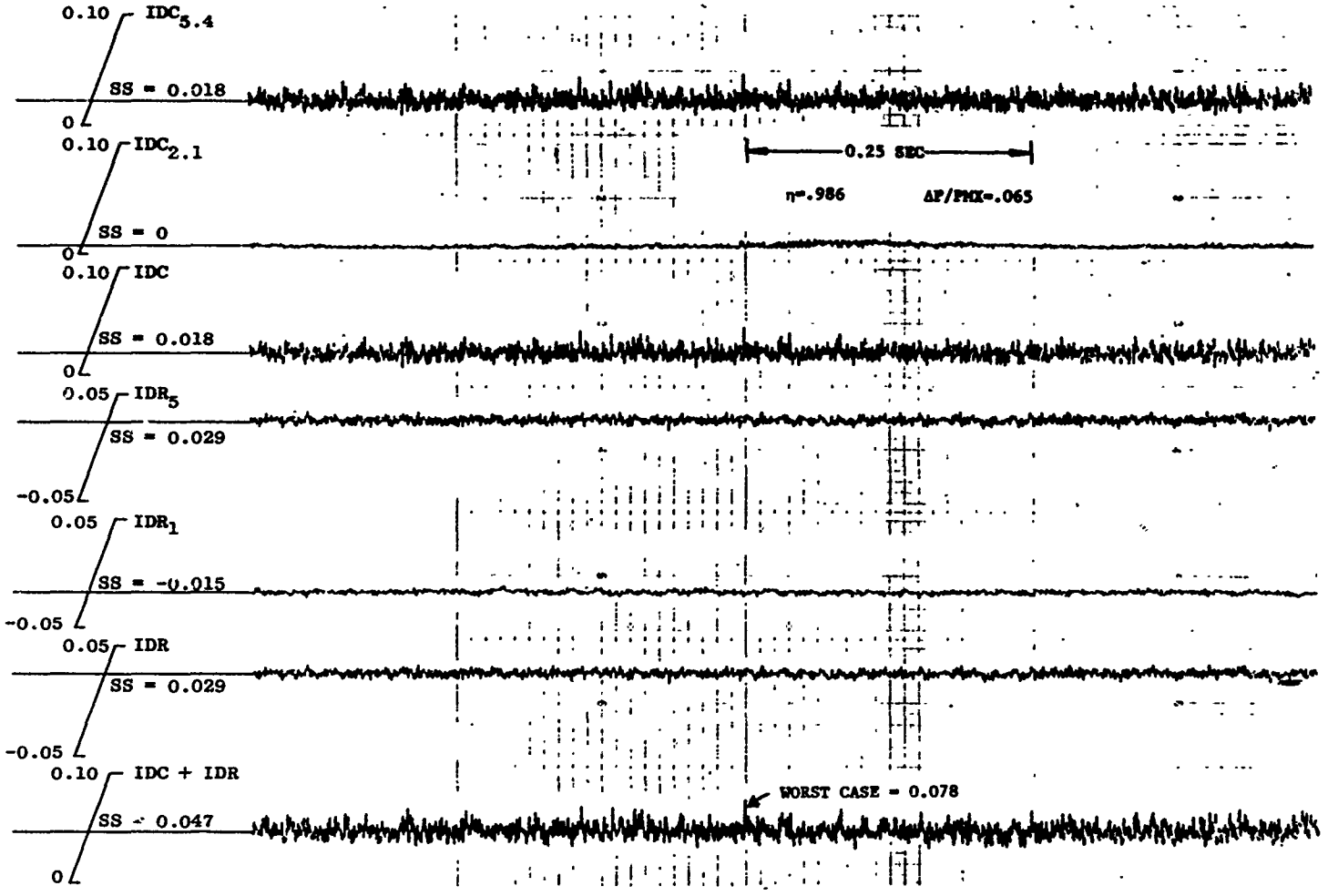

b) 0.125 Scale DDAS Inlet, 0-1000 Hz

Figure 27. Distortion Vs. Time, M = 0.9, $\alpha \approx 1.5°$, Po $\approx$ 2200 psf, Large Gap (Concluded).

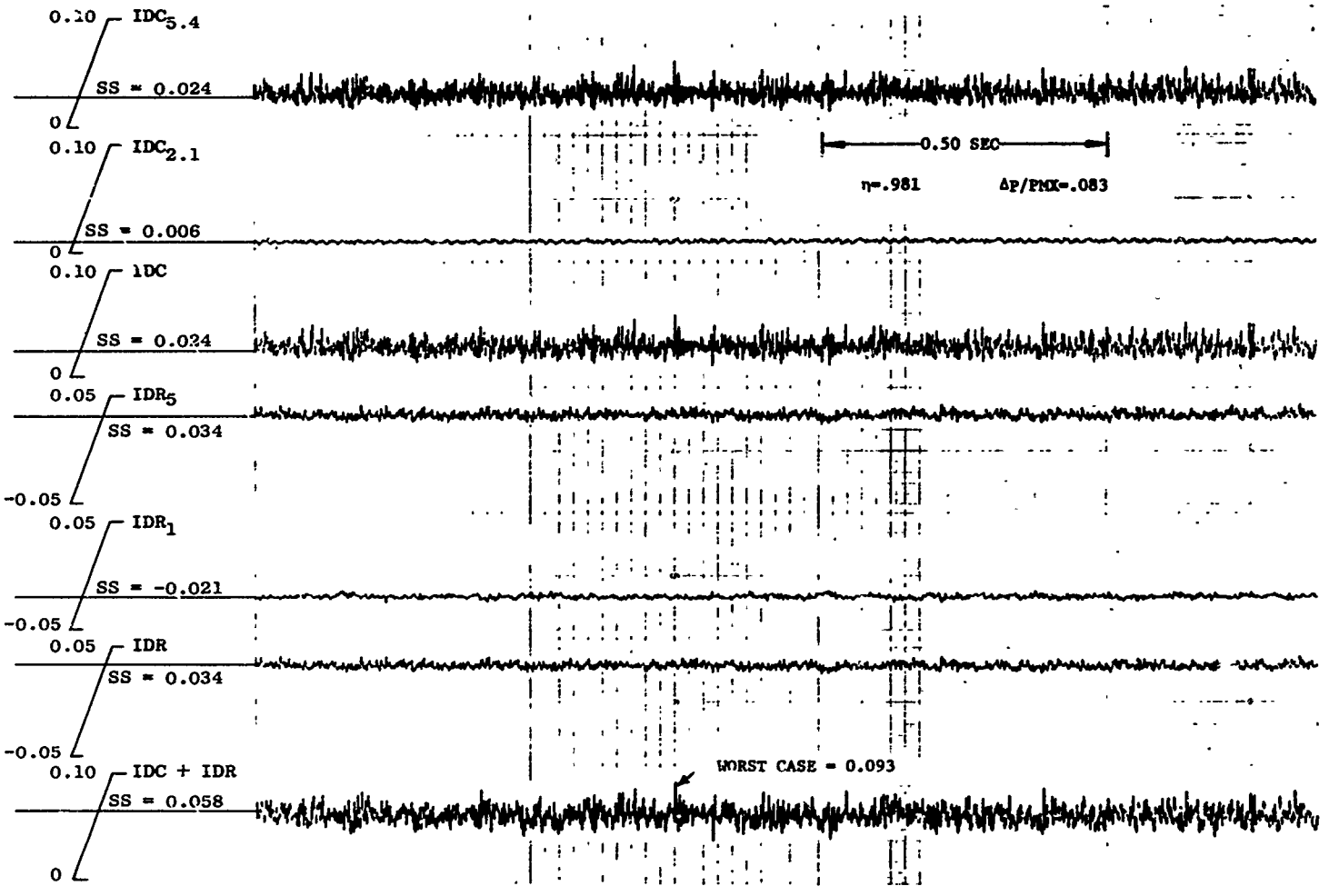

a) 0.228 Scale DDAS Inlet, 0-500 Hz

Figure 28. Distortion Vs. Time, M = 0.9, $\alpha \approx 1.5°$, Po $\approx$ 1000 psf, Large Gap.

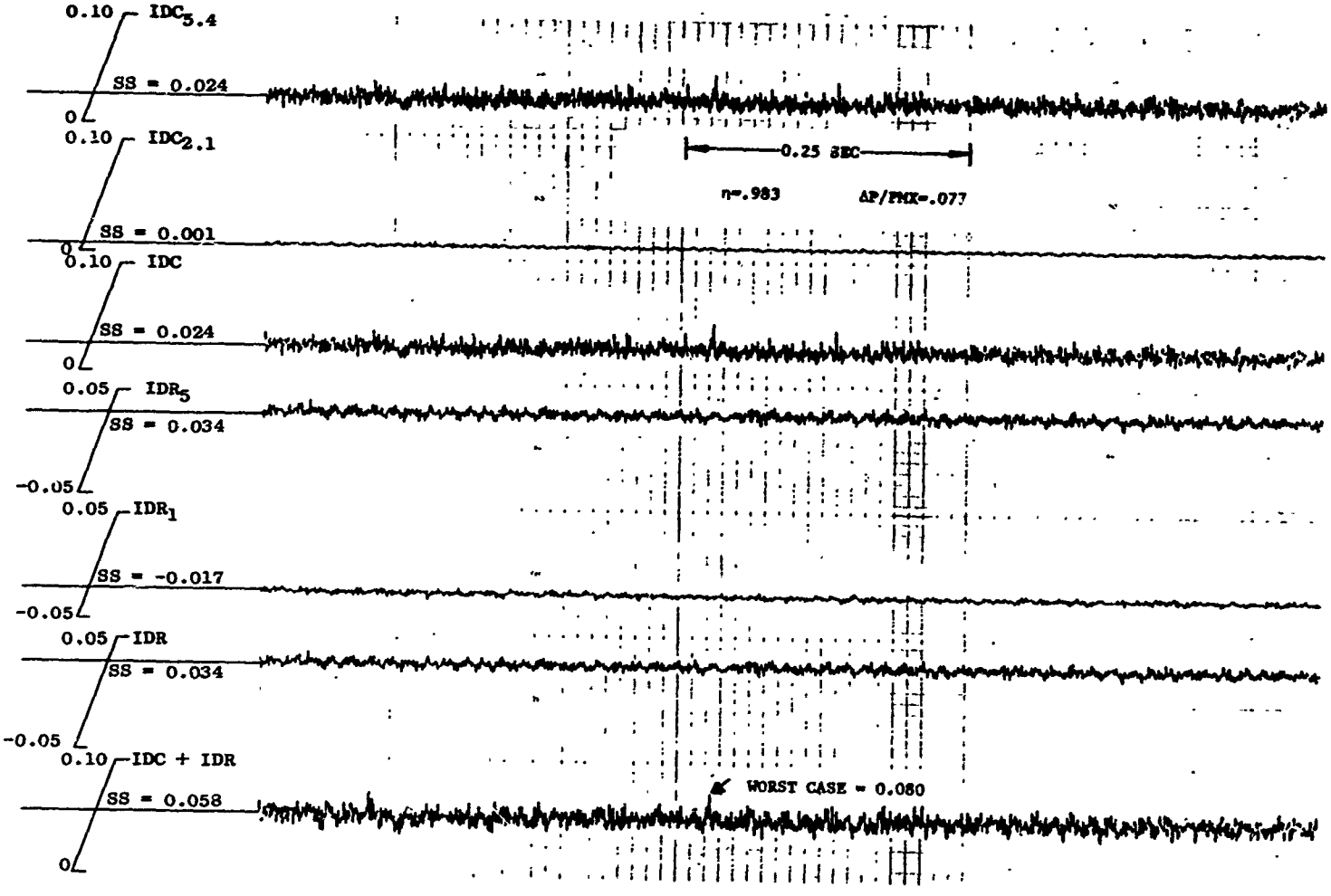

b) 0.125 Scale DDAS Inlet, 0-1000 Hz

Figure 28. Distortion Vs. Time, M = 0.9, $\alpha \approx 1.5°$, Po $\approx$ 1000 psf, Large Gap (Concluded).

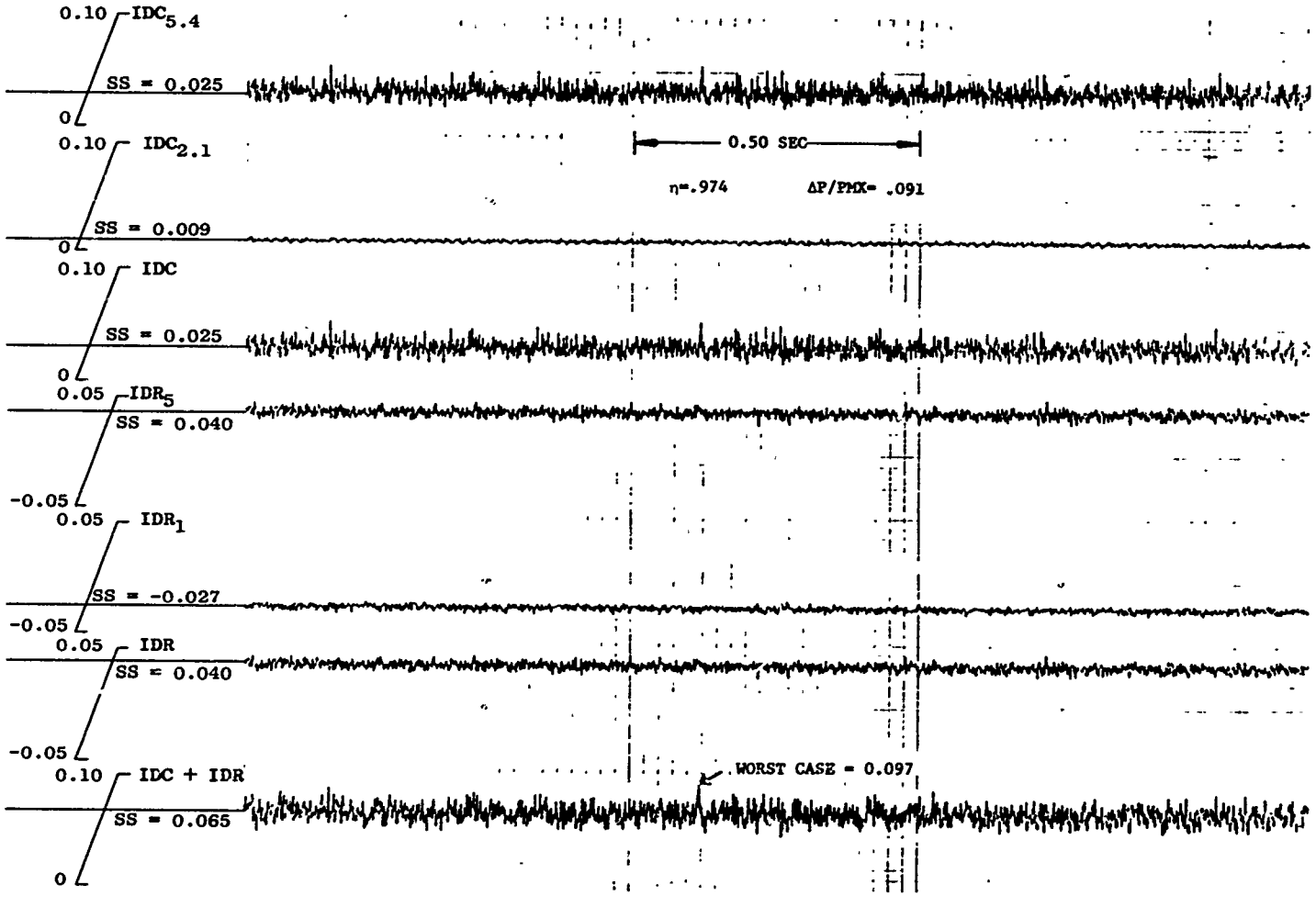

a) 0.228 Scale DDAS Inlet, 0-500 Hz, Po = 1000 psf

Figure 29. Distortion Vs. Time, M = 0.9, $\alpha \approx 5°$, Po ≈ Increasing, Large Gap.

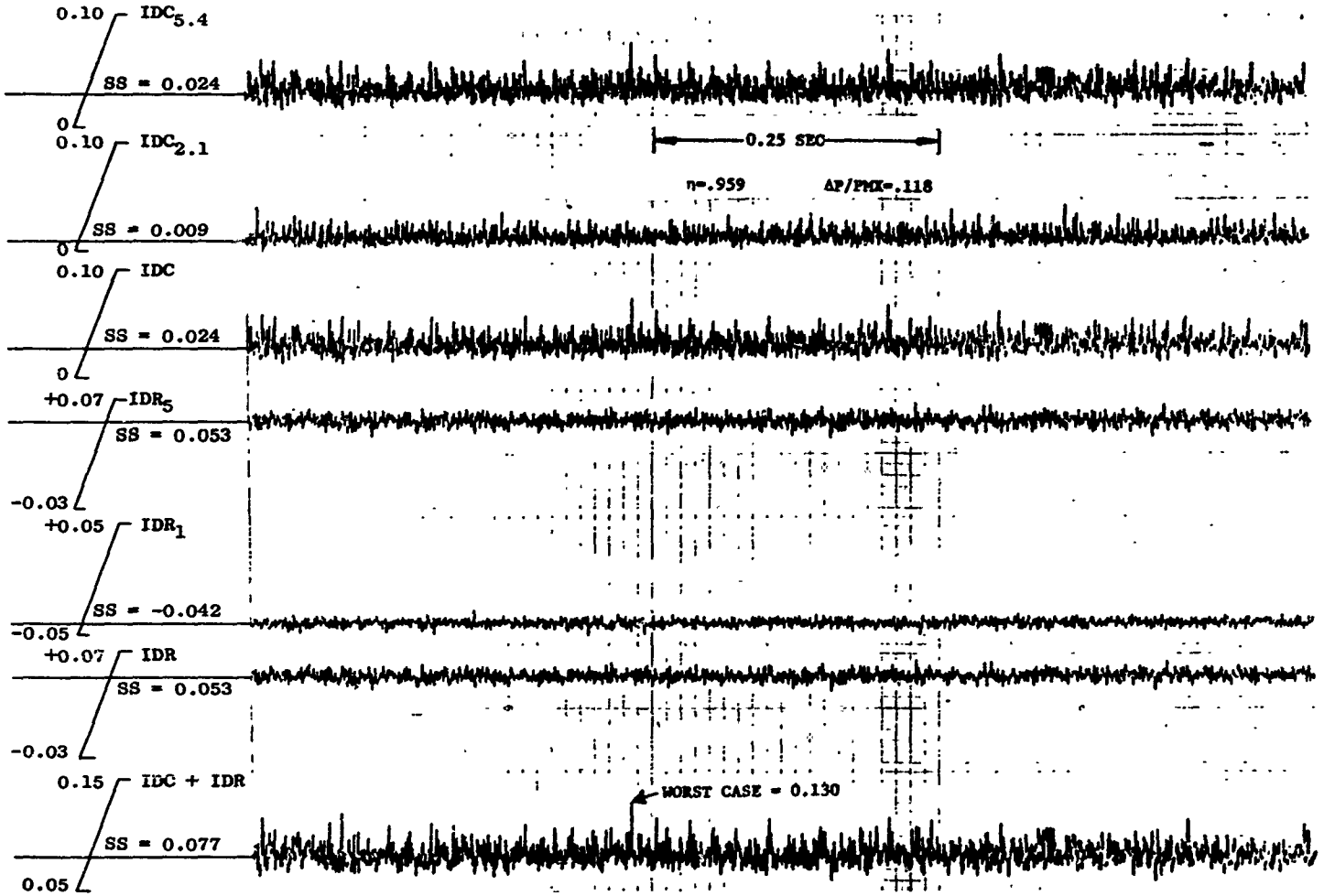

b) 0.125 Scale DDAS Inlet, 0-1000 Hz, Po = 2000 psf

Figure 29. Distortion Vs. Time, M = 0.9, $\alpha \approx 5°$, Po ≈ Increasing, Large Gap (Concluded).

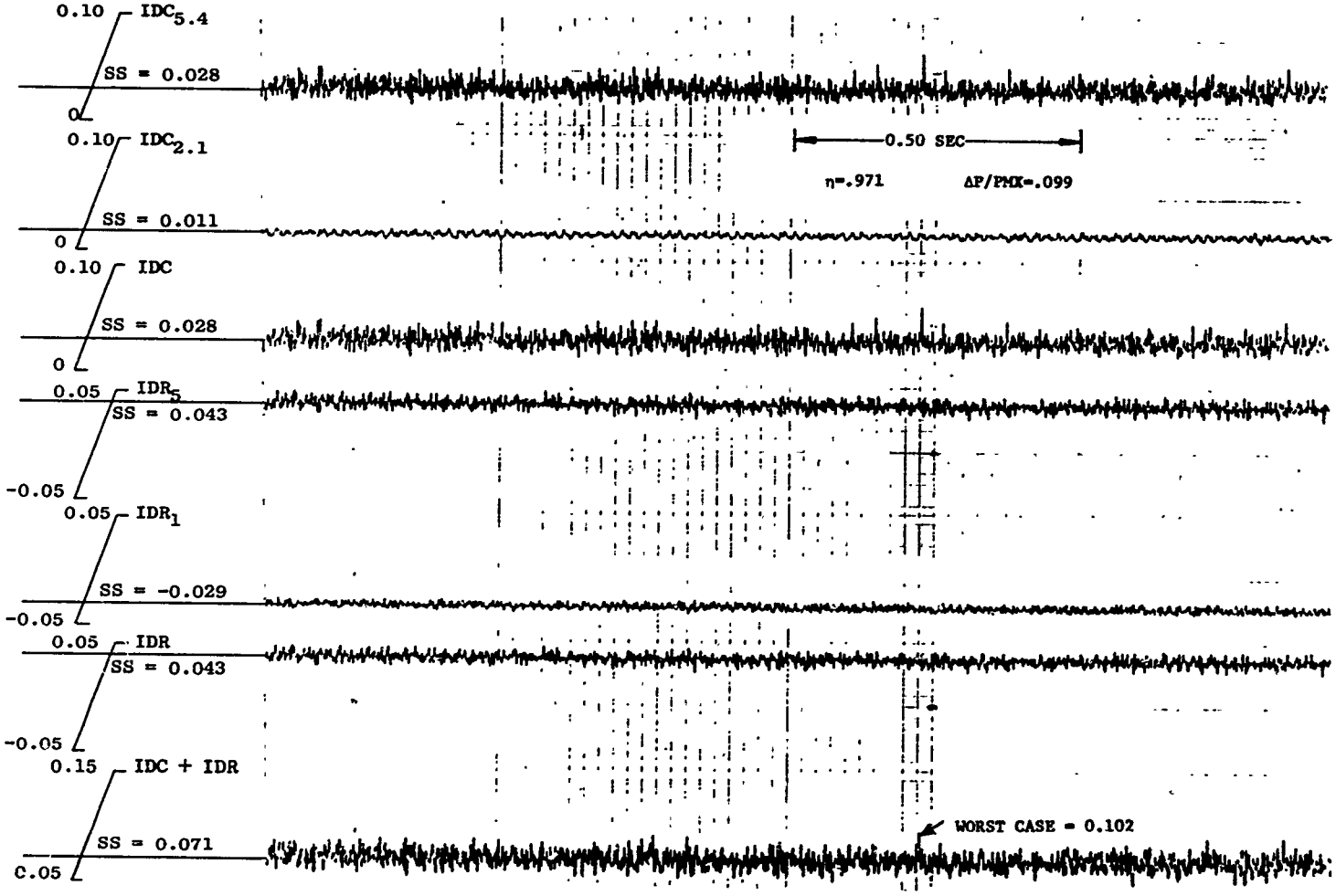

a) 0.228 Scale DDAS Inlet, 0-500 Hz

Figure 30. Distortion Vs. Time, M = 0.9, $\alpha \approx 5^{\circ}$, Po $\approx$ 500 psf, Large Gap.

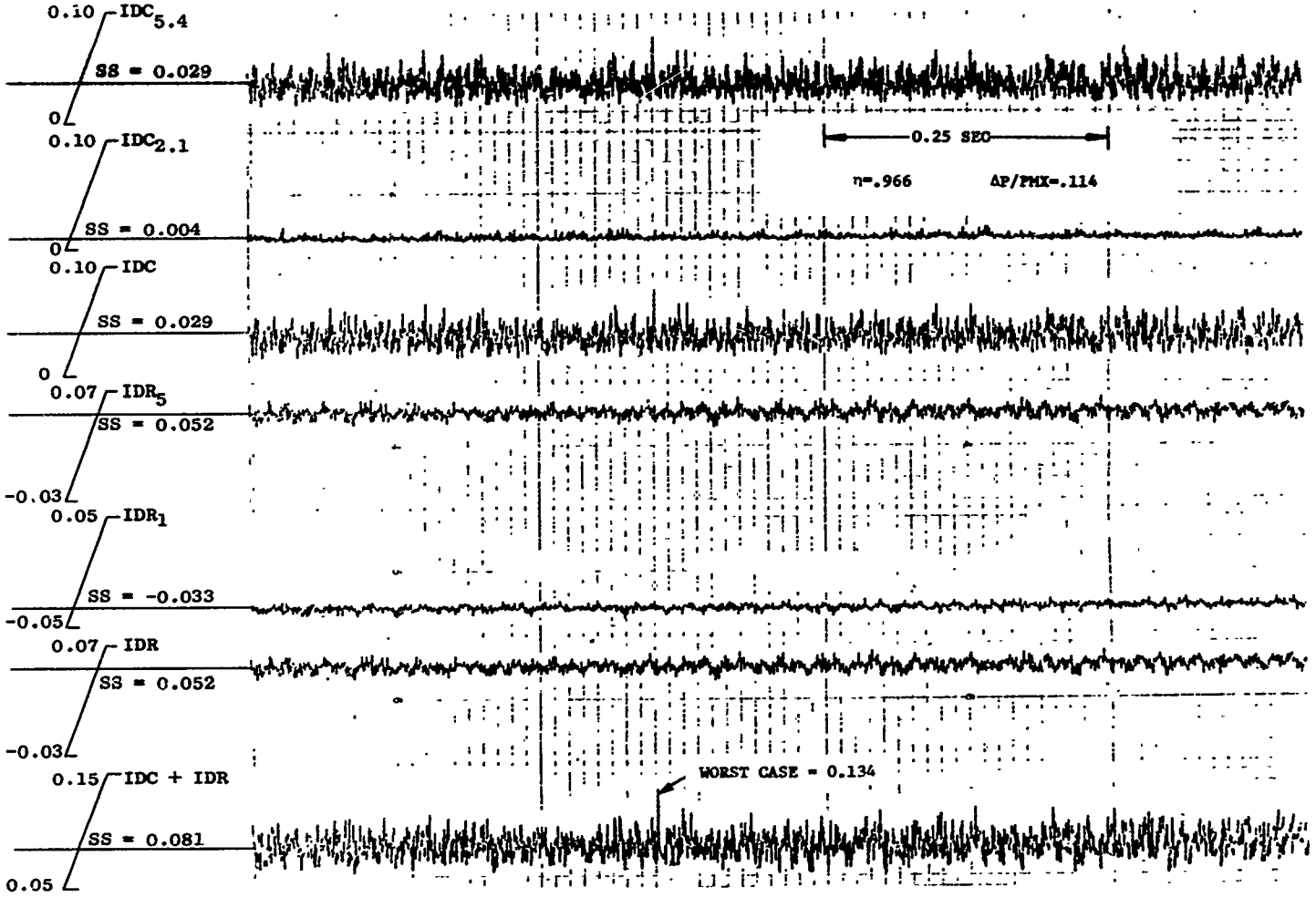

b) 0.125 Scale DDAS Inlet, 0-1000 Hz

Figure 30. Distortion Vs. Time, M = 0.9, $\alpha \approx 5°$, Po $\approx$ 500 psf, Large Gap (Concluded).

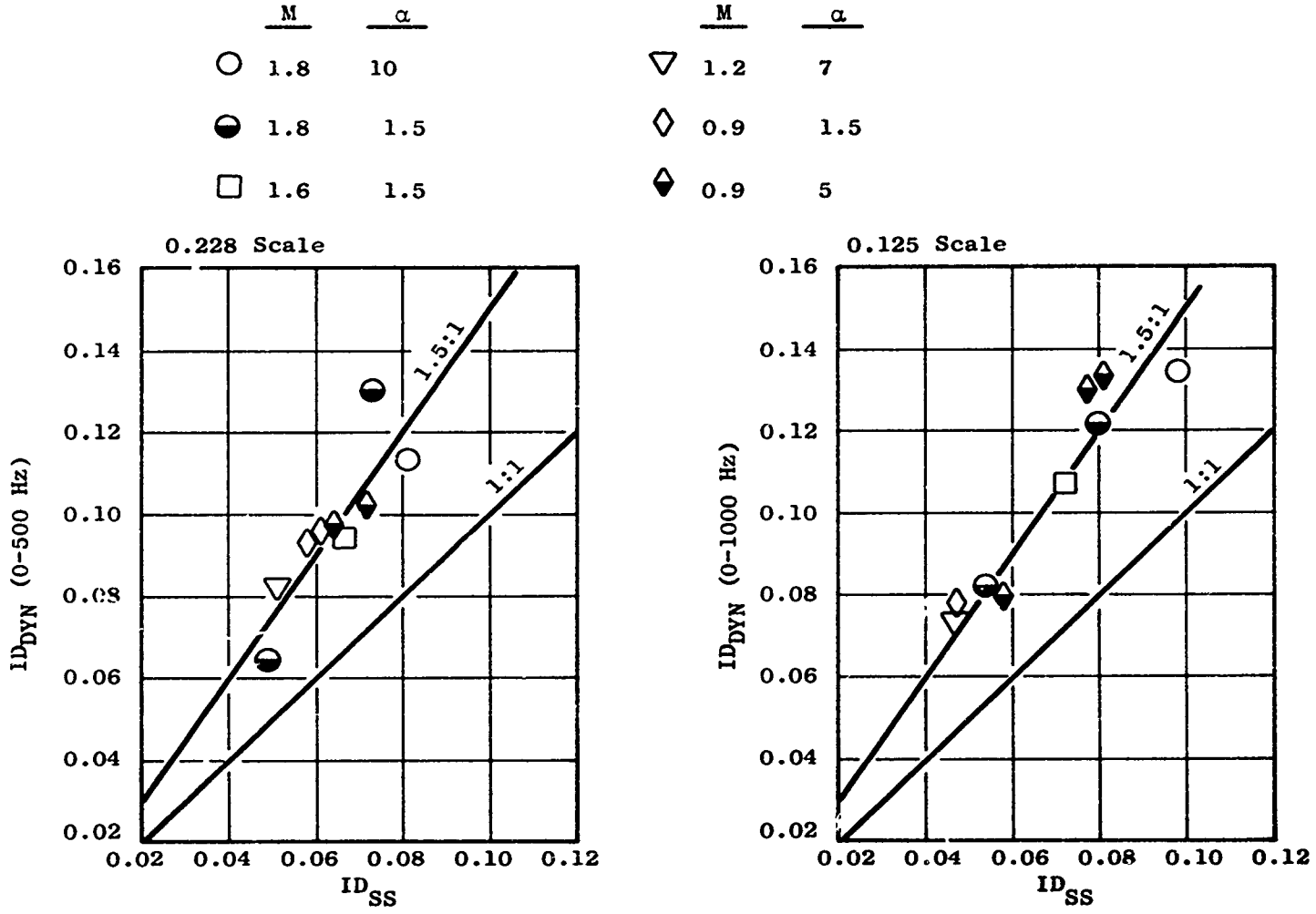

Figure 31. Peak Vs. Steady-State Distortion Levels from Analog Analysis for DDAS Inlet Models.

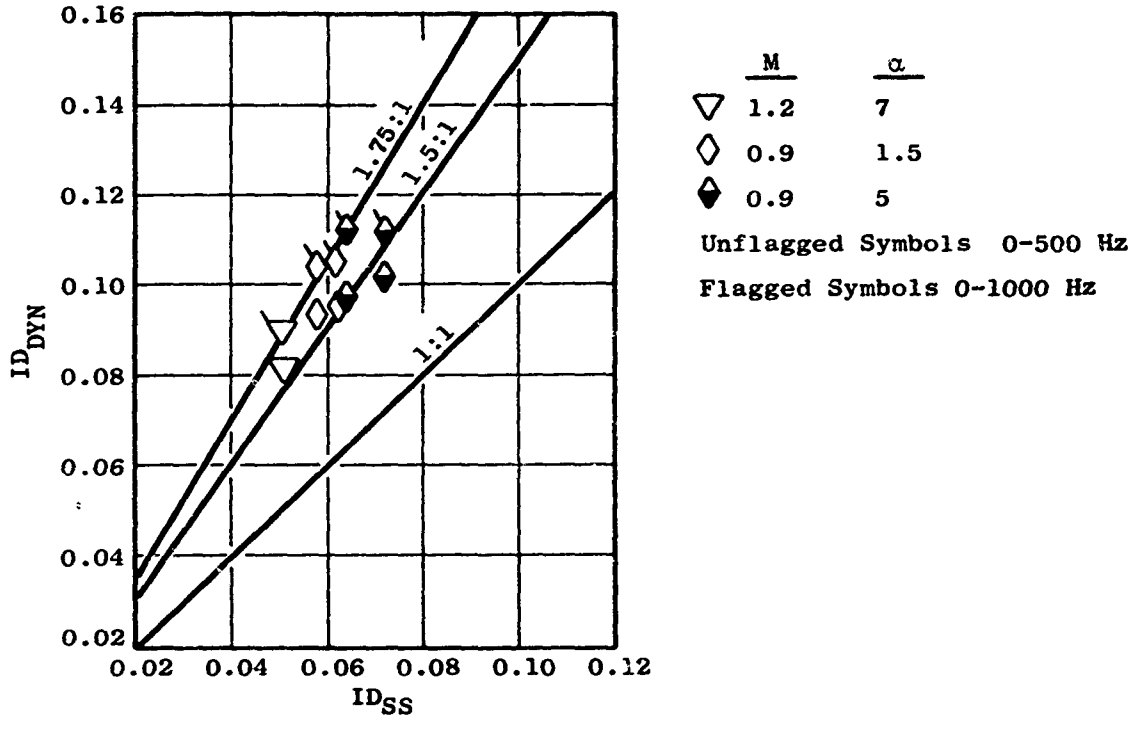

Figure 32. Peak Vs. Steady-State Distortion Levels from Analog Analysis for 0.228 Scale DDAS Inlet.

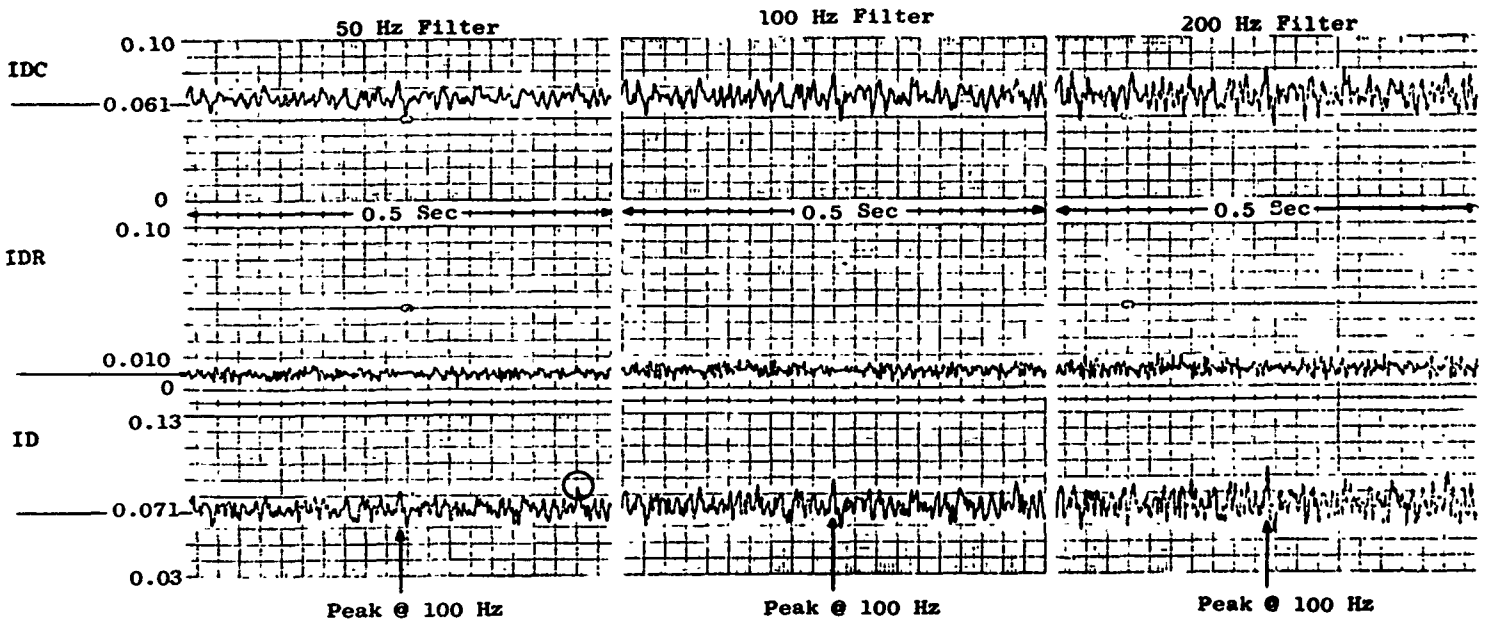

Figure 33. Distortion Vs. Time, M = 1.8, α = 11°, Small Gap, Full-Scale DDAS Inlet.

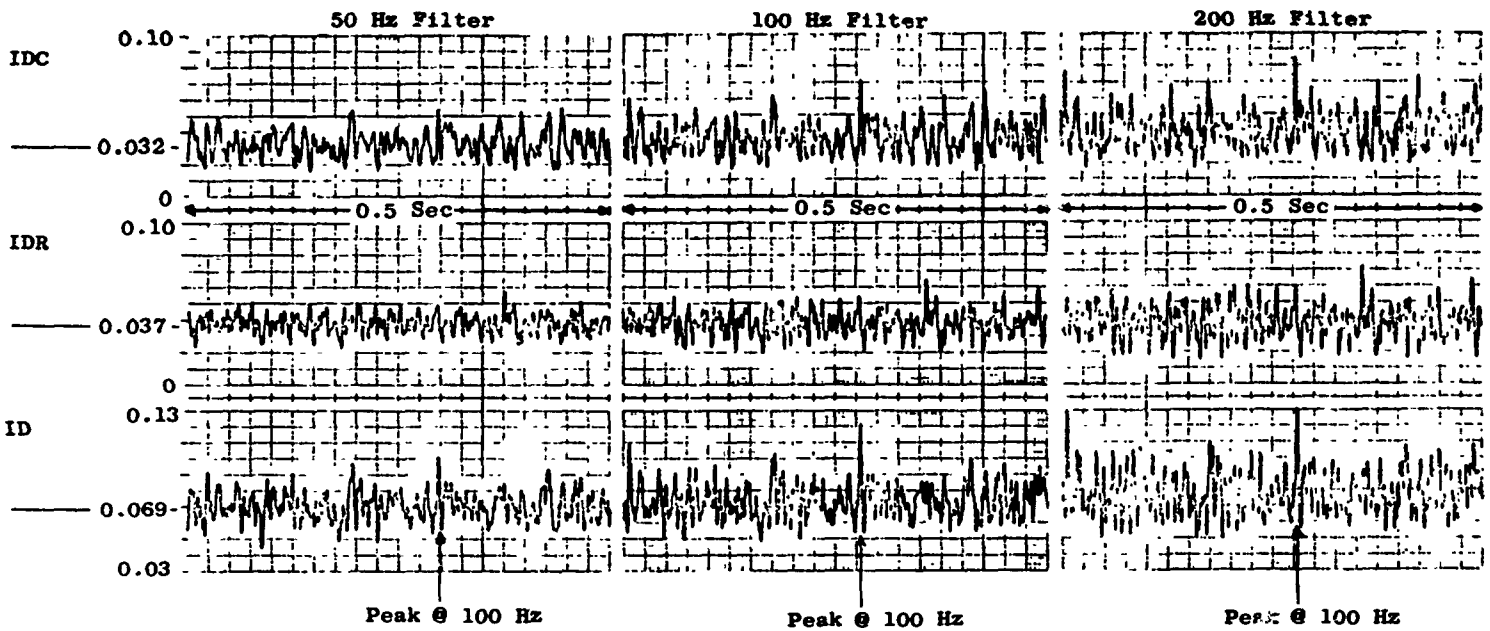

Figure 34. Distortion Vs. Time, M = 1.8, α = 2.5°, Large Gap, Full-Scale DDAS Inlet.

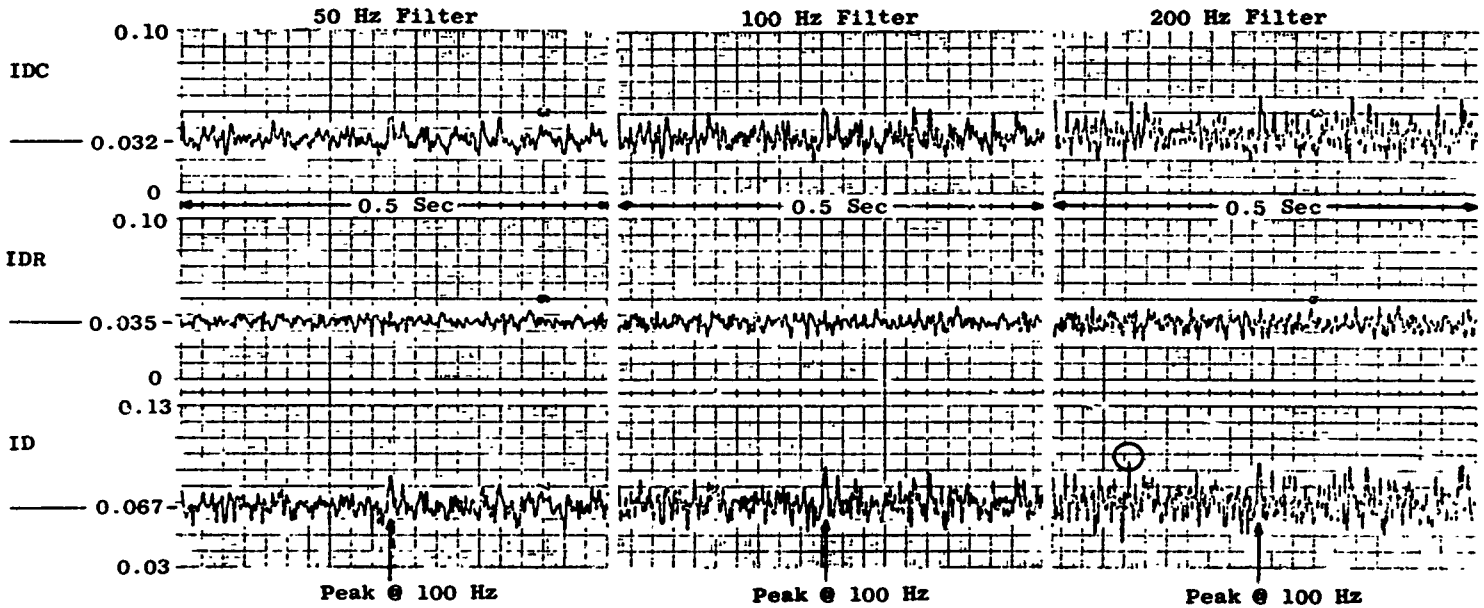

Figure 35. Distortion Vs. Time, M = 1.6, α = 2.5°, Large Gap, Full-Scale DDAS Inlet.

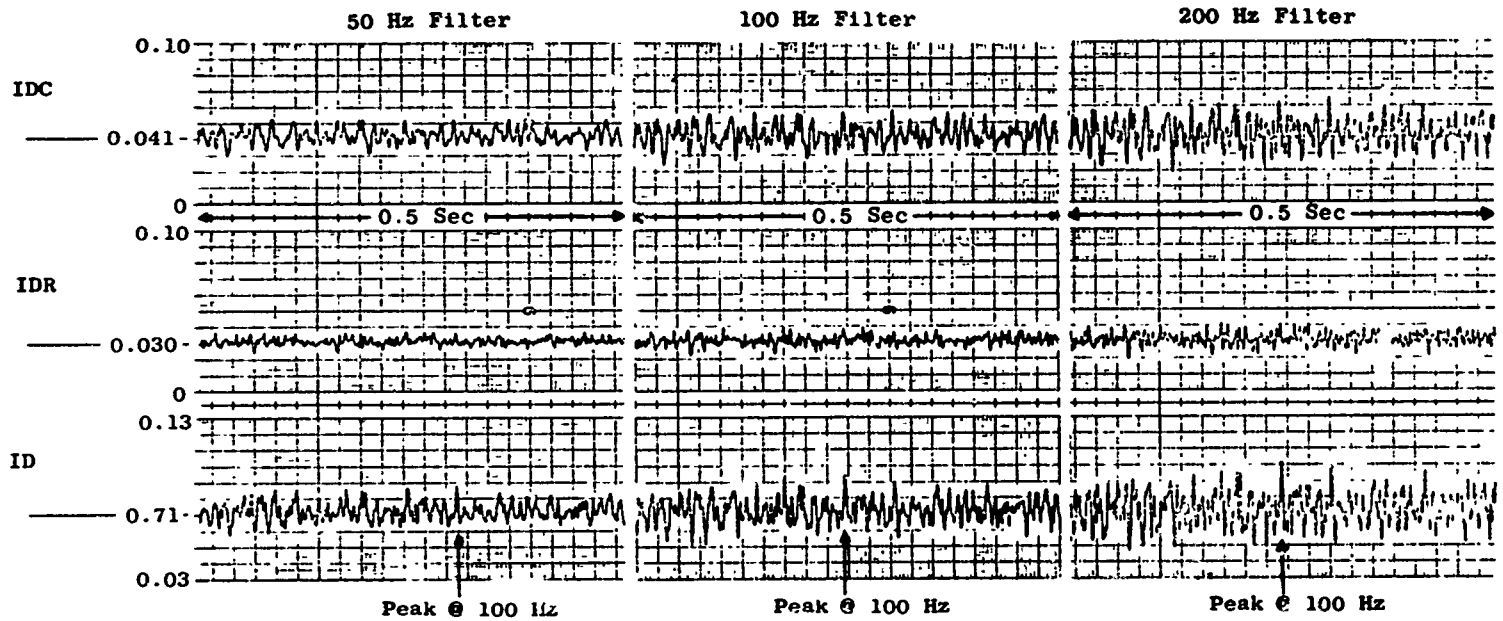

Figure 36. Distortion Vs. Time, M = 0.9, α = 5.5°, Large Gap, Full-Scale DDAS Inlet.

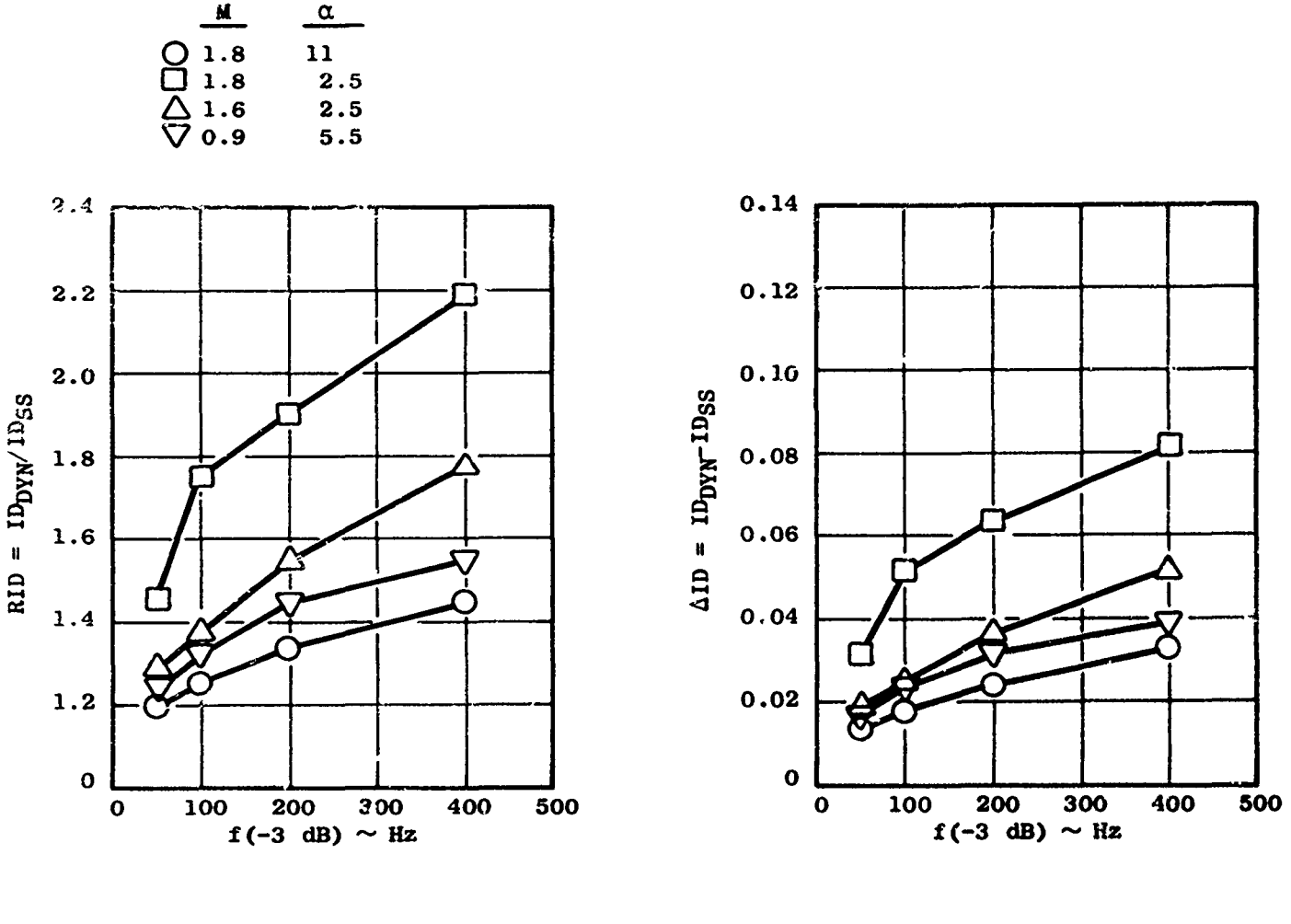

Figure 37. Filter Effects on Dynamic Distortion for Full-Scale DDAS Inlet Data.

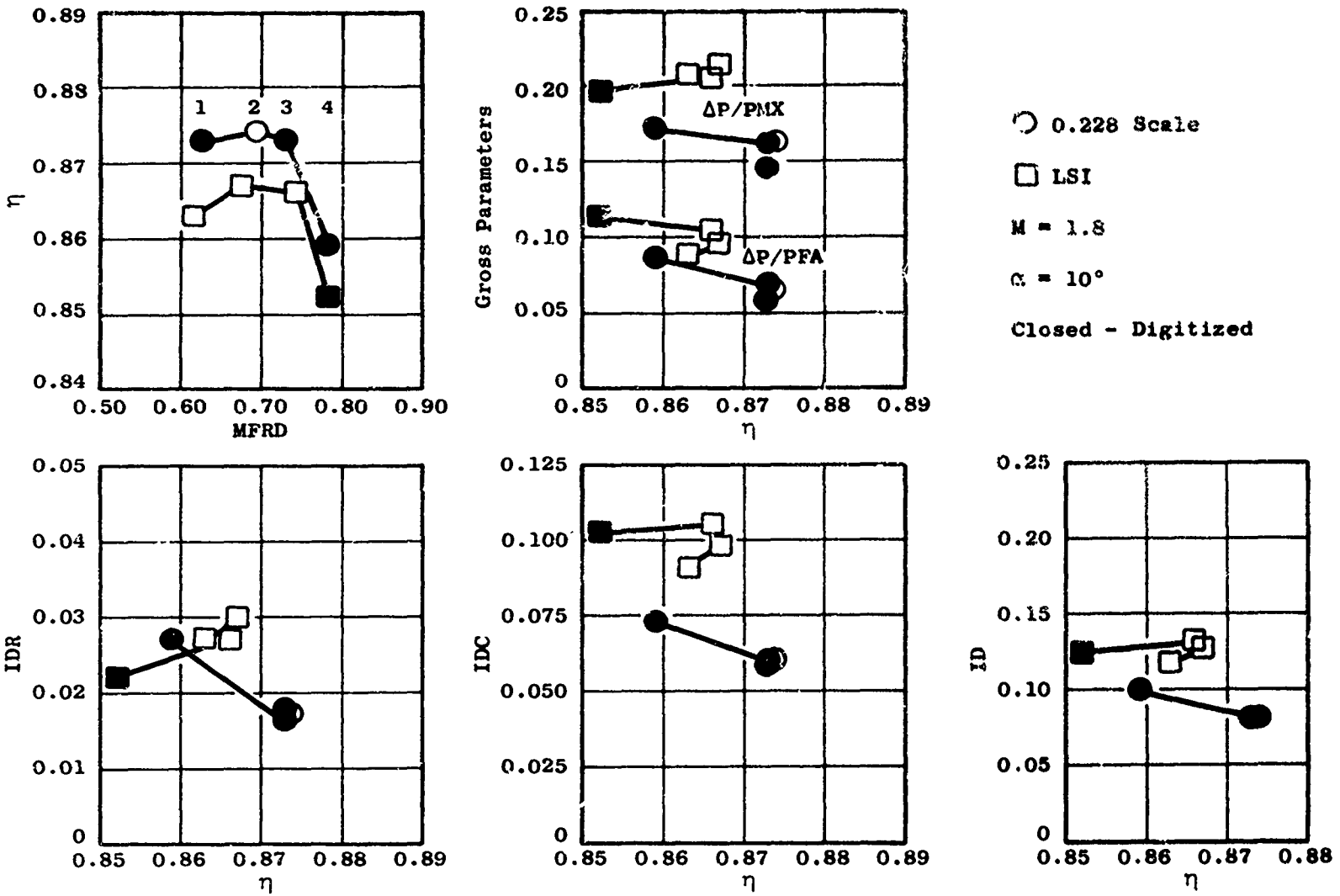

Figure 38. Recovery and Distortion Characteristics for 0.228 Scale DMAS Inlet and LSI.

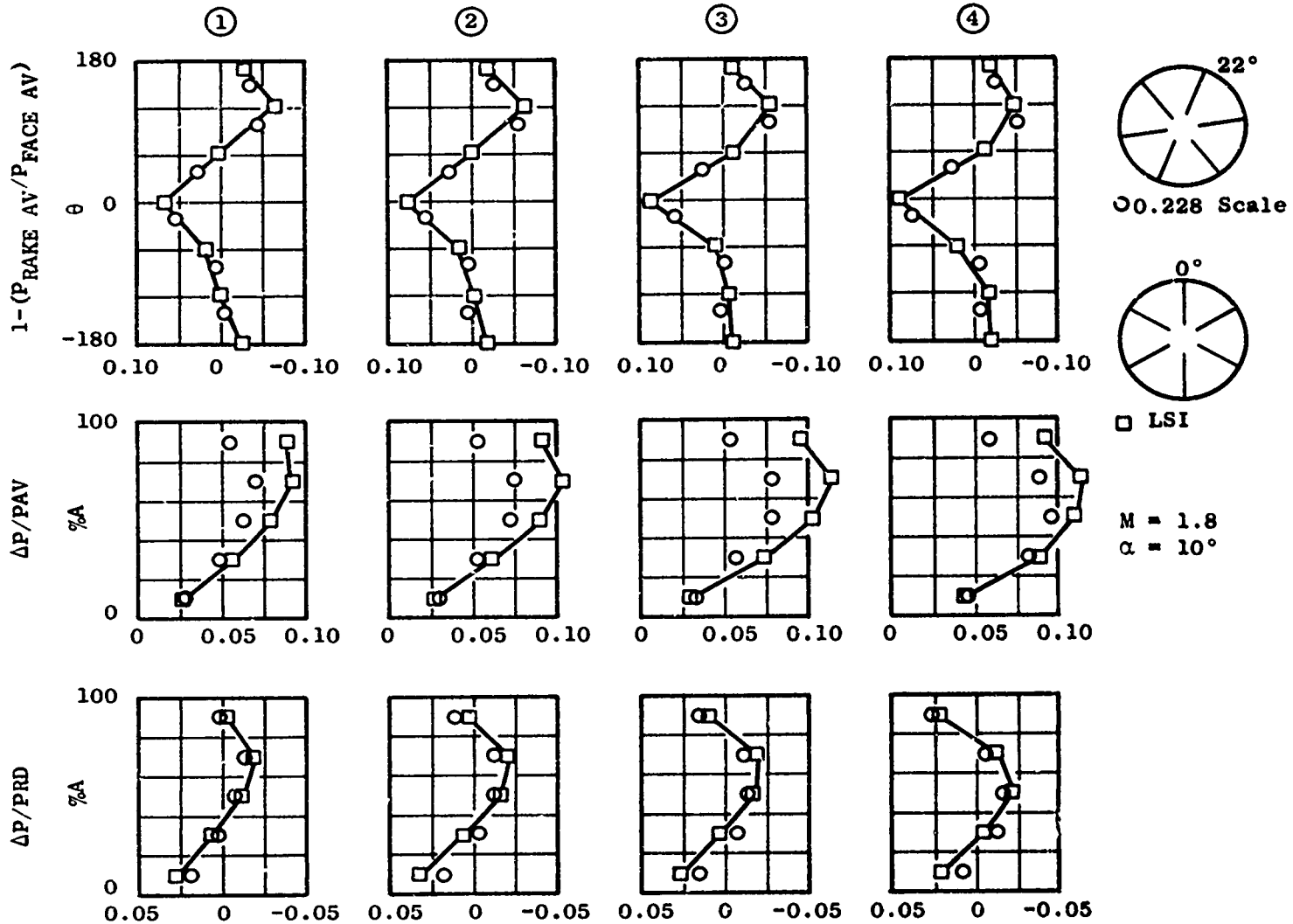

Figure 39. Mass Flow Effects on Steady-State Distortion for 0.228 Scale DDAS Inlet and LSI.

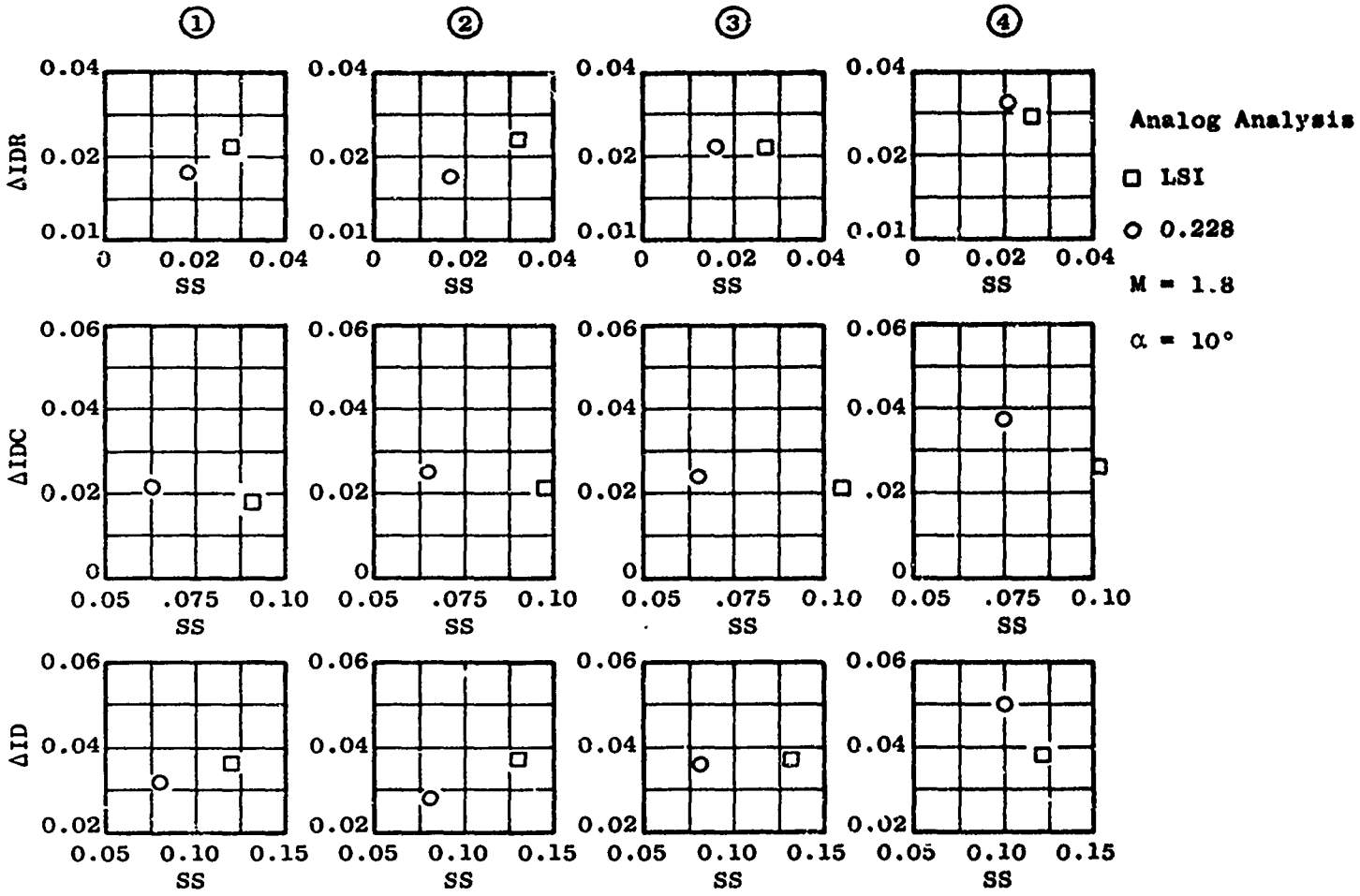

Figure 40. Mass Flow Effects on Dynamic Distortion for 0.228 Scale DDAS Inlet and LSI.

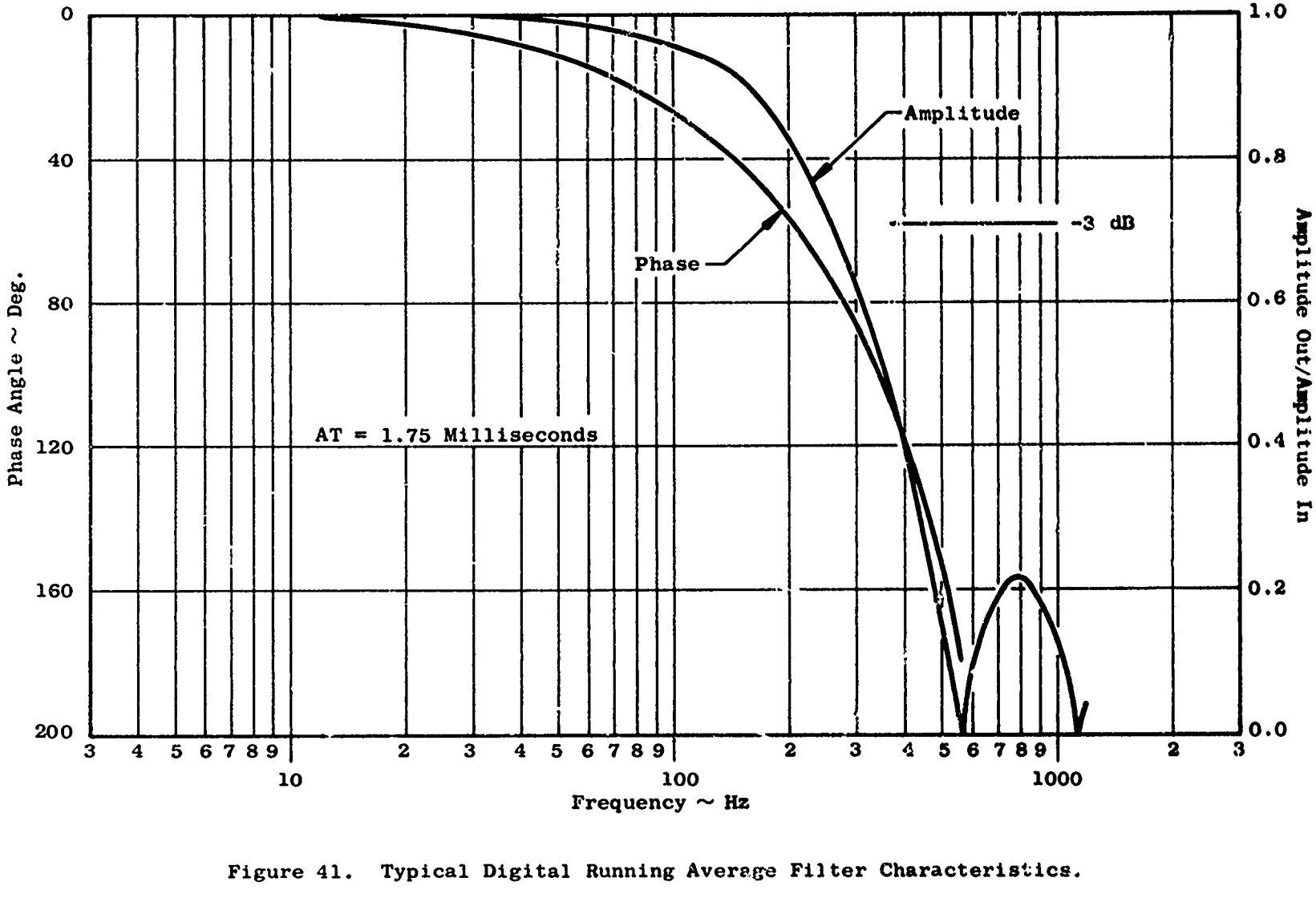

Figure 41. Typical Digital Running Average Filter Characteristics.

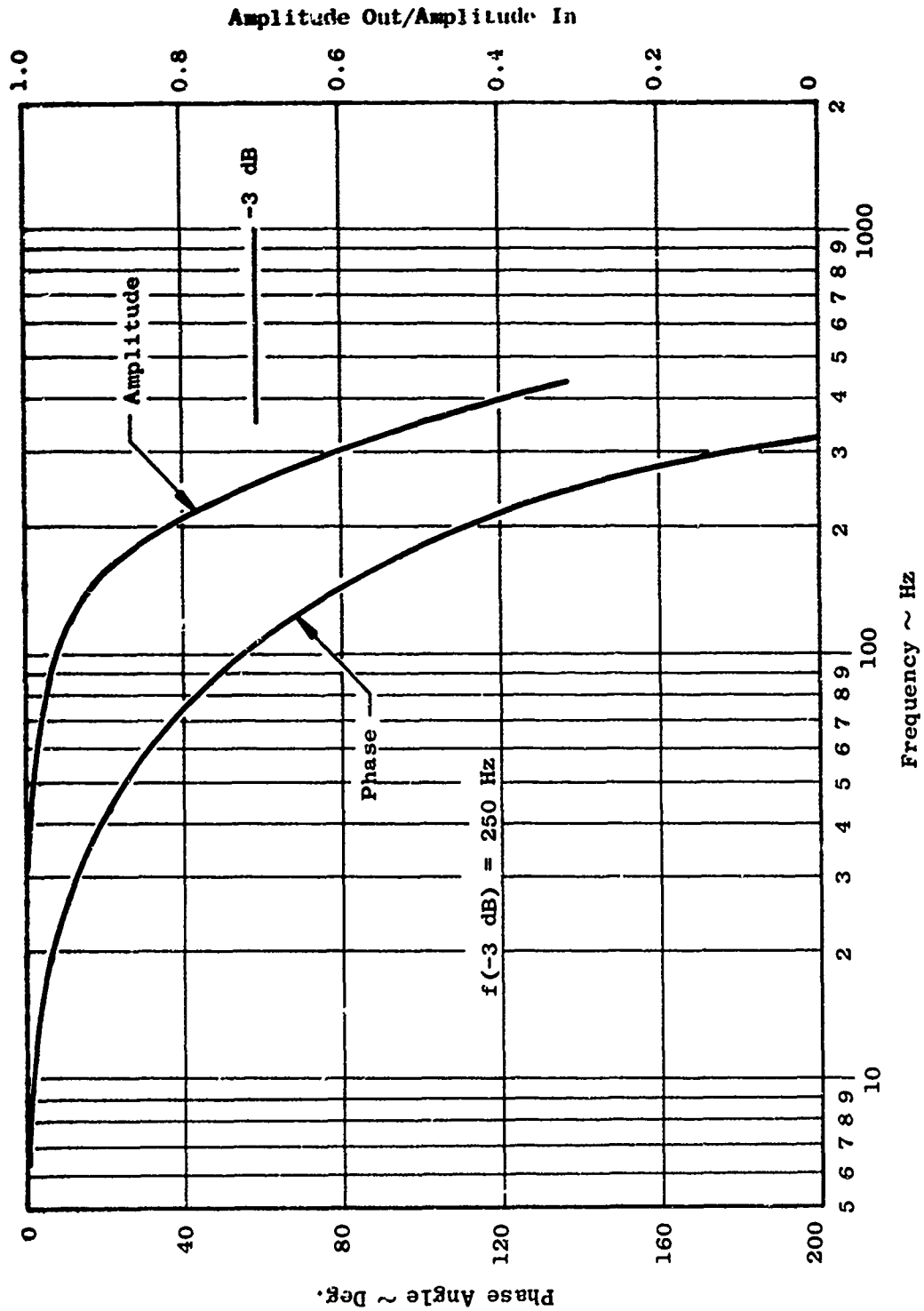

Figure 42. Typical Analog 5-Pole Linear Phase Filter Characteristics.

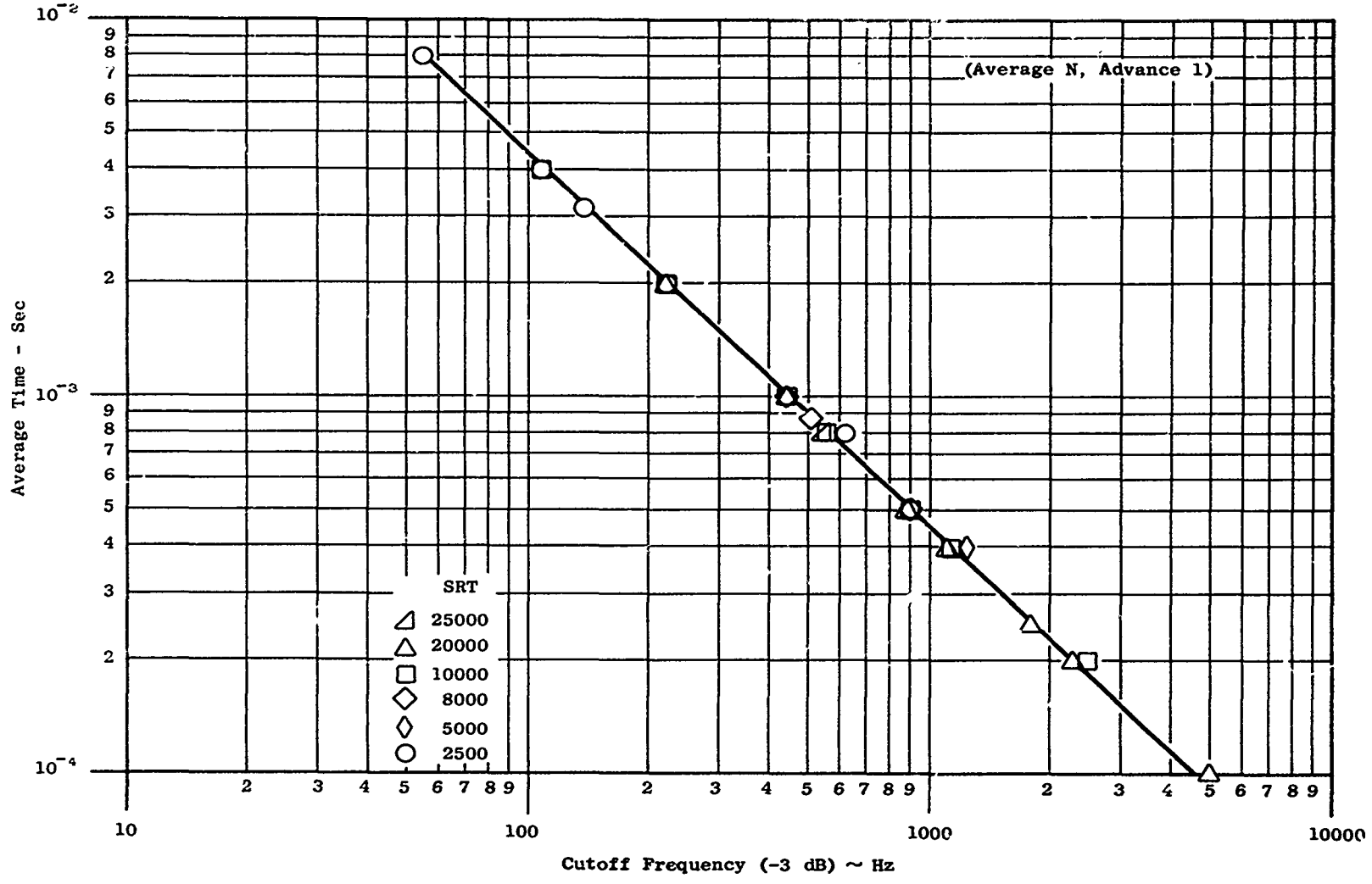

Figure 43. Average Time Vs. Cutoff Frequency for Digital Running Average.

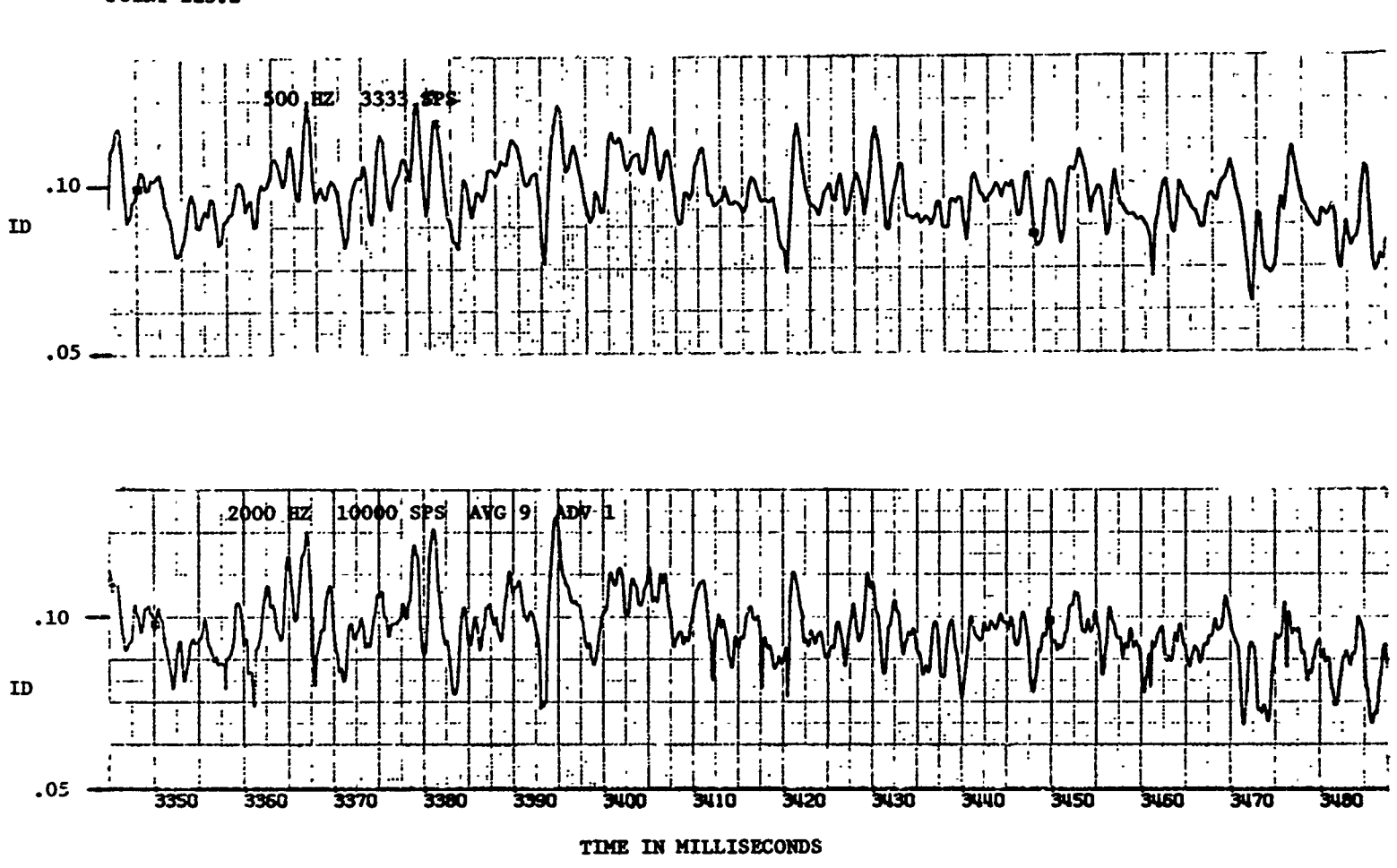

Figure 44. Analog Filter Vs. Digital Average - Comparison of Distortion Time Histories from 0.228 DDAS Inlet @ M = 1.8, α = 10°.

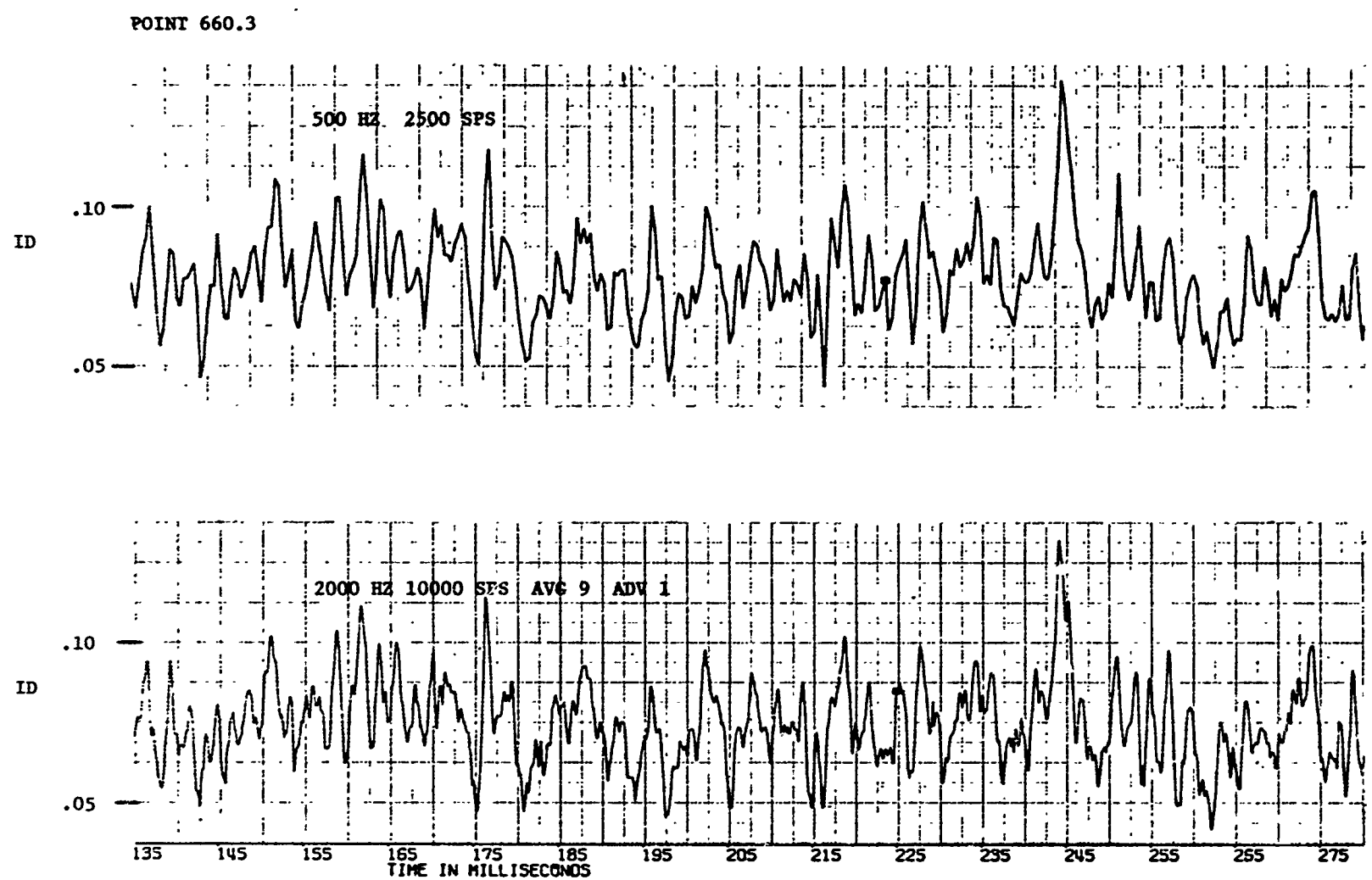

Figure 45. Analog Filter Vs. Digital Average - Comparison of Distortion Time Histories from 0.228 DDAS Inlet @ M = 0.0, α = 0°.

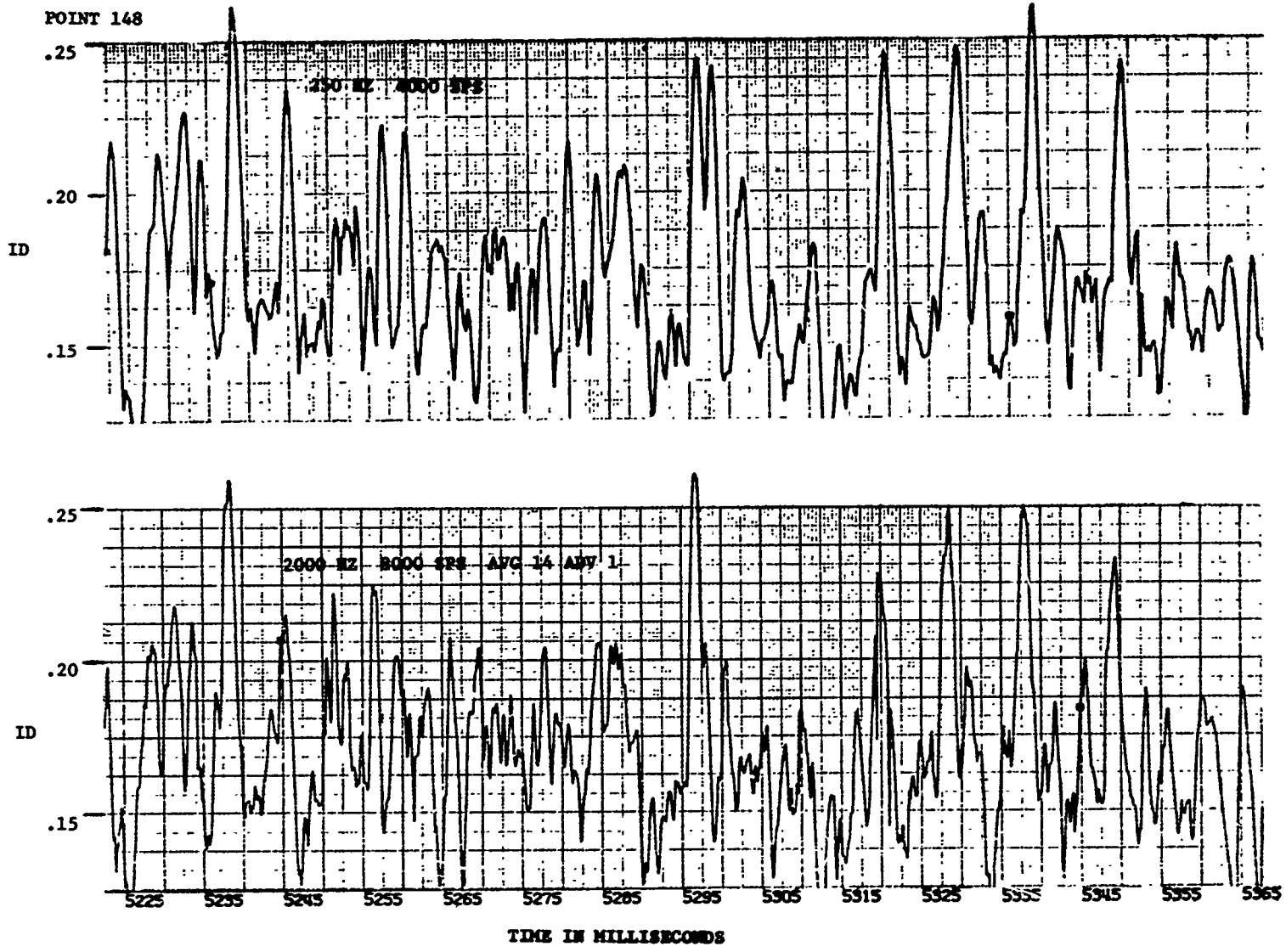

Figure 46. Analog Filter Vs. Digital Average - Comparison of Distortion Time Histories from ASMC Inlet @ M = 2.5, α = 0°.

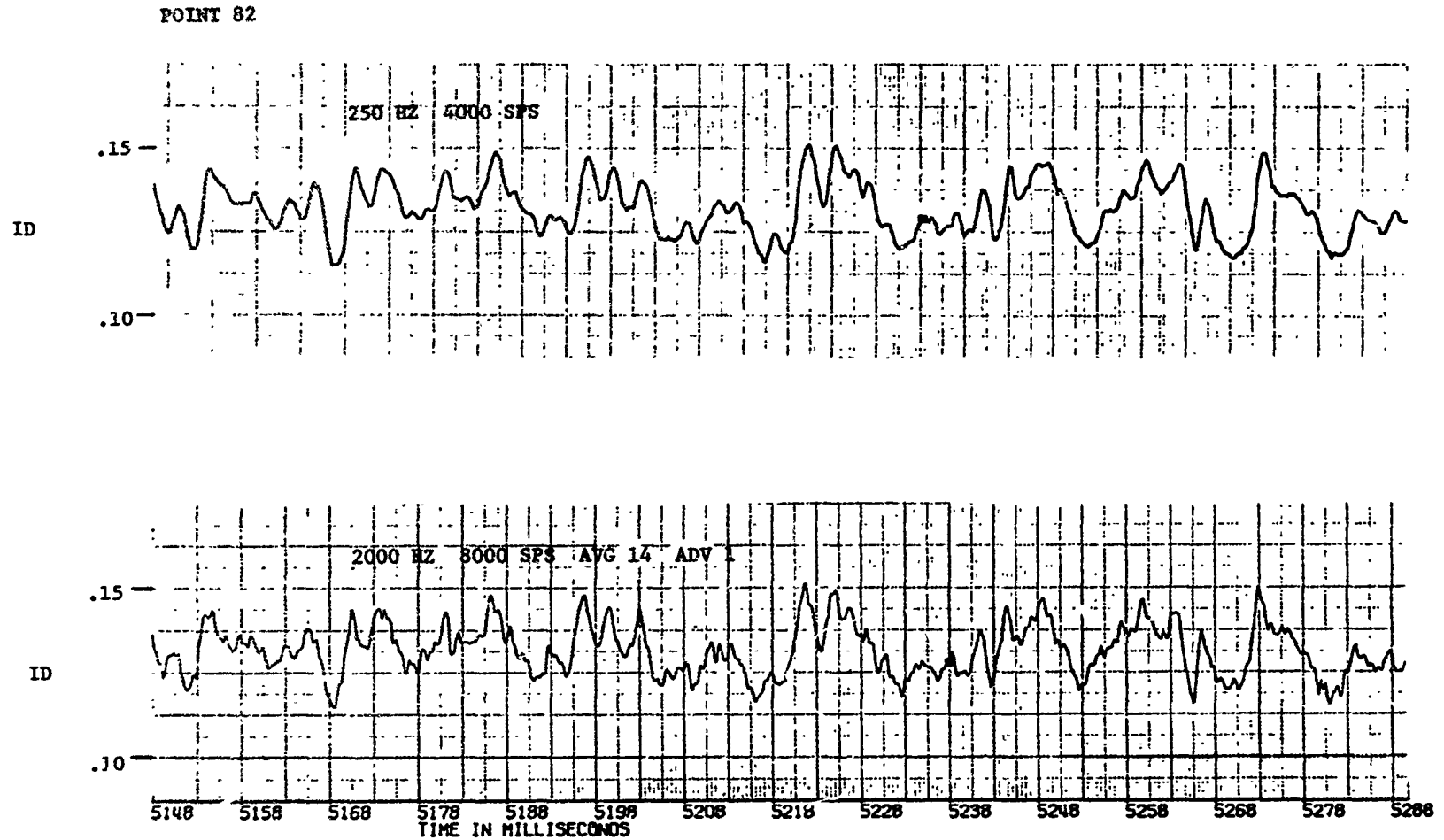

Figure 47. Analog Filter Vs. Digital Average - Comparison of Distortion Time Histories from ASMC Inlet @ M = 2.5, α = 5°.

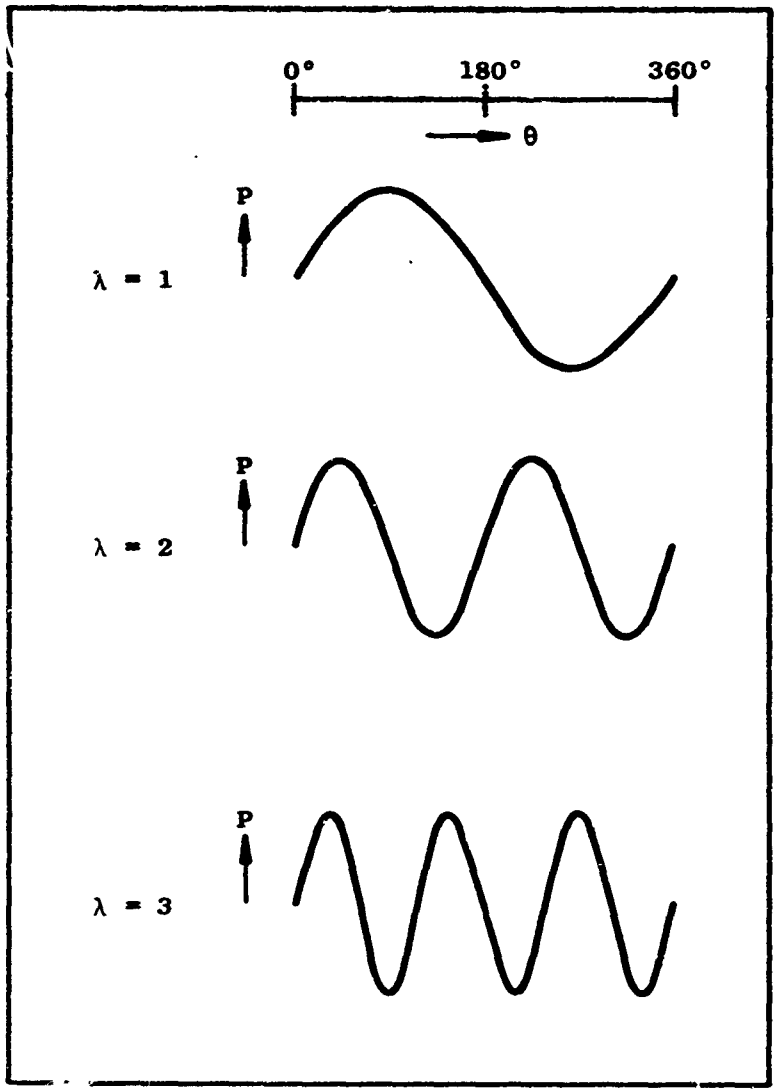

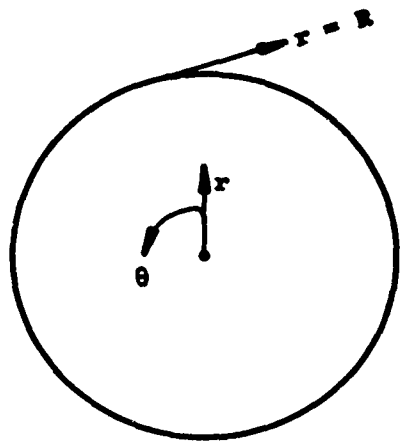

Measurement Plane
Looking Aft

Figure 48. Derivation of Average Time Parameter, λ.

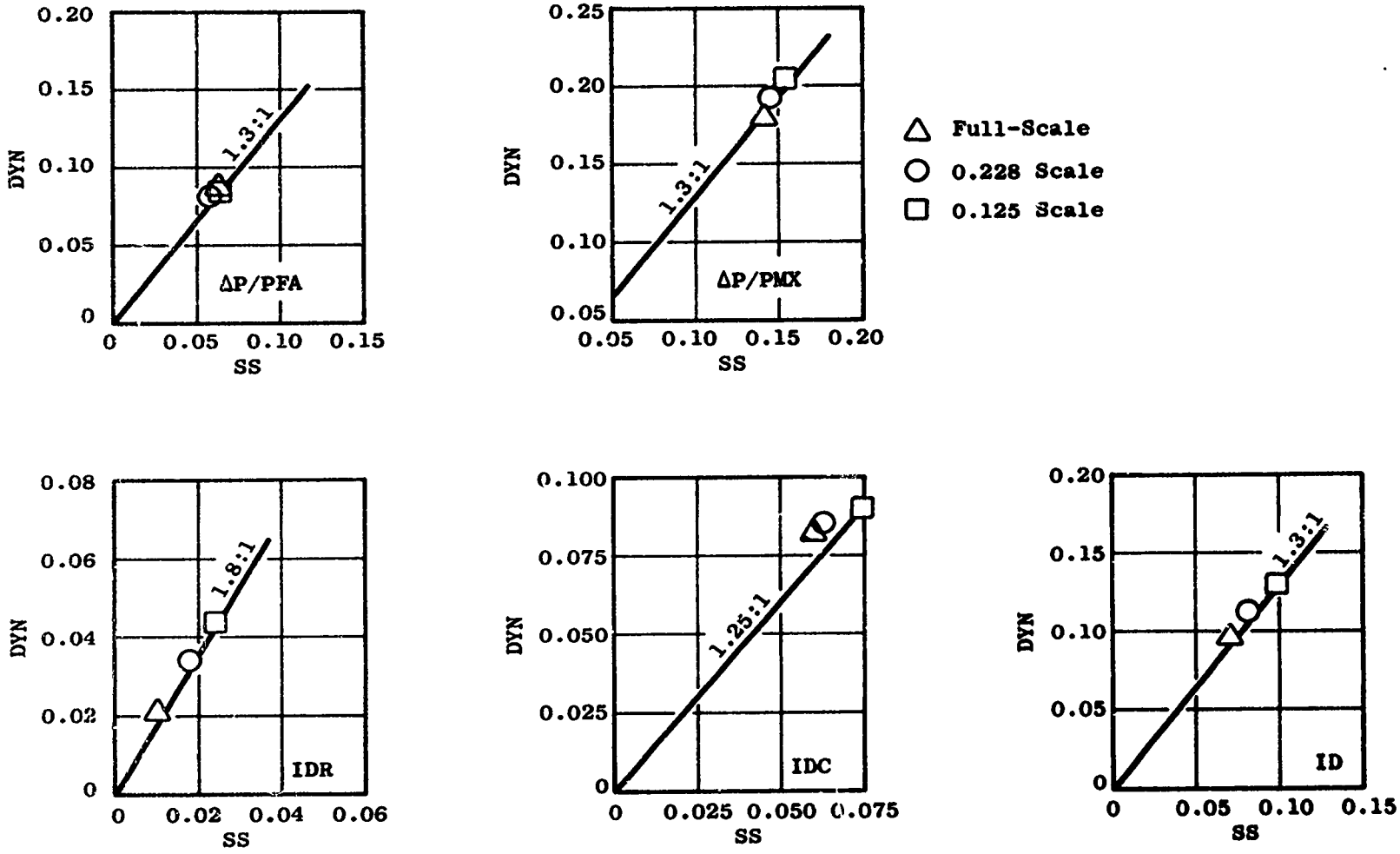

Figure 49. Distortion Parameters - Peak Dynamic Vs. Steady-State DDAS Inlet @ M = 1.8, $\alpha \approx 10°$, $\lambda \approx 1$, Po $\approx$ Constant.

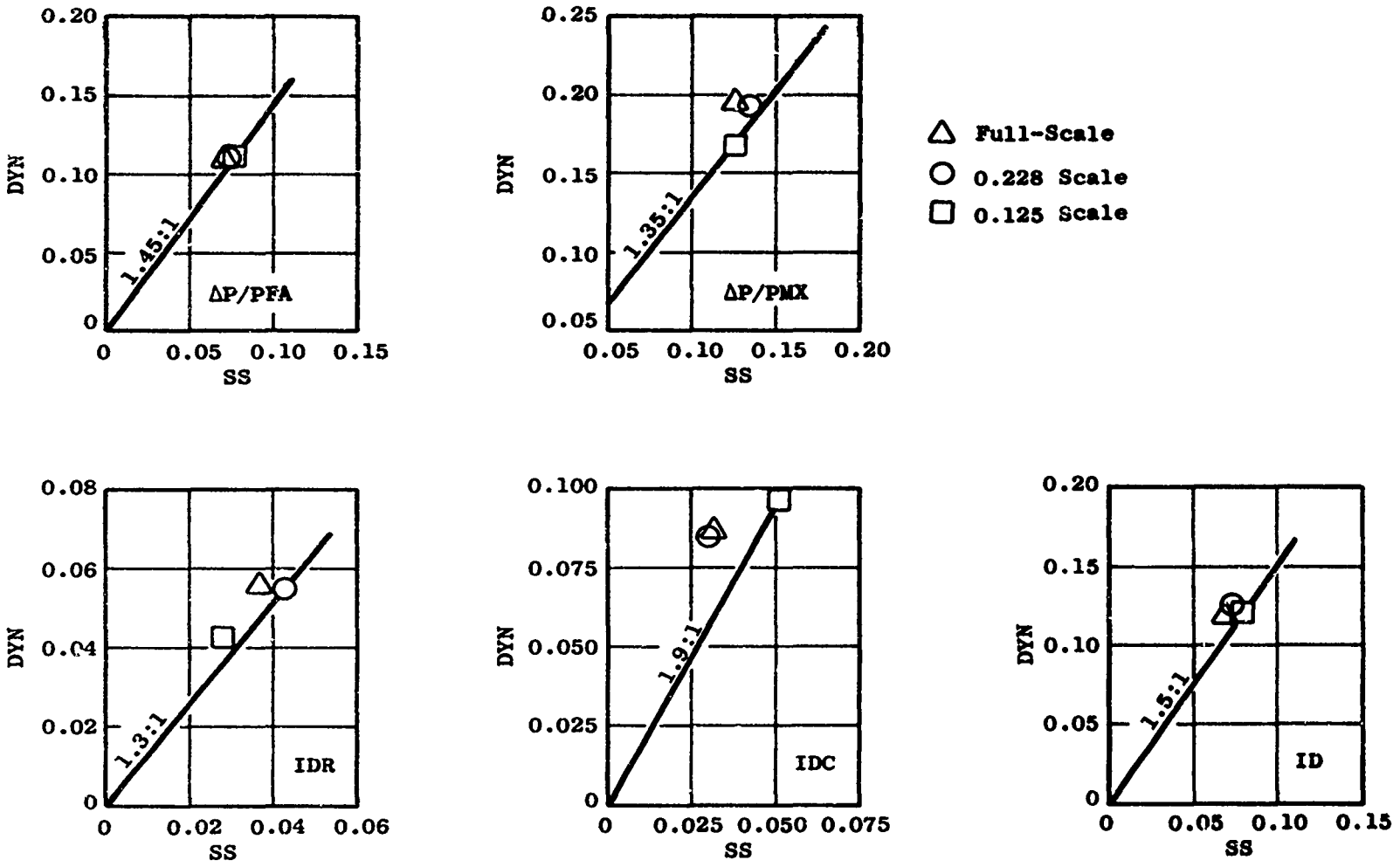

Figure 50. Distortion Parameters - Peak Dynamic Vs. Steady-State DDAS Inlet @ M = 1.8, $\alpha \approx 1.5^{\circ}$, $\lambda \approx 1$, Po $\approx$ Constant.

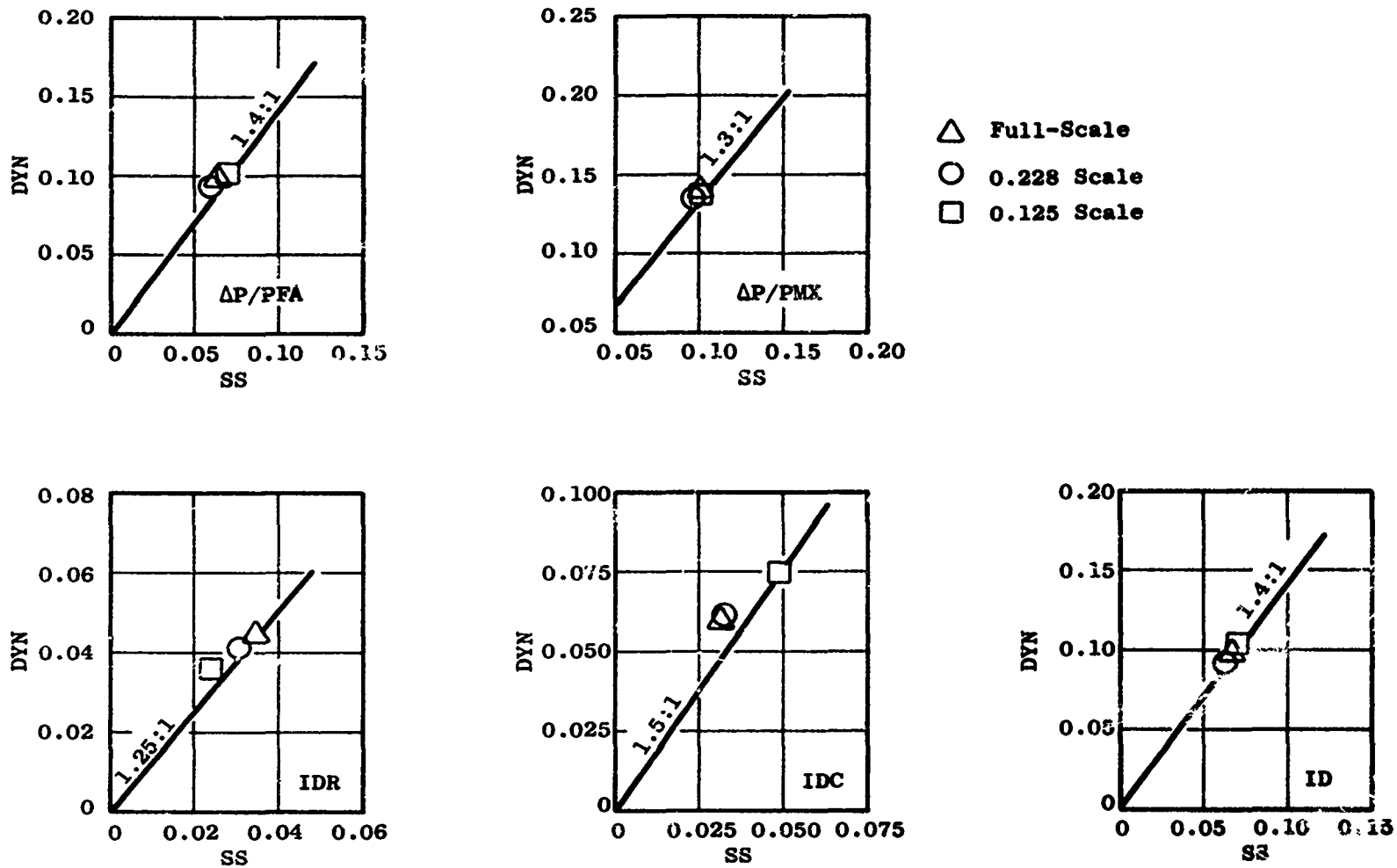

Figure 51. Distortion Parameters - Peak Dynamic Vs. Steady-State DDAS Inlet @ M = 1.6, $\alpha \approx 1.5°$, $\lambda \approx 1$, Po $\approx$ Constant.

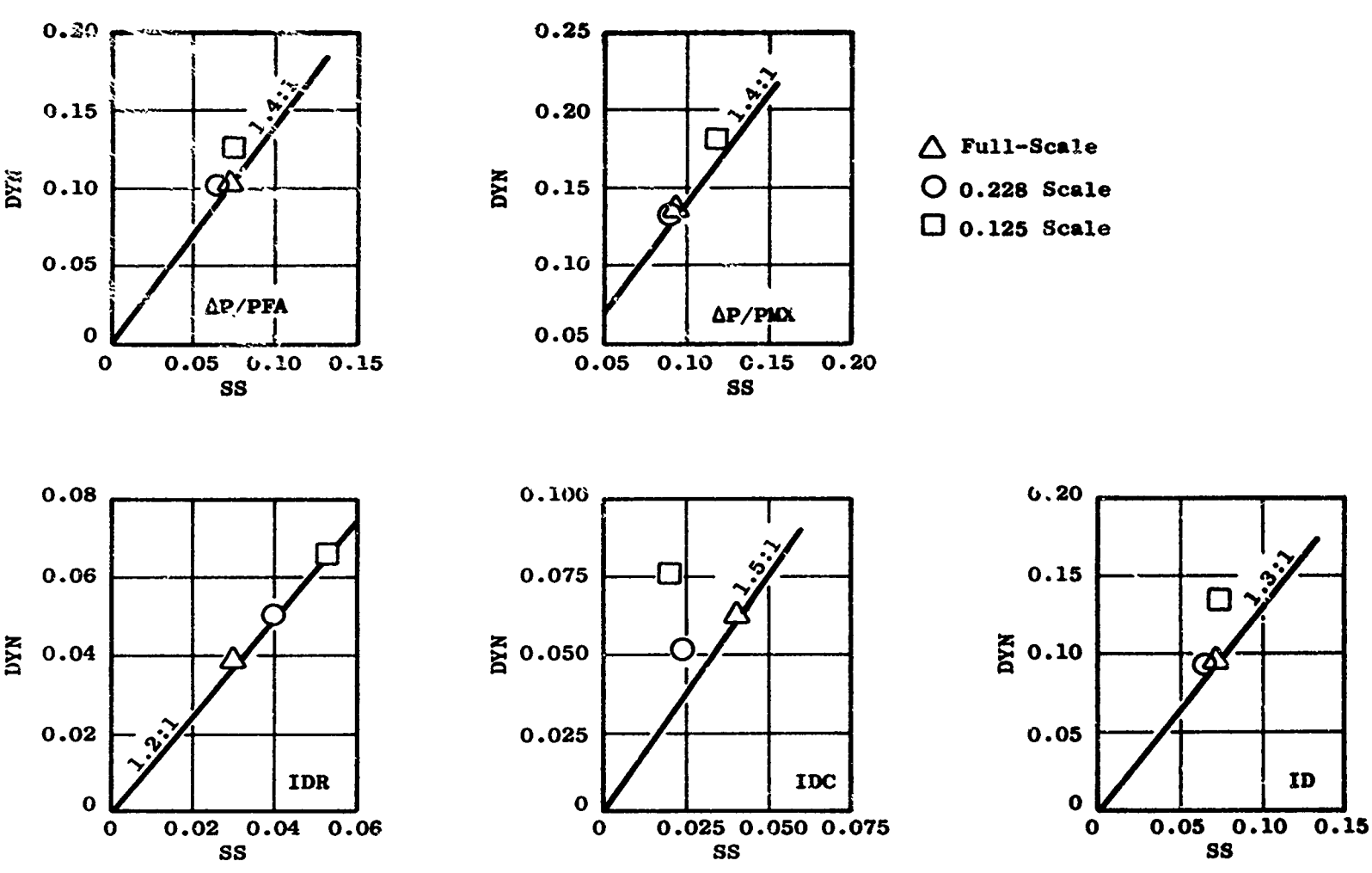

Figure 52. Distortion Parameters - Peak Dynamic Vs. Steady-State DDAS Inlet @ M = 0.9, $\alpha \approx 5°$, $\lambda \approx 1$, Re $\approx$ Constant.

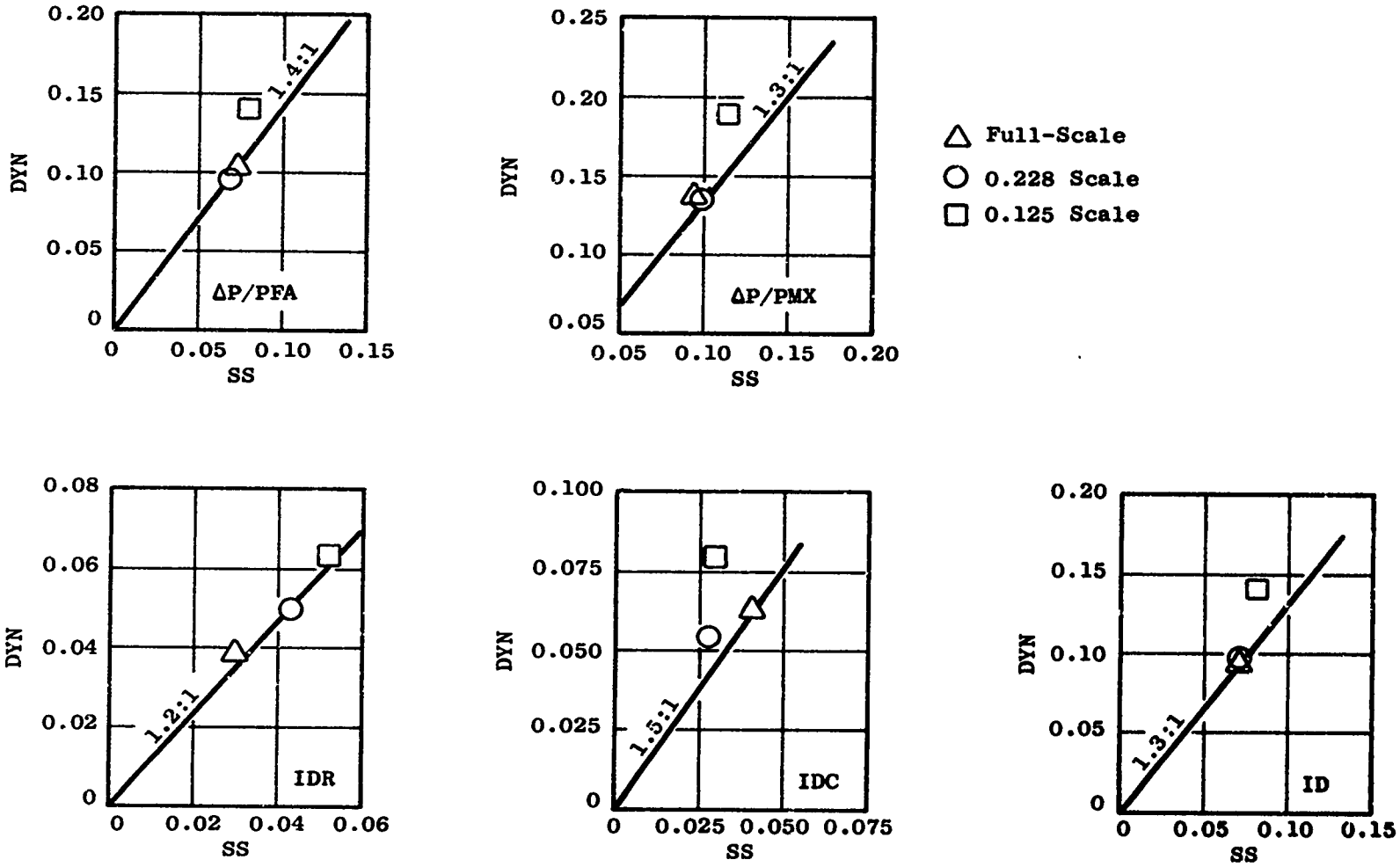

Figure 53. Distortion Parameters - Peak Dynamic Vs. Steady-State DDAS Inl t @ M = 0.9, $\alpha \approx 5°$, $\lambda \approx 1$, Po $\approx$ Constant.

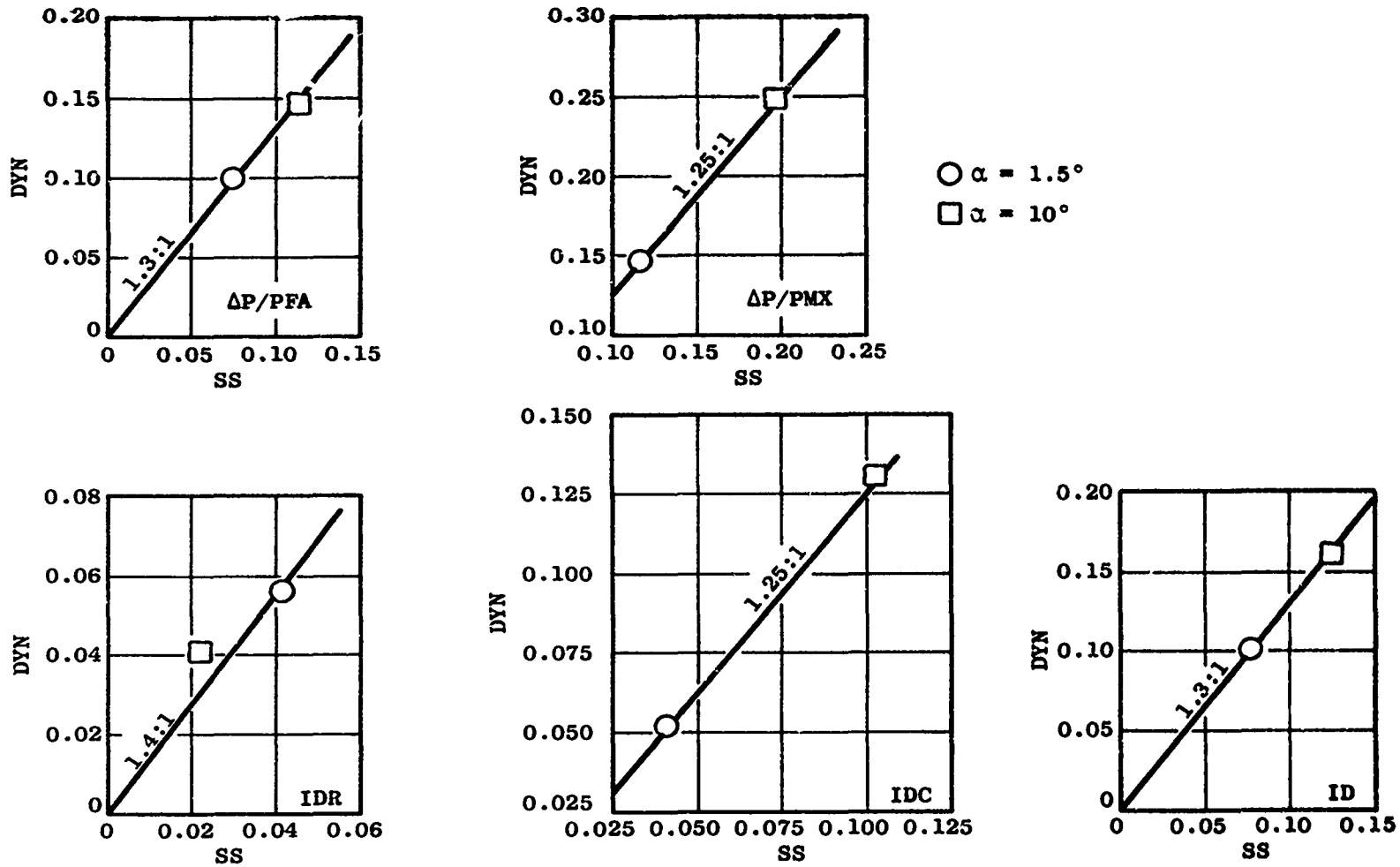

Figure 54. Distortion Parameters - Peak Dynamic Vs. Steady-State LSI @ M = 1.8, $\lambda \approx 1$.

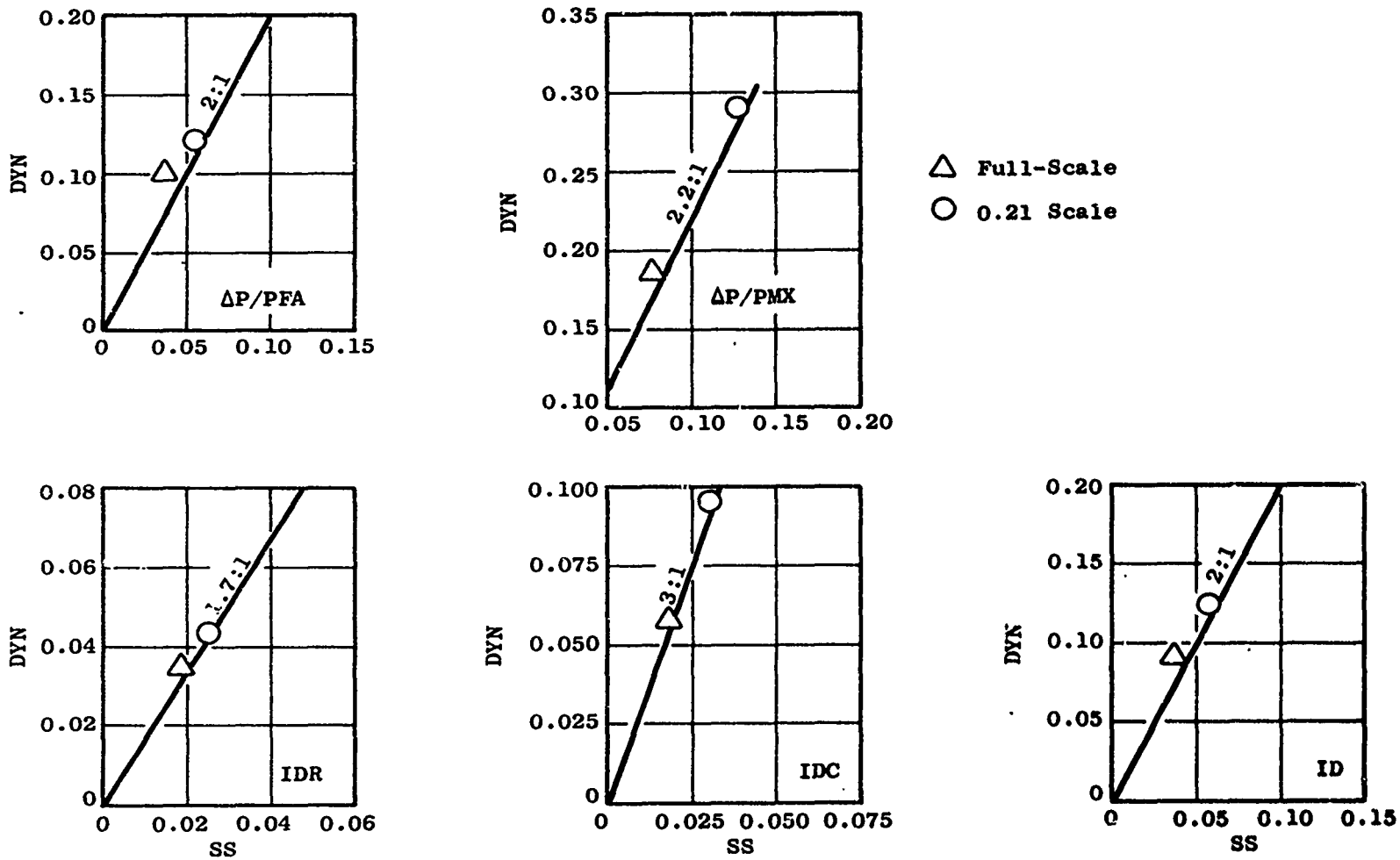

Figure 55. Distortion Parameters - Peak Dynamic Vs. Steady-State Inlet Simulator @ Low Recovery, $\lambda \approx 1$.

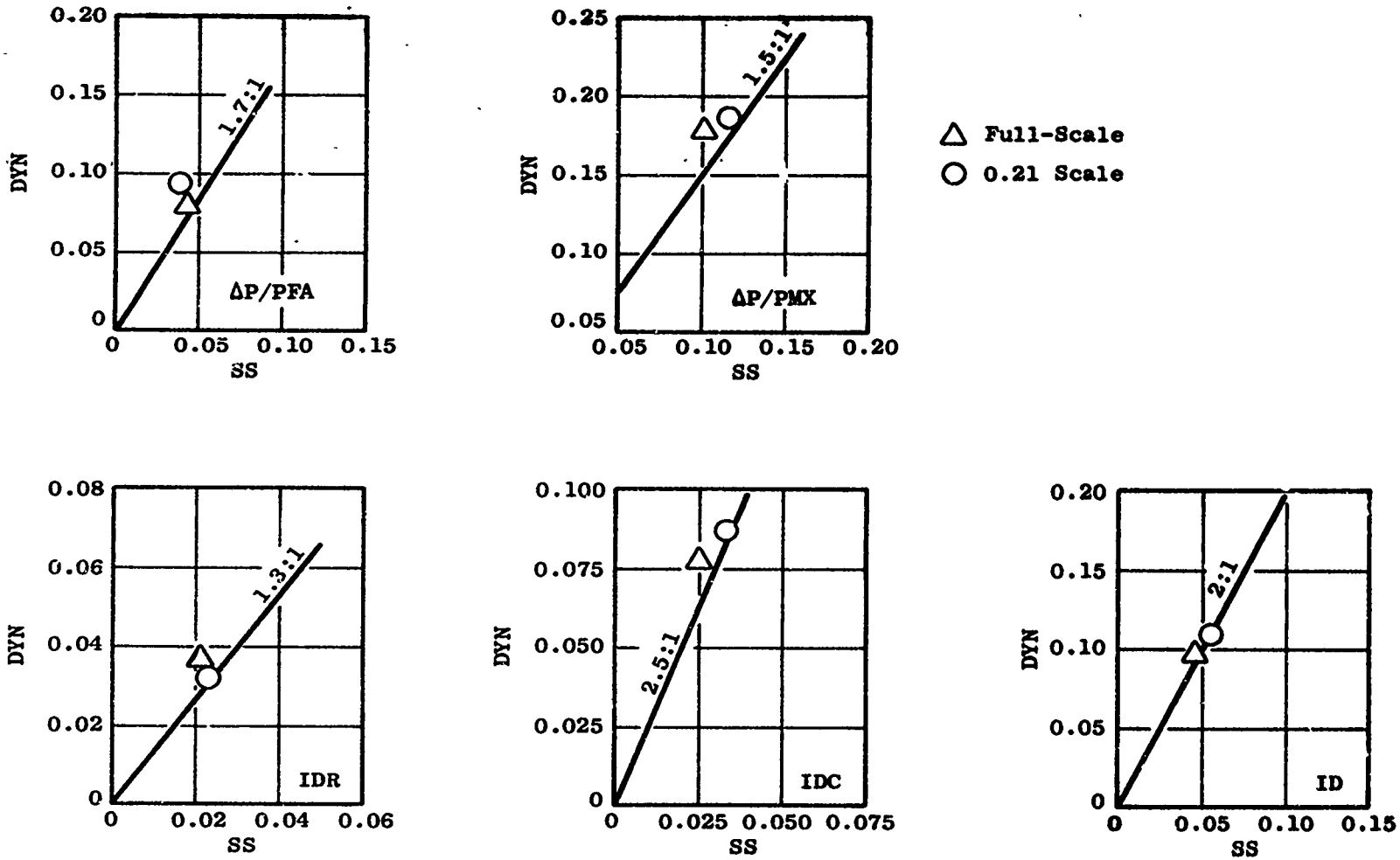

Figure 56. Distortion Parameters - Peak Dynamic Vs. Steady-State Inlet Simulator @ High Recovery, $\lambda \approx 1$.

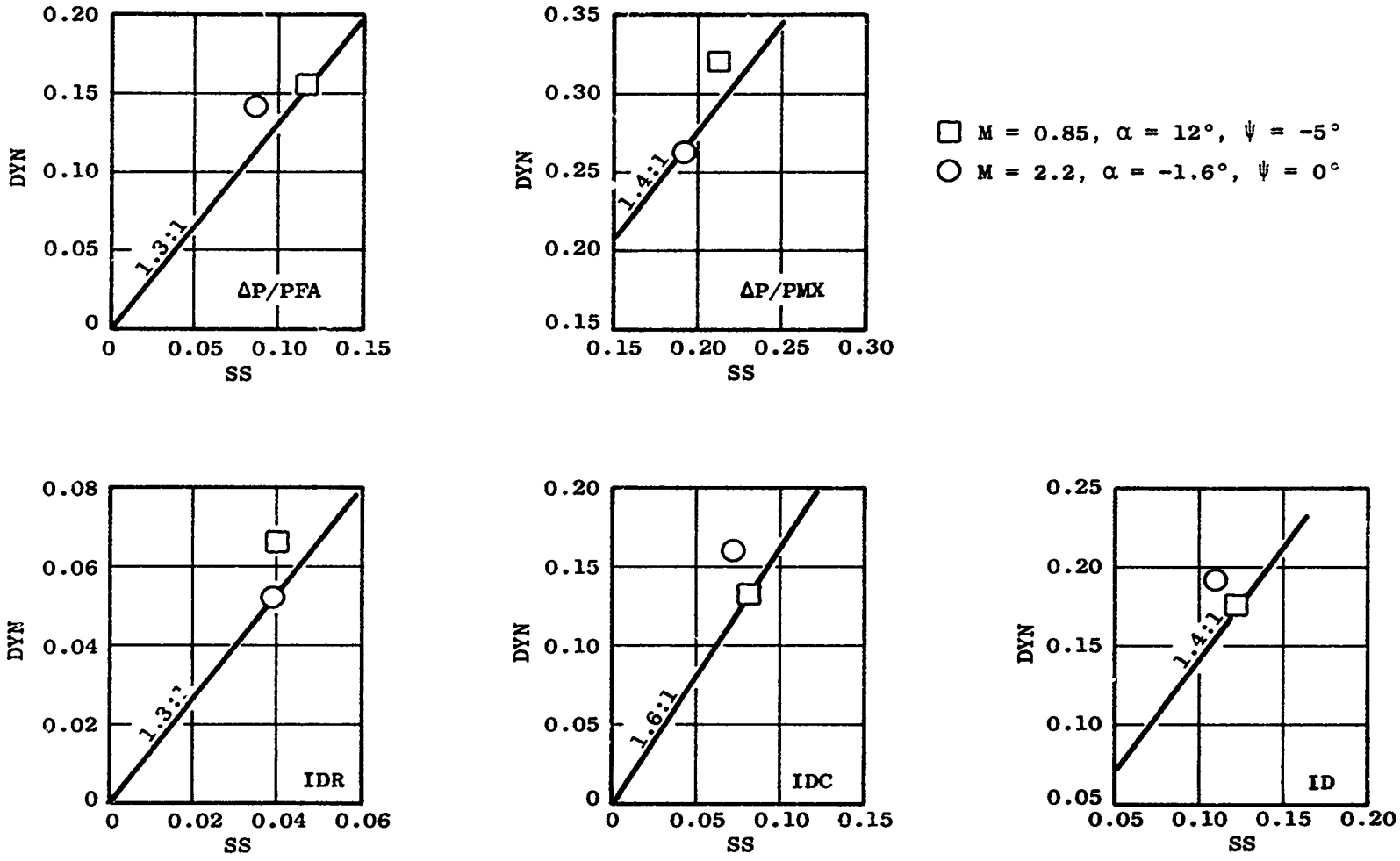

Figure 57. Distortion Parameters - Peak Dynamic Vs. Steady-State 2DMC Inlet, $\lambda \approx 1$.

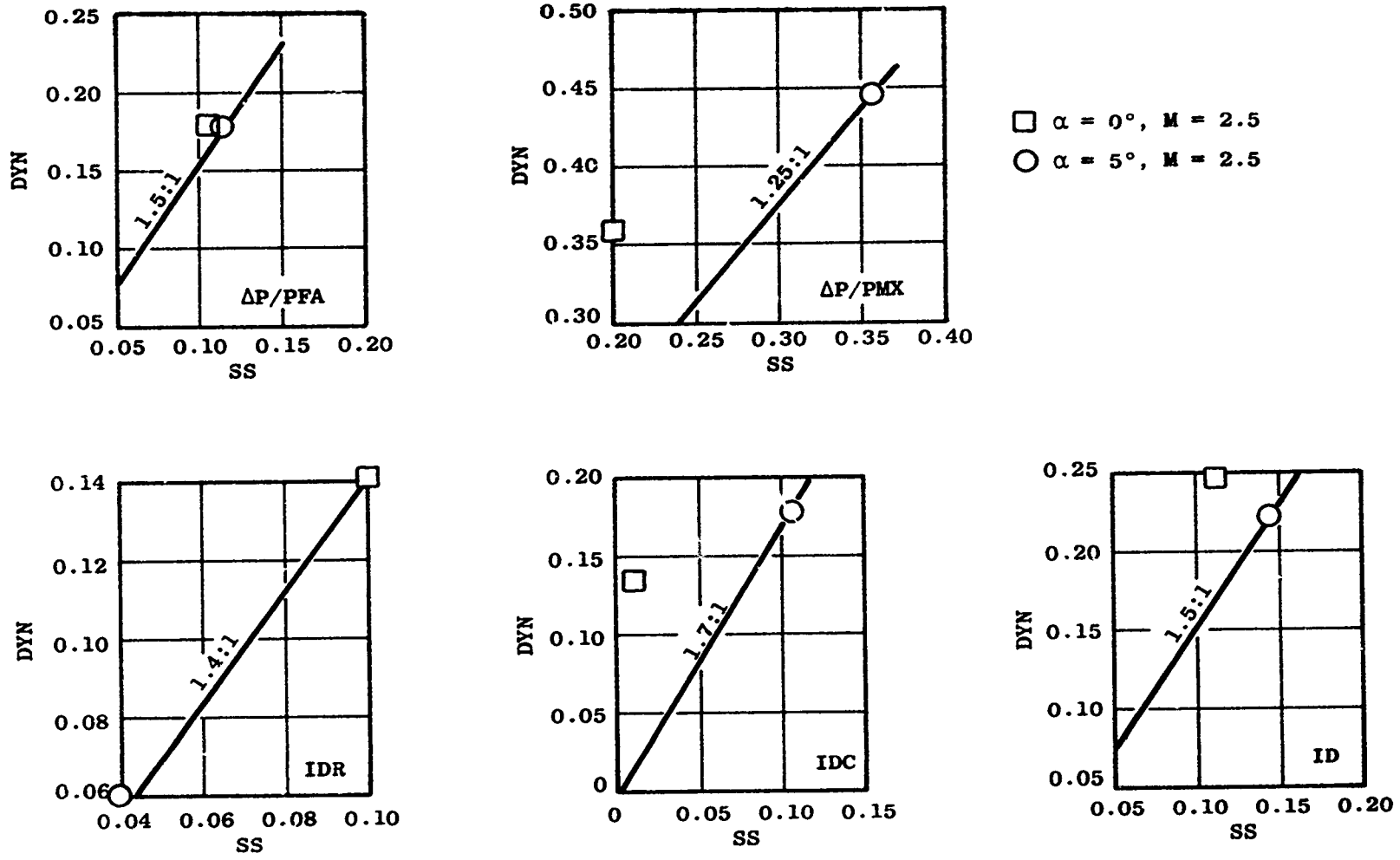

Figure 58. Distortion Parameters - Peak Dynamic Vs. Steady-State ASMC Inlet, $\lambda \approx 1$.

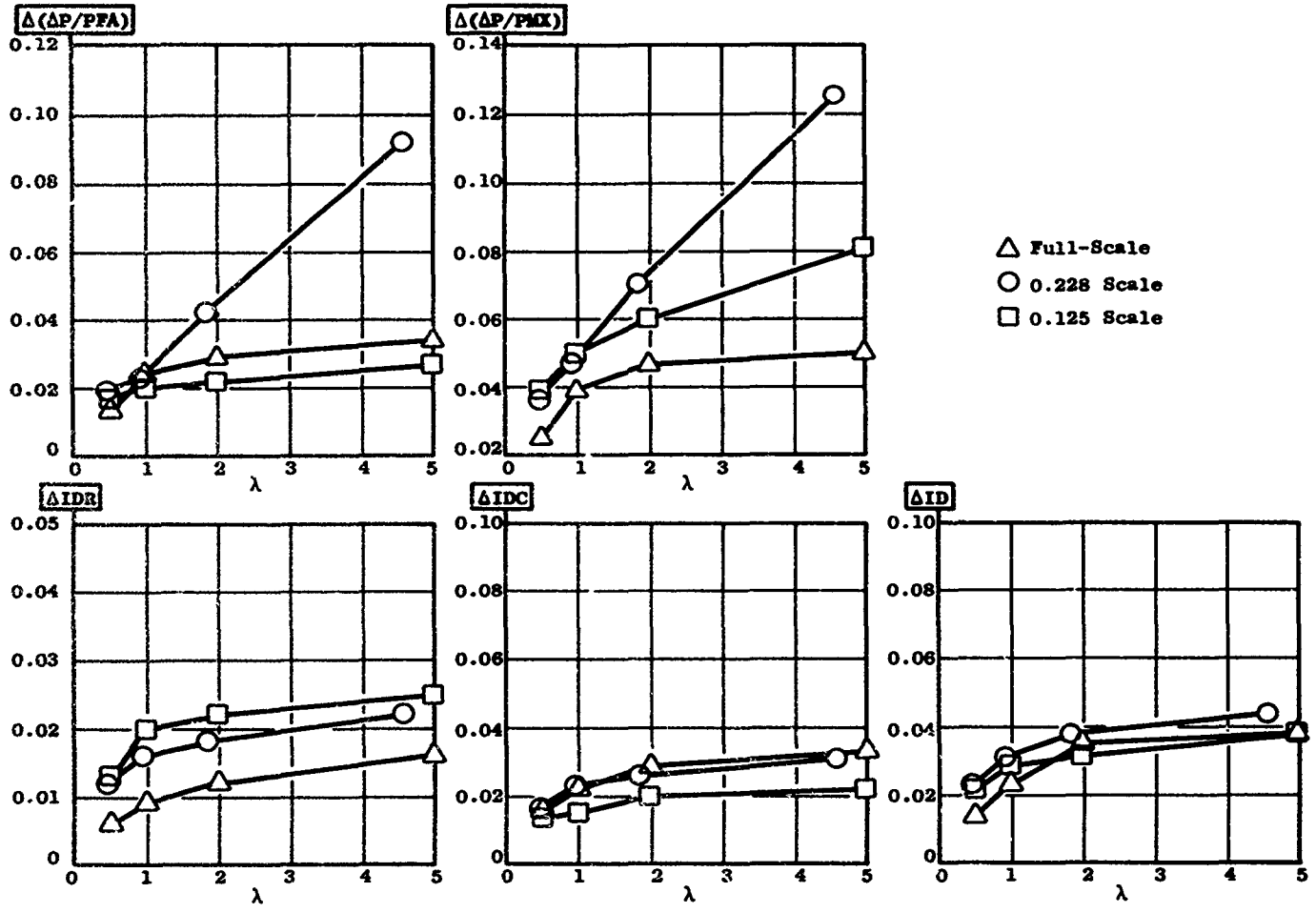

Figure 59. Average Time Effects on Peak Dynamic Distortion Parameters, DDAS Inlet @ M = 1.8, $\alpha \approx 10°$, Pc ≈ Constant.

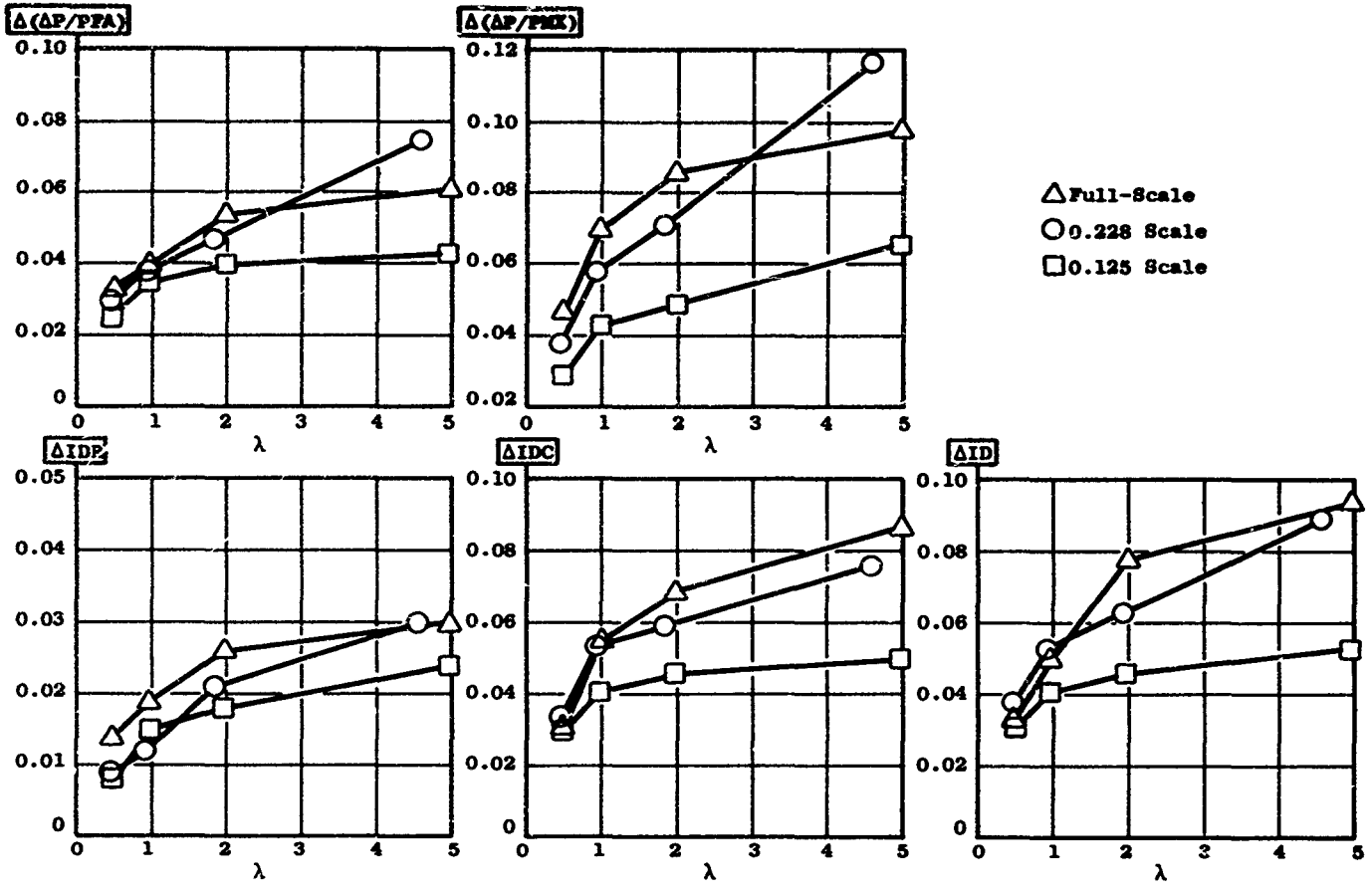

Figure 60. Average Time Effects on Peak Dynamic Distortion Parameters, DDAS Inlet @ M = 1.8, $\alpha \approx 1.5°$, Po ≈ Constant.

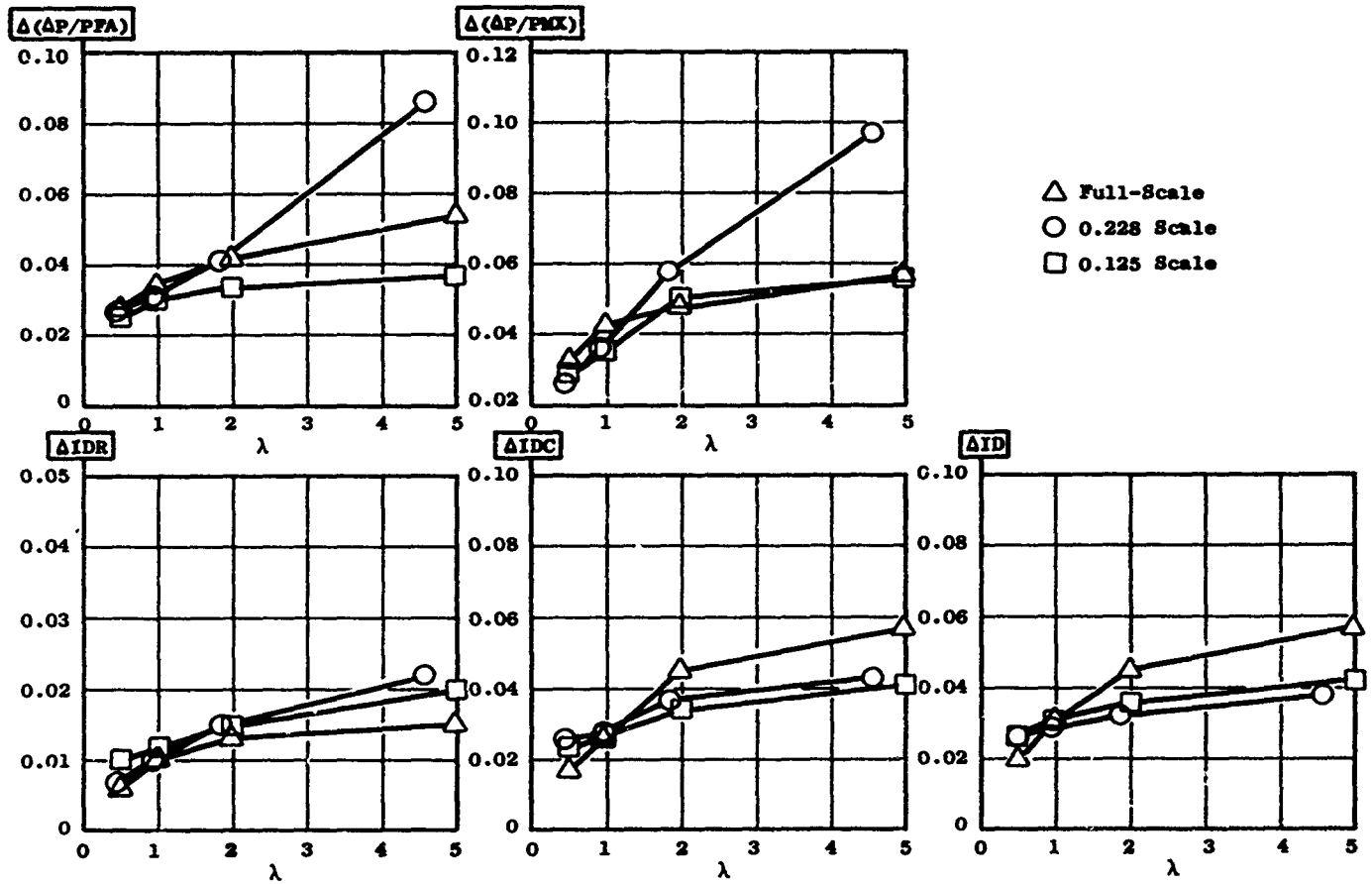

Figure 61. Average Time Effects on Peak Dynamic Distortion Parameters, DDAS Inlet @ M = 1.6, $\alpha \approx 1.5°$, Po ≈ Constant.

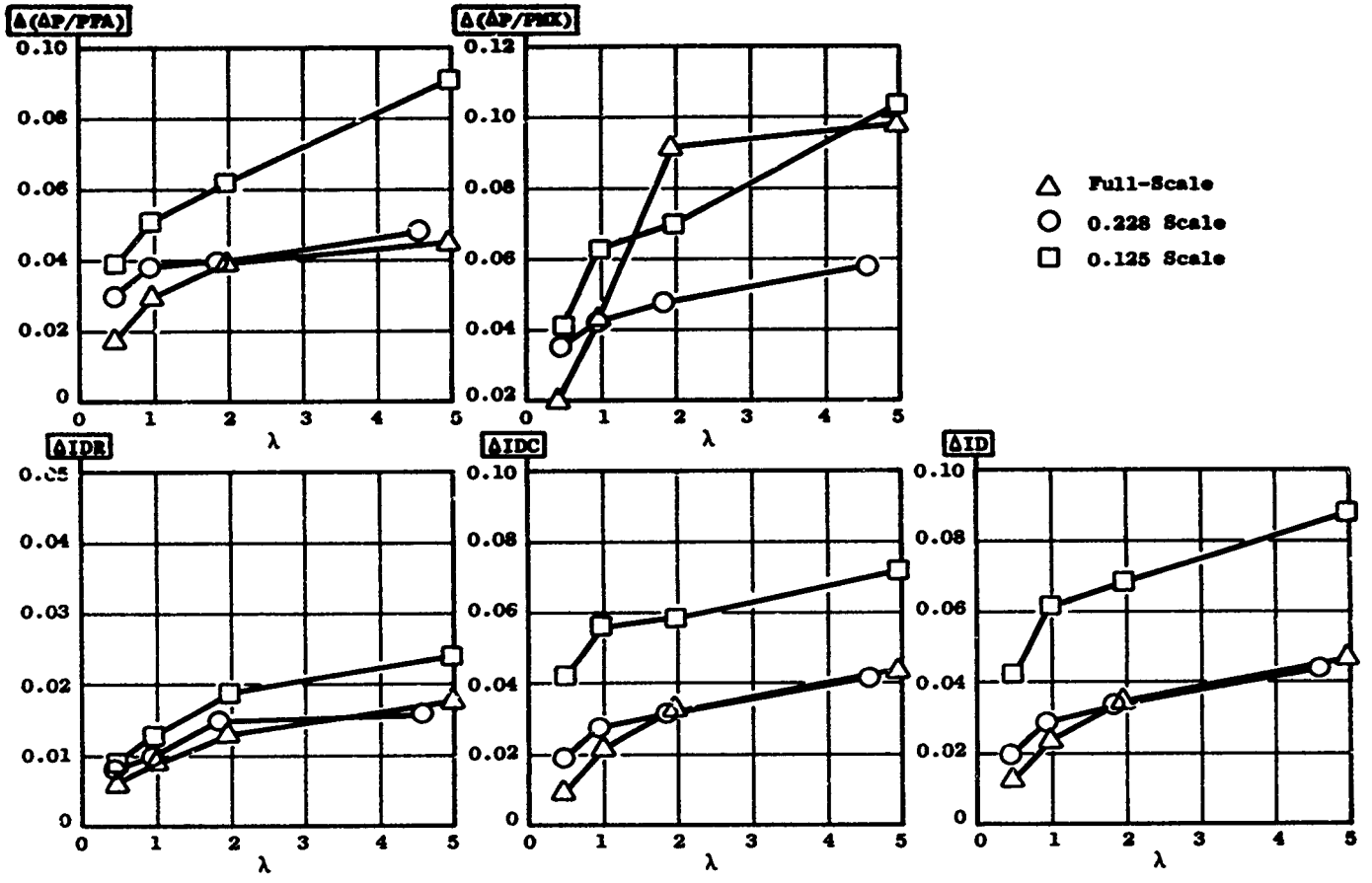

Figure 62. Average Time Effects on Peak Dynamic Distortion Parameters, DDAS Inlet @ M = 0.9, $\alpha \approx 5°$, Re ≈ Constant.

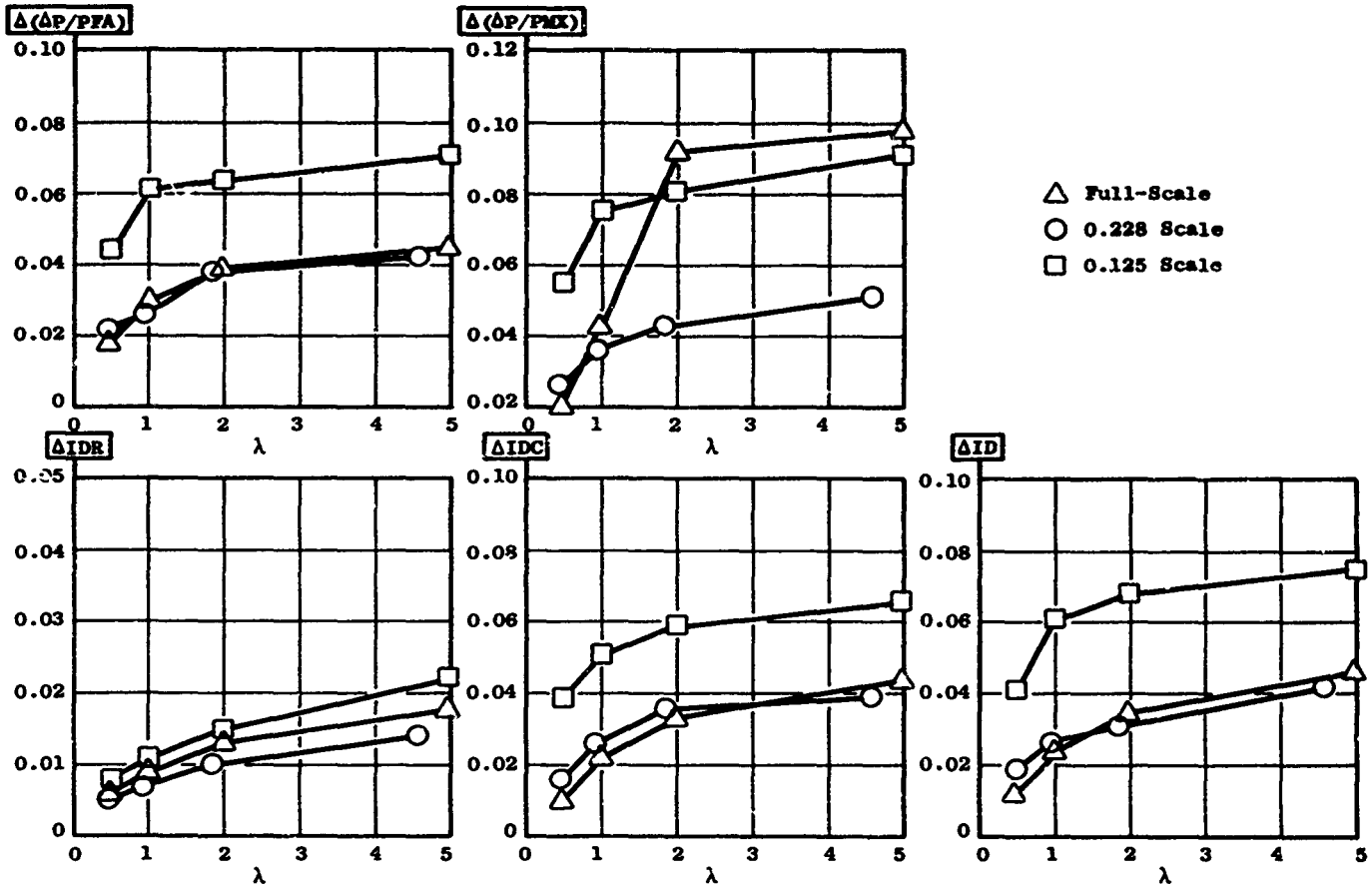

Figure 63. Average Time Effects on Peak Dynamic Distortion Parameters, DDAS Inlet @ M = 0.9, $\alpha \approx 5°$, Po ≈ Constant.

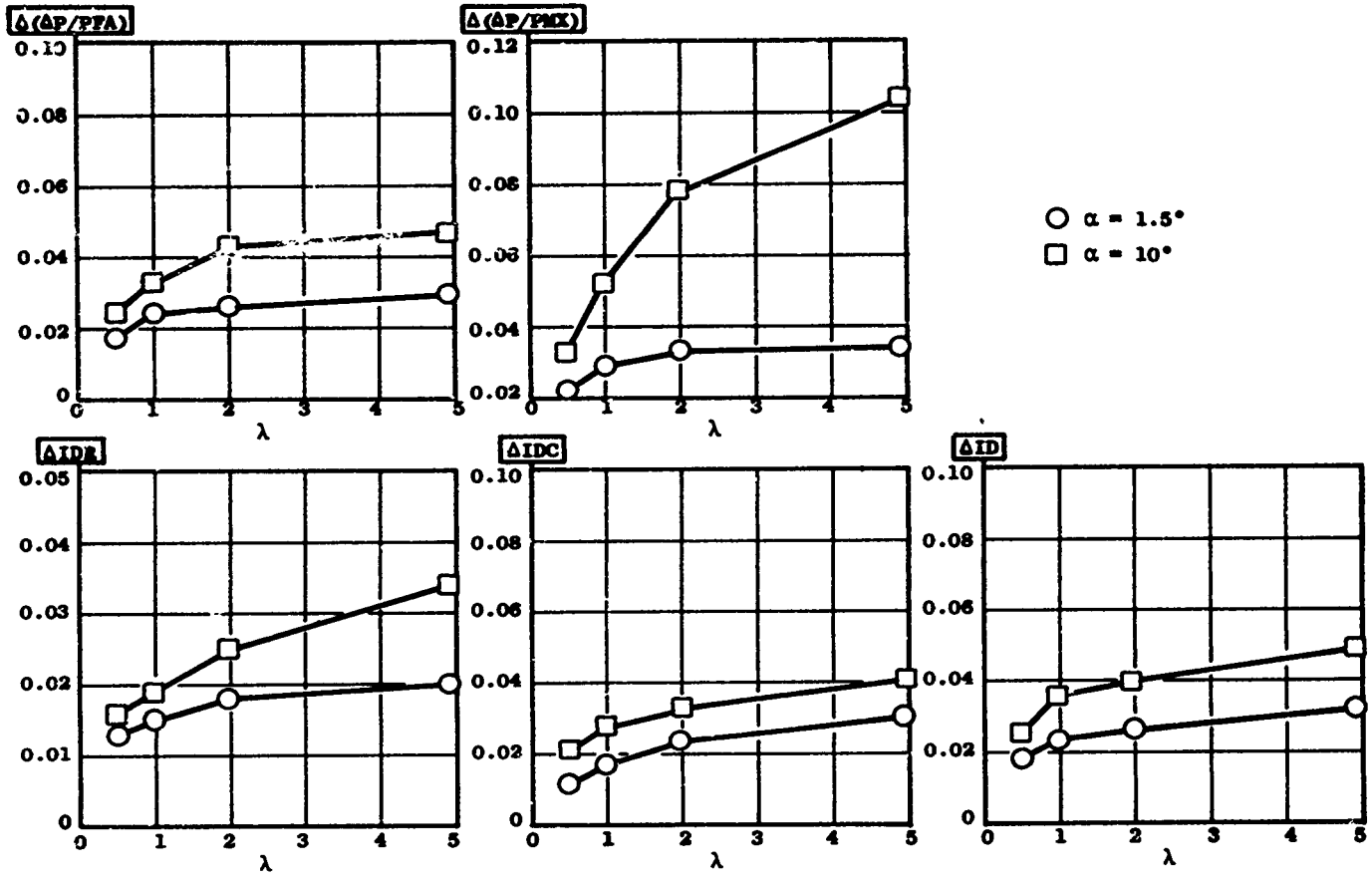

Figure 64. Average Time Effects on Peak Dynamic Distortion Parameters, LSI @ M = 1.8.

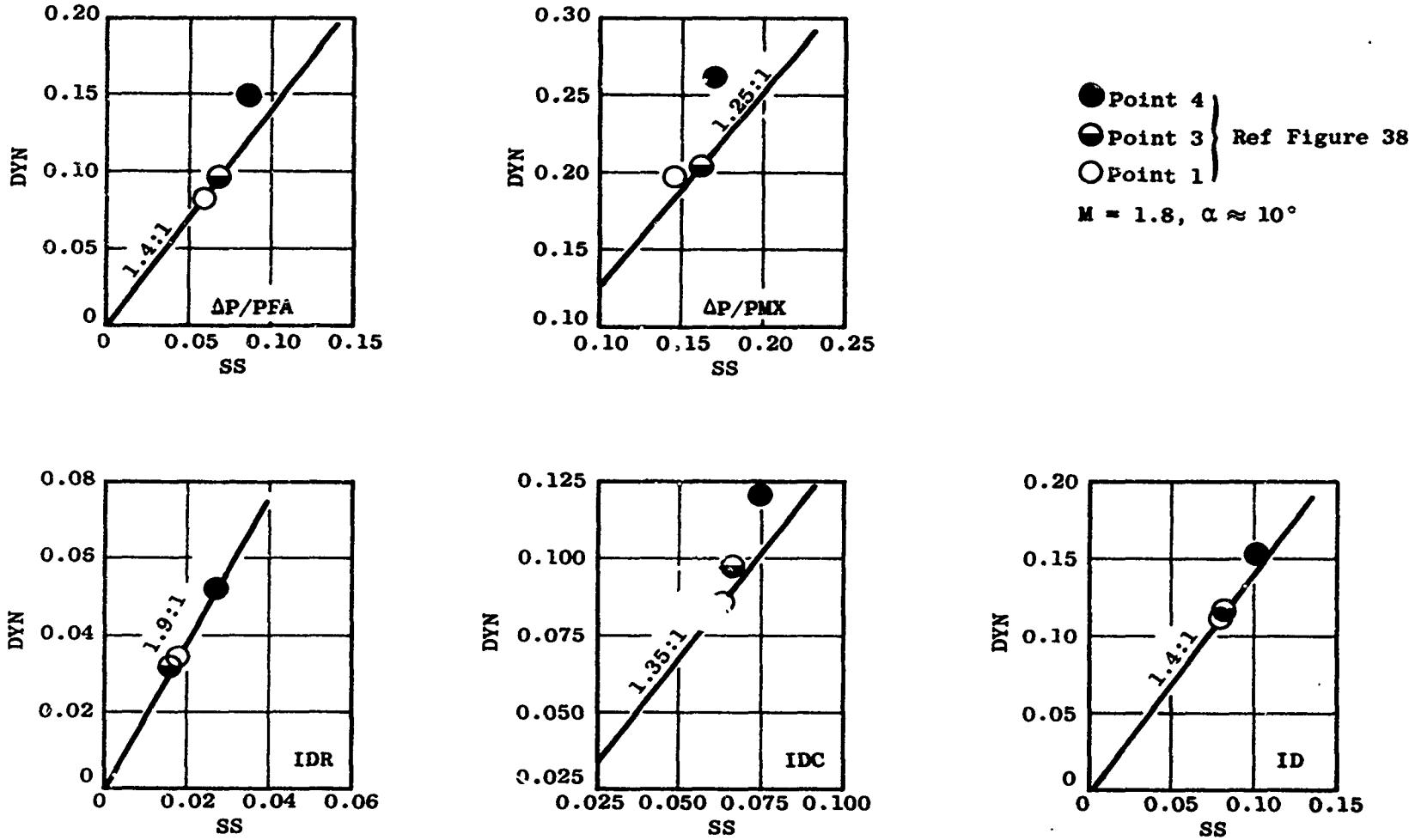

Figure 65. Mass Flow Change Effects on Dynamic Distortion, 0.228 Scale DDAS Inlet, $\lambda \approx 1.0$.

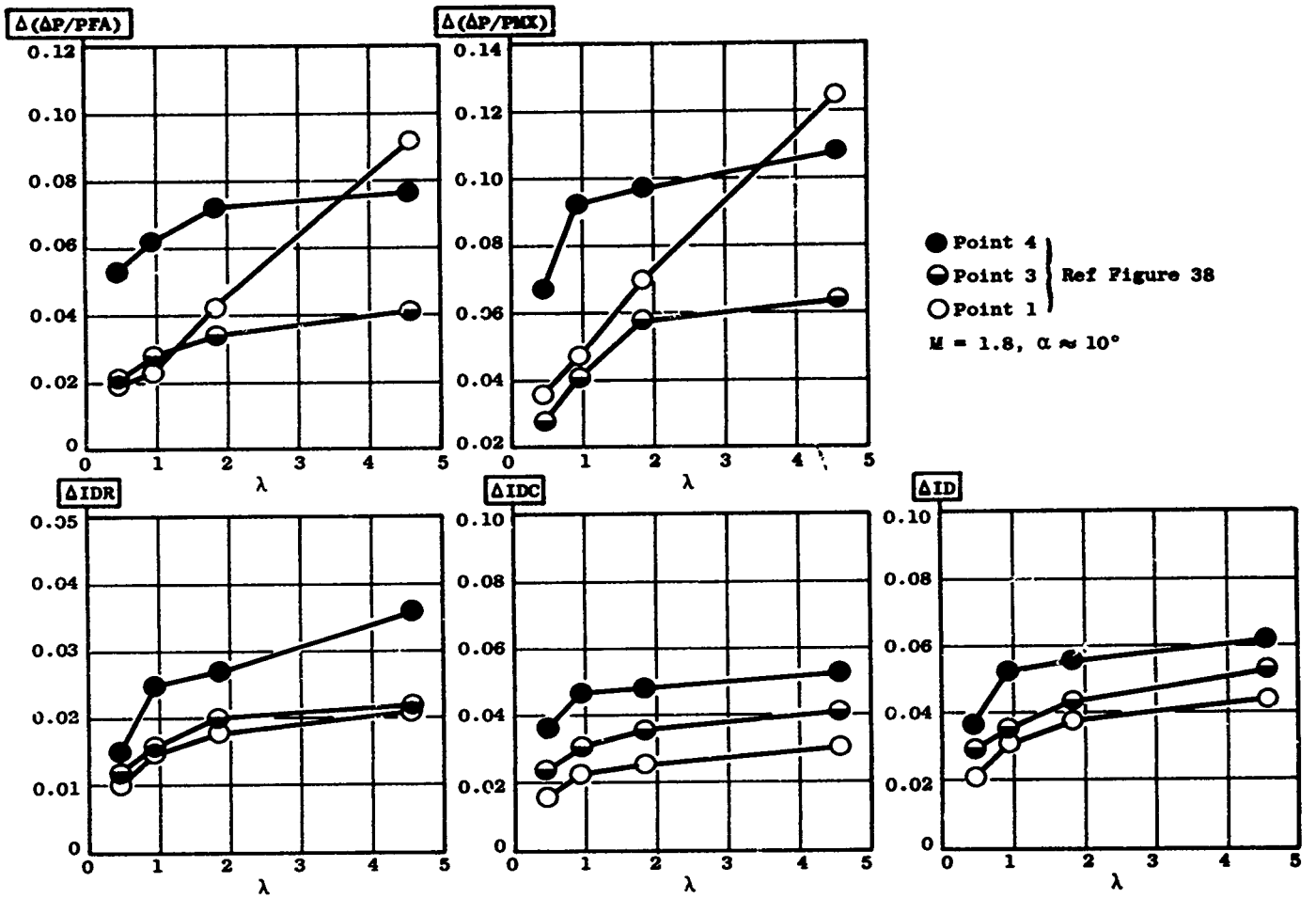

Figure 66. Mass Flow Change Effects on Dynamic Distortion, 0.228 Scale DDAS Inlet, λ = Variable.

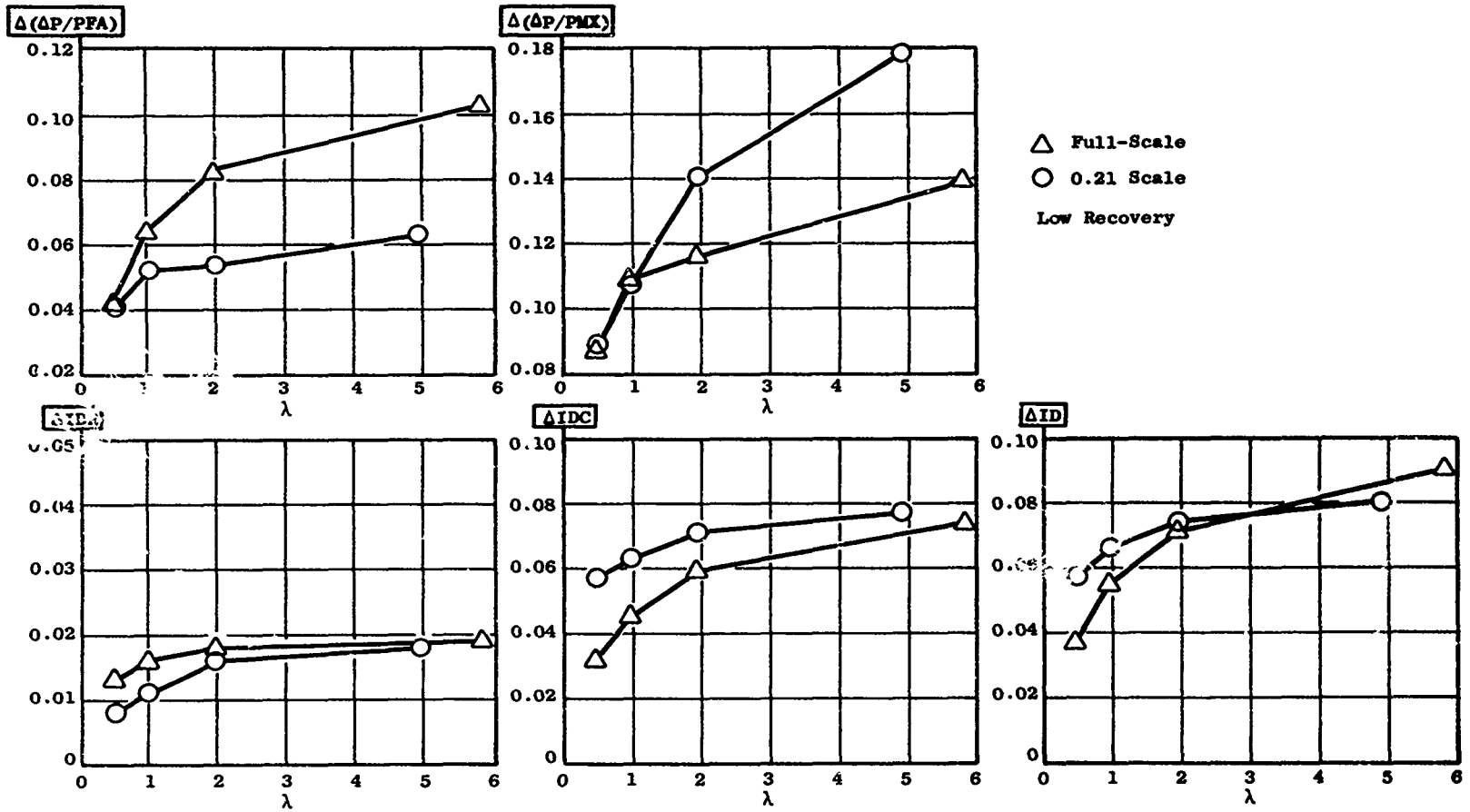

Figure 67. Average Time Effects on Peak Dynamic Distortion, Inlet Simulator, Small A*.

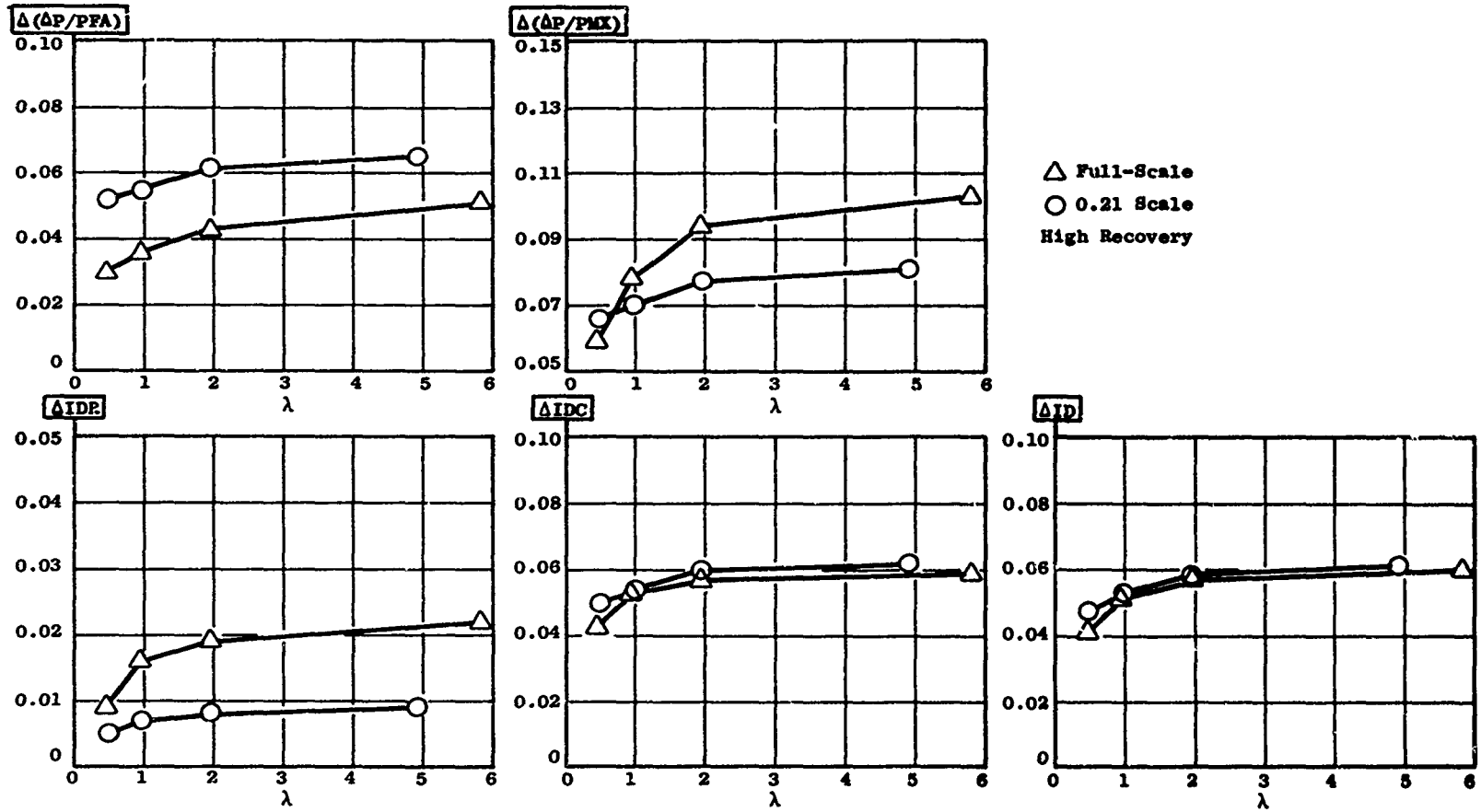

Figure 68. Average Time Effects on Peak Dynamic Distortion, Inlet Simulator, Large A*.

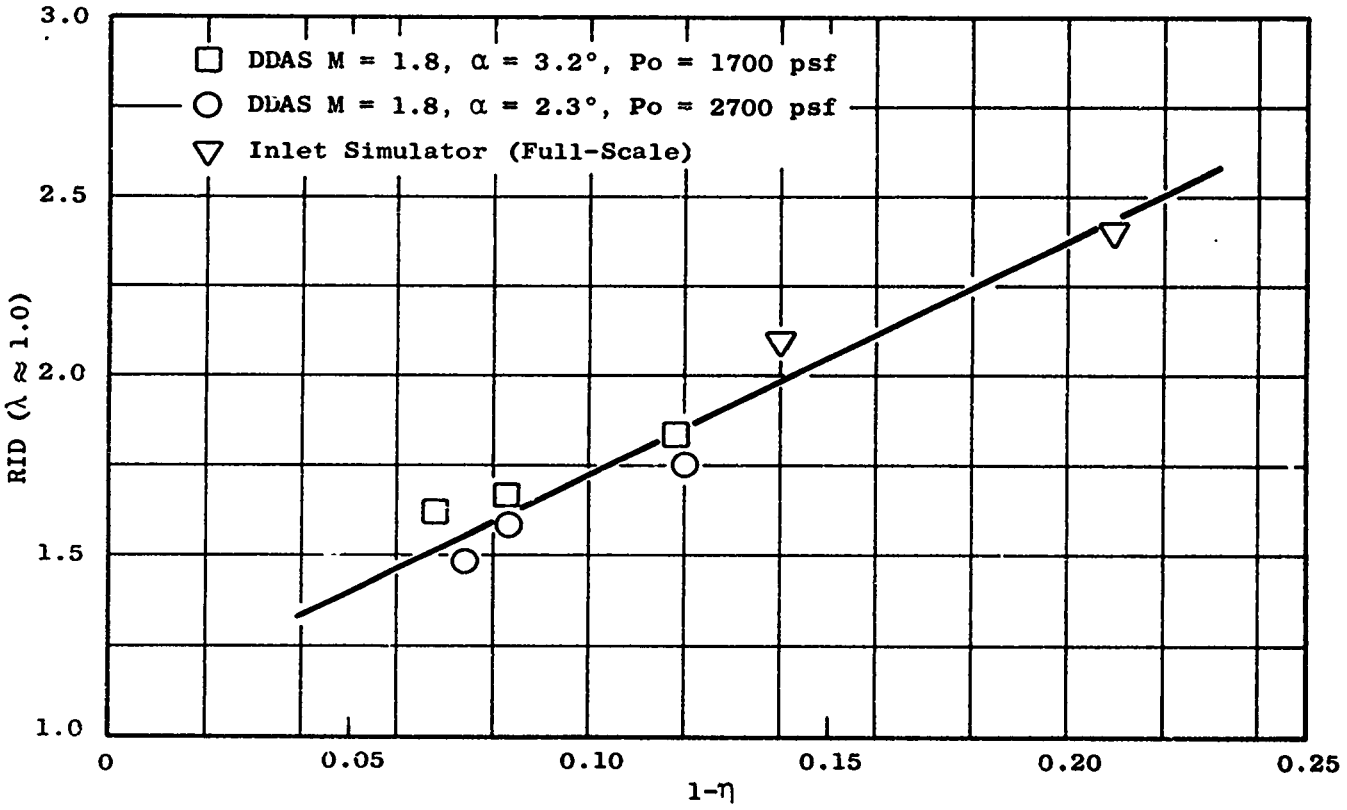

Figure 69. Supercritical Effects on Peak Dynamic Distortion.

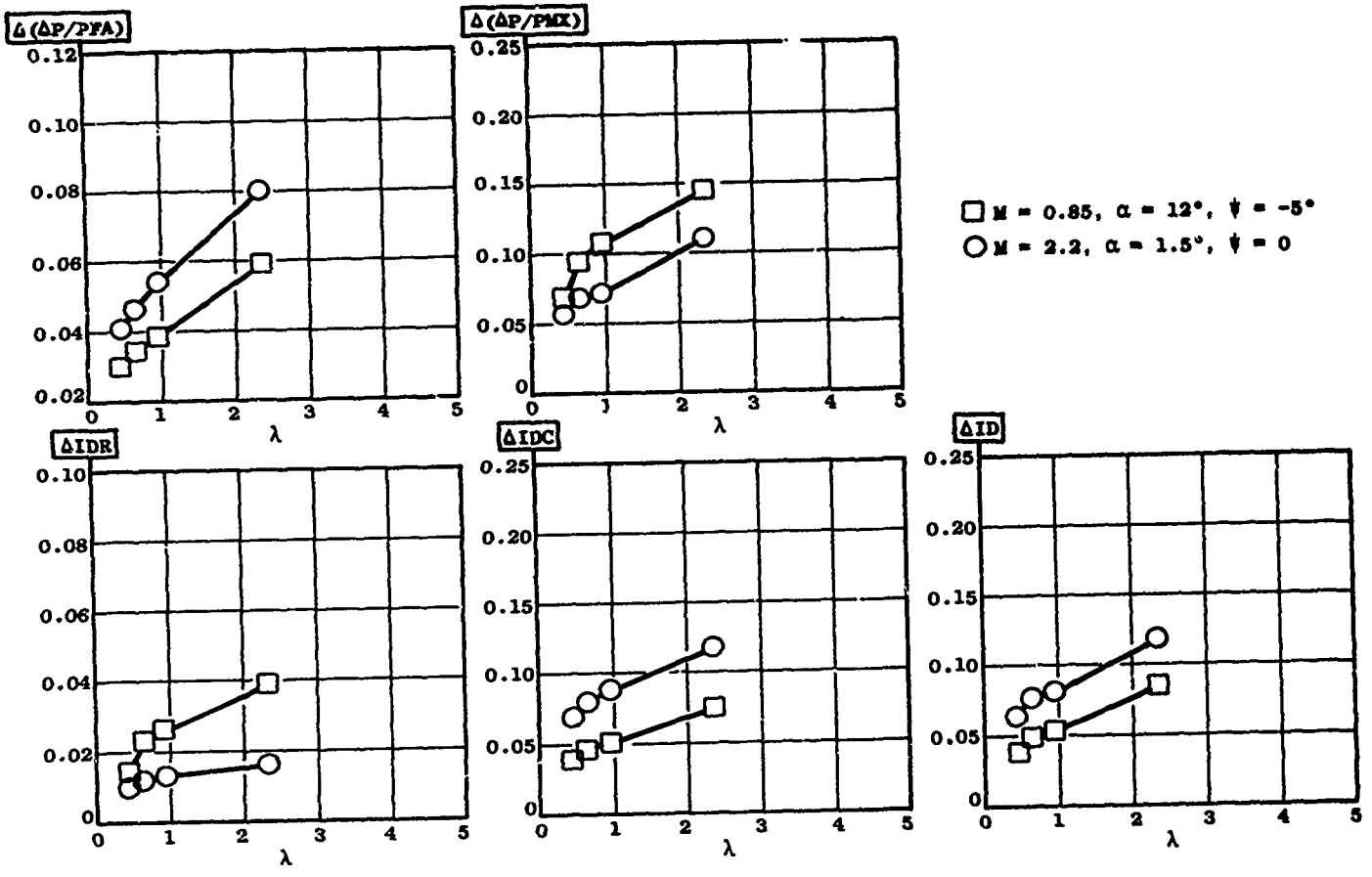

Figure 70. Average Time Effects on Peak Dynamic Distortion, 2DMC Inlet.

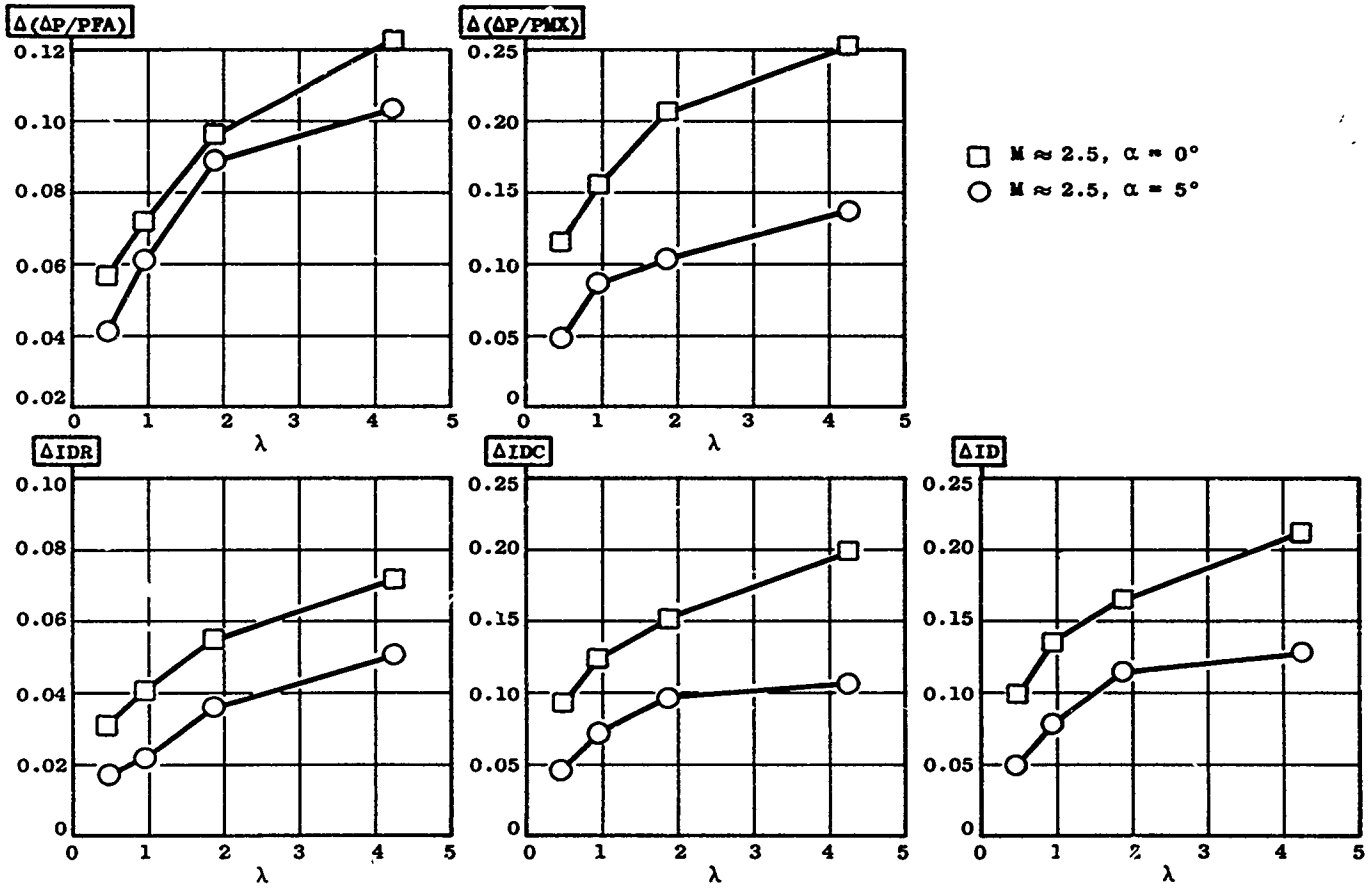

Figure 71. Average Time Effects on Peak Dynamic Distortion, ASMC Inlet.

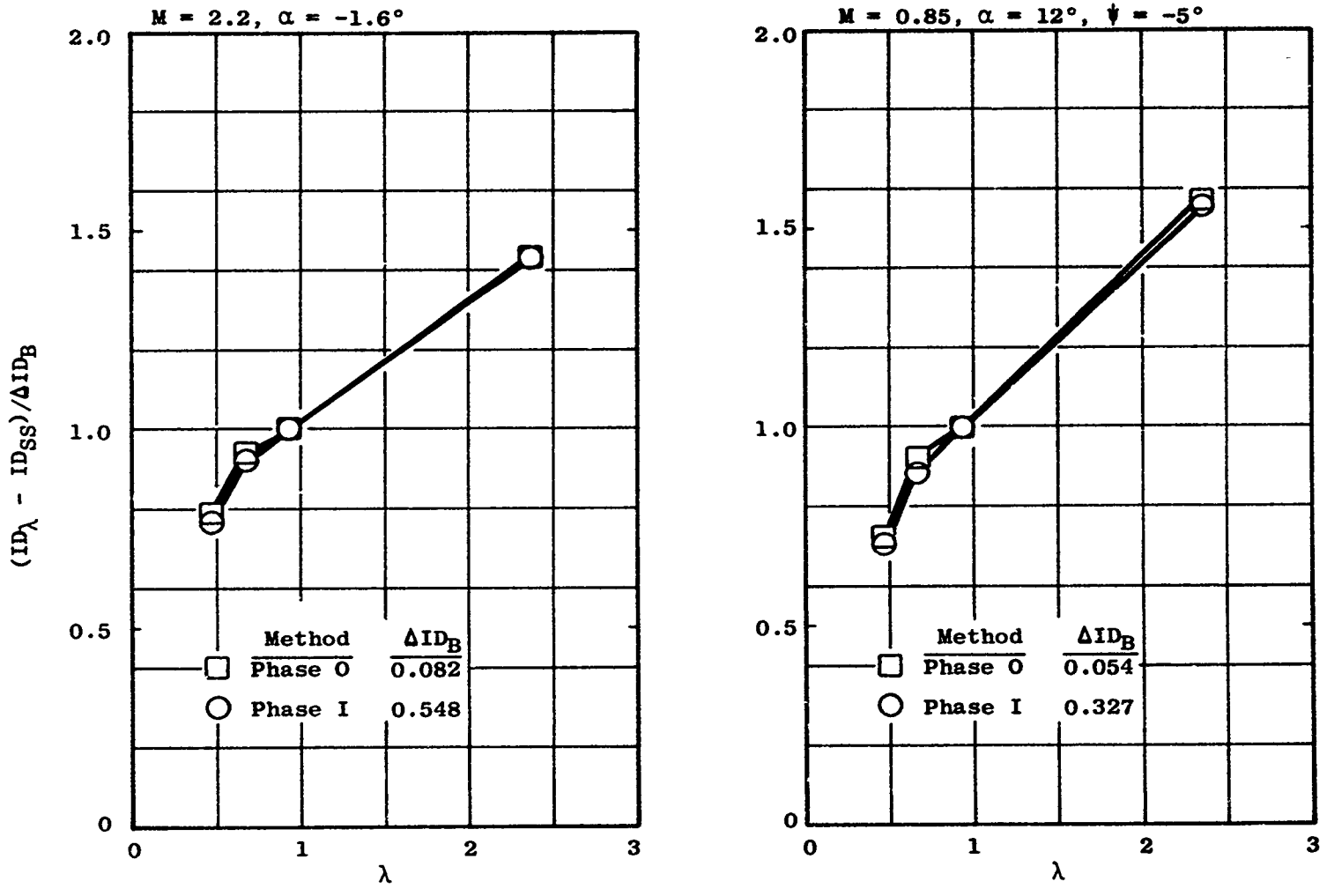

Figure 72. Parameter Combination Effects on Peak Dynamic Distortion, 2DMC Inlet.

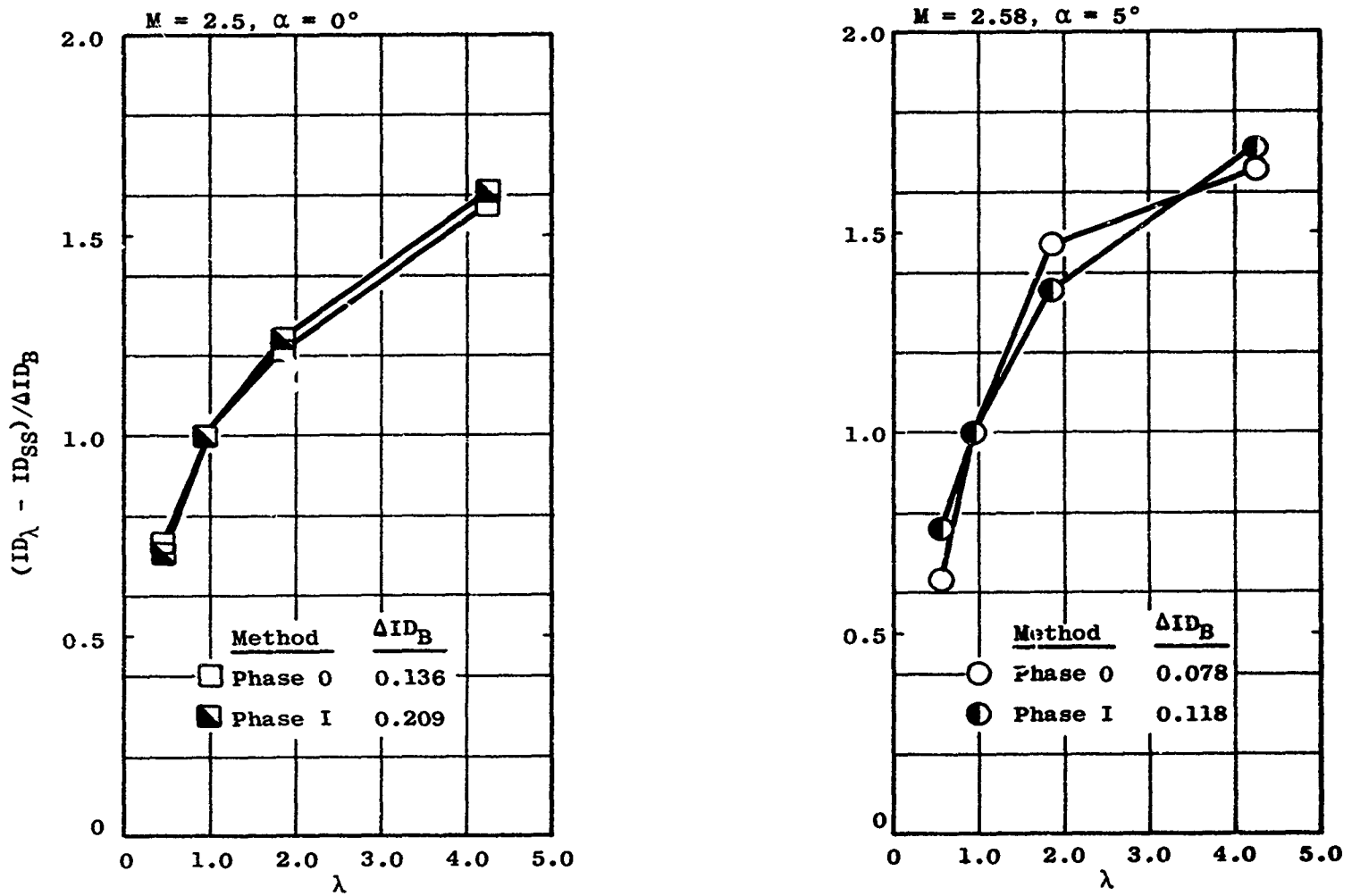

Figure 73. Parameter Combination Effects on Peak Dynamic Distortion, ASMC Inlet.

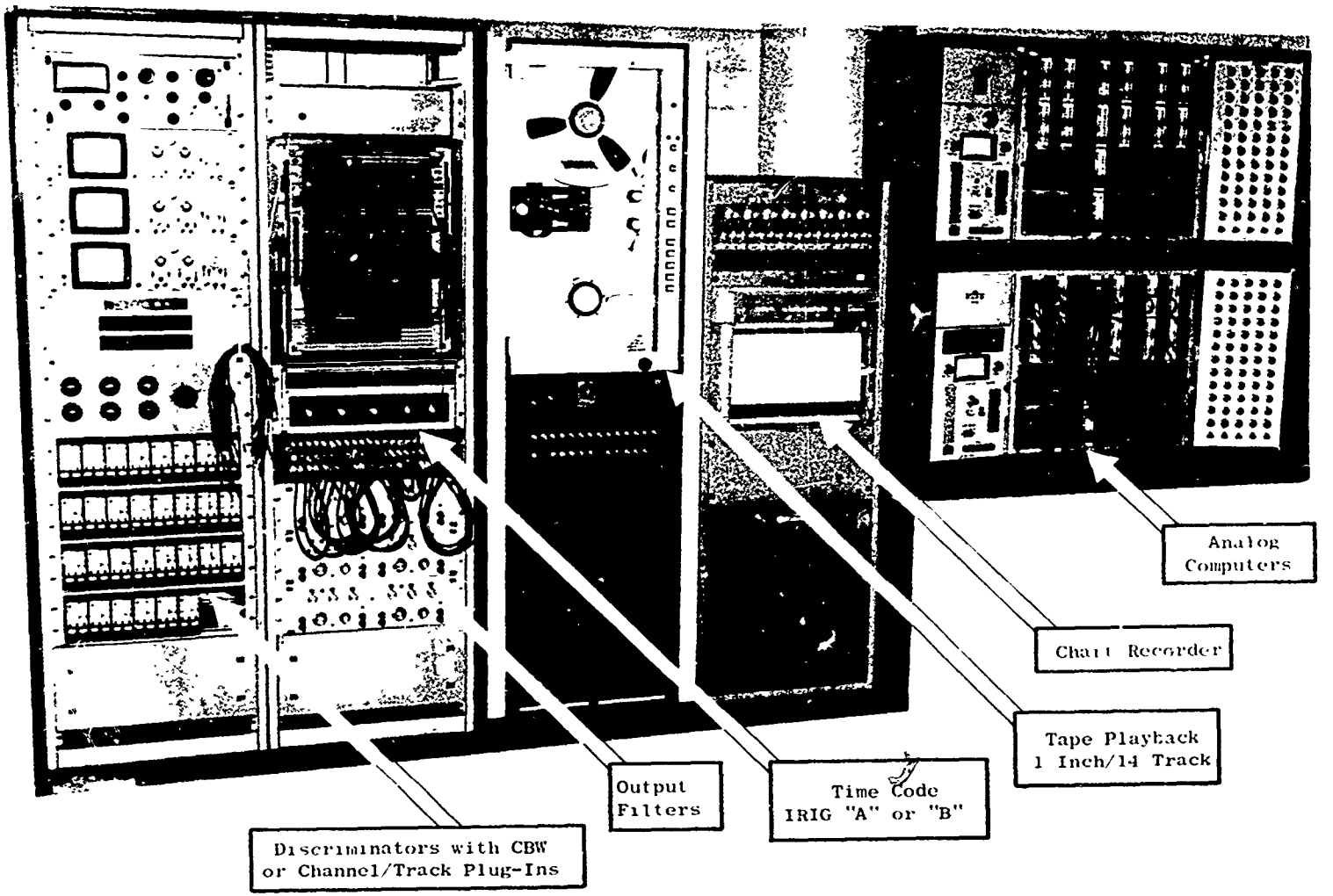

Figure 74. Stability Measurements Analysis Laboratory.

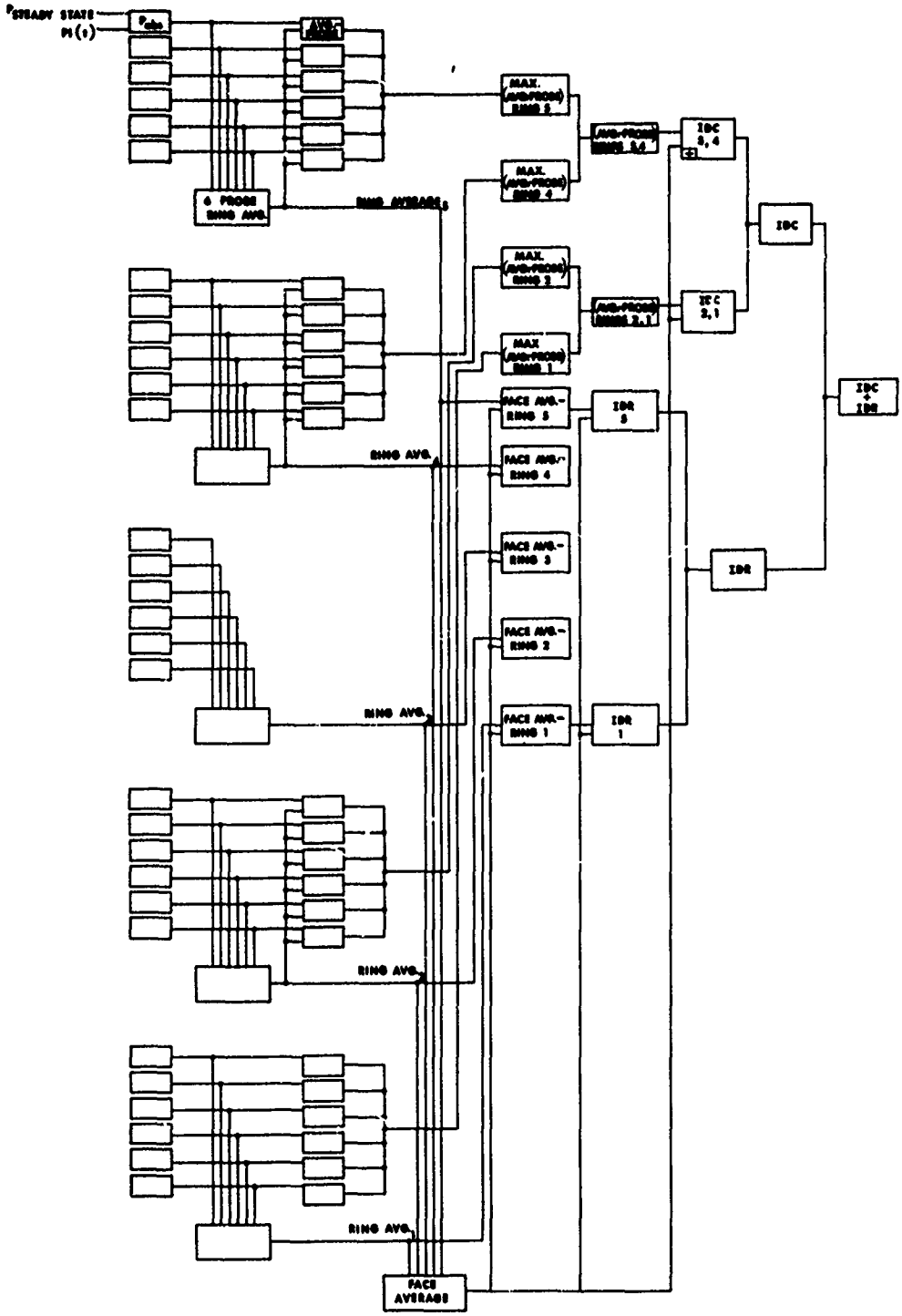

Figure 75. Analog Distortion Analyzer Block Diagram.

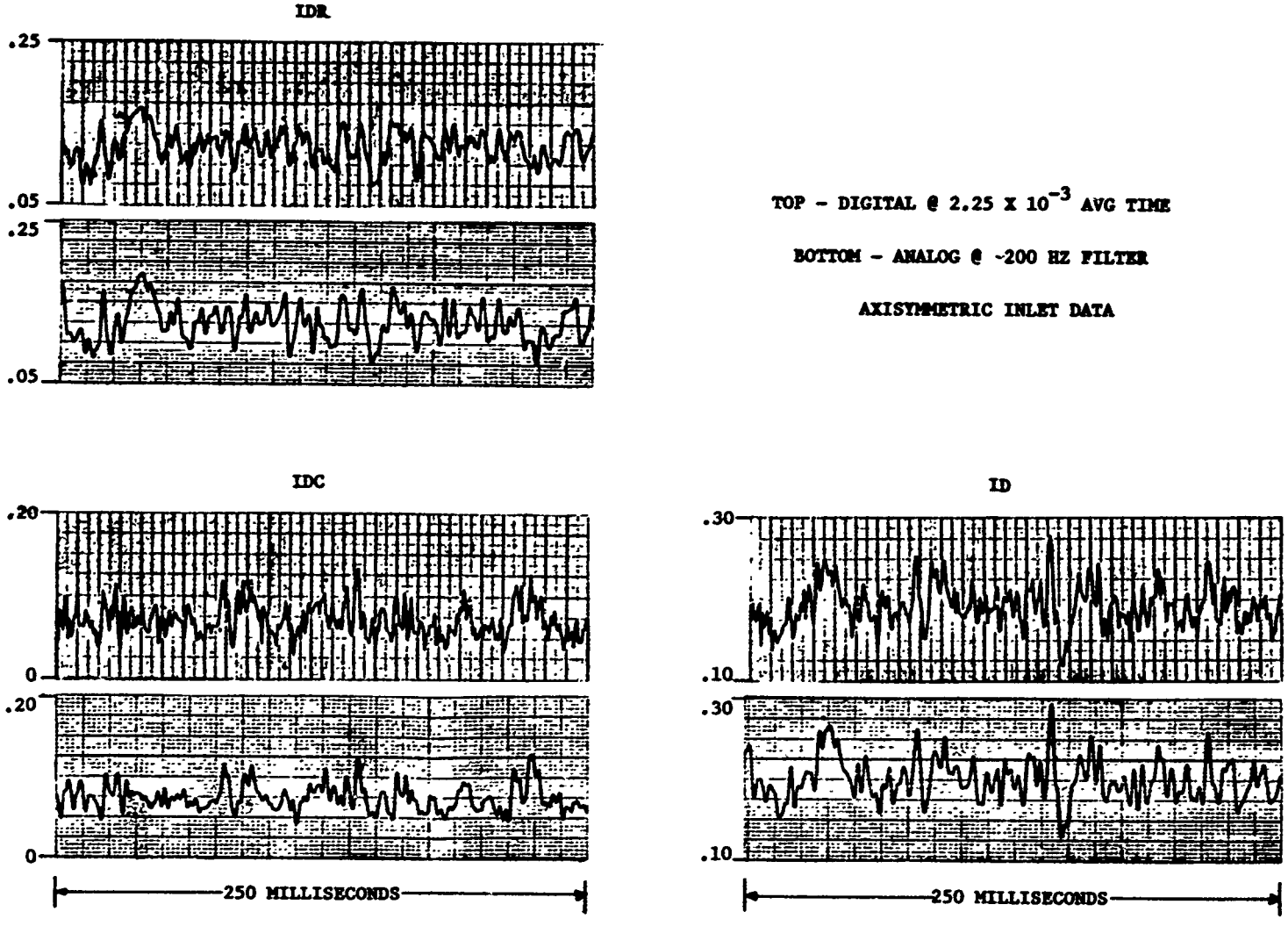

Figure 76. Analog Distortion Analysis Substantiation - Radial Component Dominates.

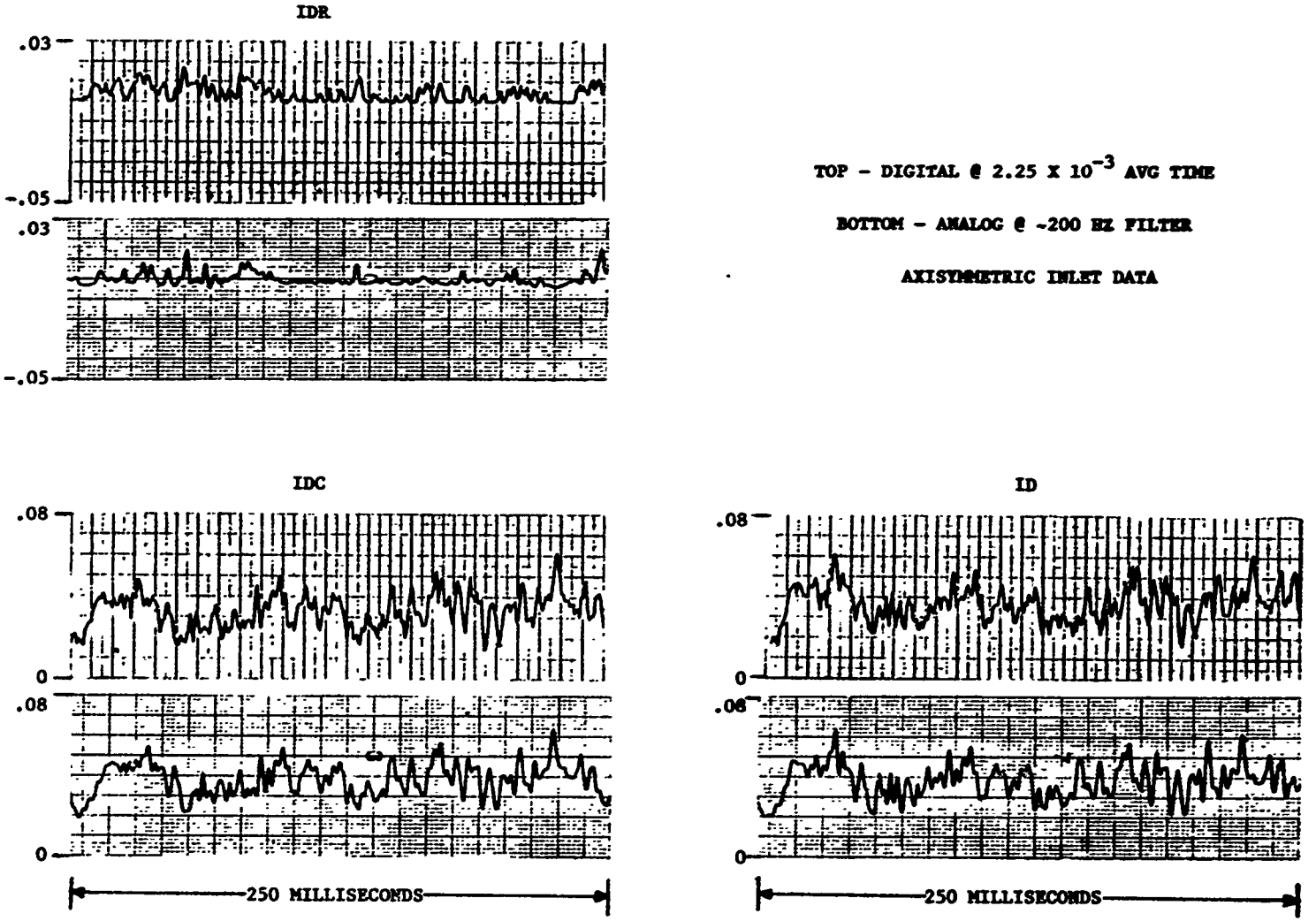

Figure 77. Analog Distortion Analysis Substantiation - Circumferential Component Dominates.

REFERENCES

1. Younghans, J.L., Moore, M.T., Collins, T.P., and Direnzi, J.G., "Inlet Flowfield Simulation Techniques for Engine/Compressor Testing," AIAA Paper #70-591 presented at AIAA 5th Aerodynamic Testing Conference, May, 1970.

2. Enochson, L.D. and Otnes, R.K., "Programming and Analysis for Digital Time Series Data," Shock and Vibration Monograph Series #SVM-3, 1968.

3. Kutschenreuter, P.H., Moore, M.T., and Collins, T.P., "Inlet Data for Engine Analysis," AIAA paper #70-1214 presented at AIAA 6th Propulsion Joint Specialists Conference, June, 1970.

4. Kutschenreuter, P.H. and Younghans, J.L., "Near Term Distortion Methodology/Task Force Results," General Electric Report TIS R70AEG410, October, 1970.